Title
Function and dynamics of microtubules and plus-end-tracking proteins during 3D epithelial remodeling

Author
Gierke, Sarah Joy

Publication Date
2012

Peer reviewed|Thesis/dissertation

Function and dynamics of microtubules and plus-end-tracking proteins during 3D epithelial remodeling

by

Sarah Gierke

DISSERTATION

Submitted in partial satisfaction of the requirements for the degree of

DOCTOR OF PHILOSOPHY

in

Biomedical Sciences

in the

GRADUATE DIVISION

ACKNOWLEDGEMENTS

First, I would like to thank my thesis advisor and mentor, **Torsten Wittmann** who, for the last 6 years, has supported my growth as a scientist and a person. When I first joined the lab he built my confidence by valuing my ideas and treating me as a colleague despite my relative inexperience. Over the years he spent countless hours with me at the microscope and staring at cell movies. I learned how to do effective, smart experiments and that it's important to quantitate EVERYTHING. He taught me how to view experiments and results with that uber-critical German eye, without feeling like he was critical of me (usually). Torsten has supported me in my career development, sending me to conferences, courses, and supporting my participation in a summer internship. In return I was happy to work hard and contribute to the success of the Wittmann lab. I'm incredibly proud to have been his first graduate student and early member of the lab and I look forward to learning of the great work coming from the Wittmann lab in the future. ; -)

I have been incredibly fortunate to have **Diane Barber** as my thesis committee chair. Because the Wittmann and Barber labs have such a close relationship, I've always felt that Diane was more like a second advisor. She has been involved in many important decisions in the direction of this project and has read countless manuscripts, fellowships, and abstracts. I also greatly value her advice on my professional development, her excitement about the SF Giants, and her hugs both in hard times and in celebration. Diane has been an amazing role model for me both scientifically and personally.

Thank you to my thesis committee member, **Keith Mostov**, for his helpful advice at all stages of my project. During the first couple years Keith invited me to present my work for his lab and I received invaluable feedback. Members of the Mostov lab provided

useful cell lines and reagents. **Dave Bryant** initially taught me the MDCK culture techniques and also spent several afternoons discussing my data and providing expertise on epithelial polarity and trafficking that were very helpful during my paper revisions. Thank you to the **Gaudenz Danuser** lab, especially **Maria Bagonis** for welcoming me to Boston for a week and teaching me Matlab and plusTipTracker.

The **Wittmann**, **Barber** and **Sophie Dumont labs** have provided an amazingly supportive, intellectual, and FUN (!) environment. I couldn't have picked a better group of people with whom to work and become lifelong friends. I still plan to crash the fantastic HSW-6 happy hours, tag along on the yearly ski and canoe trips and I look forward to visiting you all over the world (yes, Lawrence LeClaire, even you in Alabama). We've had so many wonderful scientists and I've learned so much from all of them. I want to particularly thank: **Praveen Kumar** who helped me get started when I rotated and joined, always had good scientific advice, and taught me more than I ever wanted to know about Cricket. **Karen Lyle** and I struggled together with our difficult cell culture model systems during the day and let out our frustration at Bodyjam or Bodypump at night. Karen has shown me that it is possible to be a great scientist and still have work-life balance - an invaluable lesson. Former members **Jyoti Srivastrava**, **Lawrence LeClaire**, **Jenn Haynes** and **Sam Stehbens** always had great advice, stories, cat videos and fun! I admire and appreciate **Bree Grillo-Hill, Andre Shonichen and Brad Webb** for their hard work, creativity and humor. **Hayley Pemble**, my fellow grad student, bench-mate, partner-in-crime and all around great friend has made it fun to come to work everyday. I don't think I could have finished my paper without our conversations/therapy sessions during our half-marathon training. **Claudia Bicho, Andreas Ettinger,** and **Jeffrey Van Haren** the new(er) guard in the Wittmann lab: you never know what you're going to get when someone new joins the lab, but I'm so glad we got all of you!

Thank you to the BMS staff, especially Lisa Magargal and Monique Piazza for all the administrative work, moral support, and for truly caring for me and my fellow students. To my BMS 2006 classmates, especially the Girls Book Club: **Emily Thornton, Emily Elliott, Alison Coady, Renee Greer, Kristen Coakley, Lauren Herl Martens, Kegan Donlan** and **Kate Stewart**. Such a smart and talented group! You've introduced me to new things (skiing, rockband, dominion, catch-phrase, true Harry Potter fandom, CSAs etc), supported me and listened through tough times, got me to chill out and have fun even when things were stressful (the wine helped), and all around enriched my life. I can't wait to see where we all end up and I look forward to our Google Hangouts.

To all my friends and family, especially **Neena Dagnino**, **Tara Martinez** and **Nate Bourg** and my in-laws **Marty Gierke** and **Margie Wild,** thank you for supporting me through grad school, for putting up with my busy schedule and for making the most out of the time we did have together.

Thank you to my older brothers **Bobby** and **Chris Arriola**. I grew up looking up to them and copying everything they did, and they paved the way for me. I wouldn't have had any of my successes without them showing me the way first. Thank you to my loving and caring grandparents, **Robert** and **Agnes Arriola,** who I miss everyday. They led by example the values that I think have helped me in my growth as a scientist and in any situation. These are to work hard and be helpful to others. They also taught us how to make great tamales- a gift of a great meal and great family tradition to remember them by every year.

Thank you to my parents, **Bob and Jerinda Arriola**, who have truly always supported me in whatever I wanted to do. I could not and would not have done this with out their support. They instilled curiosity in me as a kid and made our lives adventurous whenever they could. Whether it was camping and fishing in the Sierras, watching the

space shuttle land or seeing all the historic sights in New England, we were always learning new things. I also learned by watching them work hard to support our family, volunteer for our community, and participate in all my activities and interests. Thank you for being wonderful role models. Thank you for your support during this endeavor and for always being interested in my research and what I find interesting. And thank you for always being proud of me for the tiniest little accomplishments; I dedicate this great big accomplishment to you.

Finally, thank you to my amazingly supportive husband **Tom Gierke**. We were married just a few months before I started grad school and I don't think I would have gotten through that first year with out your support. Ok, our cute little kittens Dizzy and Ellie helped made it bearable too. All your sacrifices big and small on a daily basis made this possible. The late nights and weekends that you accompanied me in lab or times you missed out on vacation time because I needed to work, all contributed to this Ph.D. You believed in me all those times when I didn't. All the while, working hard and accomplishing so much in your own career. Thank you for all your love and support, I share this accomplishment with you.

Reference to published materials:

- Section III of the Introduction, Organization and Regulation of the microtubule cytoskeleton is adapted from the Introduction in Gierke S, Kumar P, Wittmann T. Analysis of microtubule polymerization dynamics in live cells. Methods Cell Biol. 2010;97:15-33.
- Table 1.1 is adapted from Table 1 in Kumar, P., & Wittmann, T. (2012). +TIPs: SxIPping along microtubule ends. Trends in Cell Biology, 22(8), 418–428.
- Chapter 1 is a reprint of the material as it appears in the published book chapter: Gierke S, Kumar P, Wittmann T. Analysis of microtubule polymerization dynamics in live cells. Methods Cell Biol. 2010;97:15-33.
- Figure 2.4 (and figure legend) is from the published article: Kumar P, Lyle KS, Gierke S, Matov A, Danuser G, Wittmann T. GSK3beta phosphorylation modulates CLASP-microtubule association and lamella microtubule attachment. J Cell Biol. 2009 Mar 23;184(6):895-908.
- Chapter 4 is a reprint of the material as it appears in the published article: Gierke S, Wittmann T. EB1-recruited microtubule +TIP complexes coordinate protrusion dynamics during 3D epithelial remodeling. Curr Biol. 2012 May 8;22(9):753-62. The coauthor listed in this publication, Torsten Wittmann, directed and supervised the research that forms the basis for the dissertation.

Function and dynamics of microtubules and plus-end-tracking proteins during 3D epithelial remodeling

Sarah Joy Gierke

ABSTRACT

Epithelial remodeling, in which apical-basal polarized cells switch to a migratory phenotype, plays essential roles in development and disease of multicellular organisms. How cytoskeleton dynamics, especially microtubule dynamics, are controlled and contribute to epithelial remodeling in a more physiological three-dimensional (3D) environment is not understood. We optimize confocal live-cell imaging to analyze microtubule function and dynamics during 3D epithelial remodeling of polarized Madin-Darby kidney epithelial cells that undergo a partial epithelial-to-mesenchymal transition (pEMT) in response to hepatocyte growth factor (HGF). We found that cellular extensions at the basal surface of HGF-treated cysts are densely packed with microtubules. Computational tracking of EB1-2xEGFP showed large numbers of microtubules growing persistently from the apical domain into these extensions and an increase in microtubule growth rate in response to HGF. We tested the role of microtubule plus-end-tracking protein (+TIP) complexes in 3D epithelial remodeling by depleting cells of EB1, an adaptor protein that mediates recruitment of other +TIP proteins to growing microtubule plus ends. In EB1-

depleted cells, microtubules displayed rapid lateral and retrograde movements demonstrating that EB1 is required to stabilize and organize microtubules in HGF-induced extensions. EB1-depleted cysts formed shorter, more branched, extensions suggesting that EB1 is required for productive HGF-induced extension outgrowth. Analysis of cell-matrix interactions and F-actin dynamics revealed that control extensions progressively pulled on and deformed the extracellular matrix (ECM) typically with one F-actin-rich protrusion near the cell tip with cell-matrix adhesions that turned over in a coordinated fashion. In contrast, EB1-depleted cells produced multiple highly dynamic protrusions with nascent adhesions that were uncoordinated, mislocalized and did not productively engage the matrix. As a result EB1-depleted extensions rapidly protruded, retracted and changed direction. Finally we show that trafficking of VAMP3-positive vesicles to the protrusion tip is disrupted in EB1-depleted cells. Together these data suggest that EB1-mediated organization of the MT cytoskeleton and associated vesicle delivery to the tip of HGF-induced extensions are likely required to coordinate cell-matrix adhesion and protrusion dynamics during 3D epithelial remodeling. It will be important in the future to investigate a broader role for EB1-mediated +TIP complexes in other normal and disease states of epithelial remodeling.

TABLE OF CONTENTS

LIST OF TABLES

LIST OF FIGURES

INTRODUCTION

I. Epithelial Remodeling

Epithelial cell layers constitute the barriers that define the inside and outside of multicellular organisms (O'Brien et al., 2002). The function of epithelial cells, those that line the internal organs for example, depends on a precise regulation of cell polarity and cell shape. Epithelial cells are typically polarized with three plasma membrane surfaces. These include an apical surface that faces a lumen or the topological outside of the organism, a lateral surface that forms contacts with adjacent cells and a basal surface that interacts with extracellular matrix proteins (ECM) to organize the tissue (O'Brien et al., 2002). This cellular organization is termed apical-basal polarity and is critical to normal epithelial function and homeostasis. However, changes in this organization, referred to herein as epithelial remodeling, play a central role in normal development and disease of multicellular organisms (Bryant and Mostov, 2008; Affolter et al., 2009).

One underlying process of epithelial remodeling is the epithelial-mesenchymal transition (EMT). During EMT, apical-basal polarized epithelial cells undergo changes in transcription factor activation, cell surface protein expression, mRNA expression, organization of the cytoskeleton and interactions with the extracellular matrix. The end result is a mesenchymal cell phenotype, characterized by increased dissociation and migration from the epithelial layer and invasion in the surrounding environment (Kalluri and Weinberg, 2009). EMT occurs in distinct biological contexts resulting in different functional outcomes. An

effort to categorize EMT based on these outcomes has been proposed as the following three subtypes (Kalluri and Weinberg, 2009):

- Type 1: EMT that occurs during embryo implantation, embryogenesis and organ development and includes gastrulation and neural crest cell migration. The mesenchyme resulting in this category of EMT can subsequently transition back to epithelia (mesenchymal-epithelial transition; MET), for example during branching morphogenesis of the mammary gland or kidney tubule.
- Type 2: EMT of established epithelia during wound healing or in response to inflammation and fibrosis.
- Type 3: EMT associated with cancer progression and metastasis.

EMT can take place in individual cells, defined groups within the epithelium or can be a whole epithelial structure that switches to a single mesenchyme (Duband, 2010). Furthermore, EMT can occur to different extents depending on the context. For example, partial EMT is the transient adoption of some mesenchymal characteristics without complete or permanent loss of the epithelial phenotype (Bryant and Mostov, 2008).

Many of the molecular players that determine epithelial or mesenchymal phenotypes and those that signal EMT have been identified (Kalluri and Weinberg, 2009). In polarized epithelia, the distinct apical plasma membrane domain is separated from the basolateral plasma membrane by junctional complexes of adherens and tight junctions. This polarity is thought to be established by the cooperation of three different cellular machineries: polarized trafficking machinery, domain-identity machinery, and 3D organization machinery

(Mellman and Nelson, 2008; Tanos and Rodriguez-Boulan, 2008). Polarized trafficking, via secretory and endocytic mechanisms, is required for sorting and delivering plasma membrane proteins and lipids to the correct apical or basolateral domains. Polarity protein complexes control the assembly of the tight junctions that divide the two domains and establish the domain identity for either side. The Scribble complex (Scribble, LGL, DGL) establishes the basolateral surface, while the Par (Par3, Par6, aPKC) and Crumbs (Crumbs/PALS/PAT J) complexes establish the apical surface and the location of the tight junctions. Interactions of proteins within each complex and between complexes regulate and maintain this localization: The PAR complex reinforces apical Crumbs complex localization while PAR and Scribble complexes mutually antagonize each other so that PAR is apical and Scribble is basal. How these complexes bind to the plasma membrane is poorly understood. Furthermore, it is unclear how the Crumbs and Scribble complexes establish and maintain the apical and basolateral identities of the plasma membrane (Tanos and Rodriguez-Boulan, 2008; Mellman and Nelson, 2008). Finally the 3D organization machinery is comprised of a network of GTPases and their regulators that relay signals from cell-cell adhesions and cell-substrate adhesions to orient cells and coordinate the other two machineries (Tanos and Rodriguez-Boulan, 2008; Mellman and Nelson, 2008). For example, MDCK epithelial cyst formation is initiated by GTPase Rac1-dependent adhesion to laminin, signaling the position of the basal surface and orienting the apical surface to be established at the opposite end of the cell (O'Brien et al., 2001). The asymmetric distribution of PtdIns(3,4,5)P3 to

the basolateral membrane and PtdIns(3,4)P2 to the apical membrane is also important in domain identity and is thought to be mediated by localization and activation of regulators PI3K and PTEN (Martín-Belmonte et al., 2007; Martín-Belmonte and Mostov, 2007). It is unclear how phospholipid asymmetry functions in apical-basal polarity but it may contribute to localization of polarity proteins and proper vesicle trafficking and fusion (Mellman and Nelson, 2008). Taken together, the epithelial program can be characterized by the expression of junctional proteins (E-cadherin, desmoplakins, occludins and claudins), polarity complex proteins (Par and Crumb) and extracellular matrix proteins/basement membrane (laminins) (Duband, 2010; Nelson, 2009; Tanos and Rodriguez-Boulan, 2008).

Several growth factors and morphogens, including transforming growth factor-β (TGF–β), bone morphogenetic proteins (BMPs), hepatocyte growth factor (HGF), fibroblast growth factor (FGF), Wnt proteins and Notch proteins, have been identified to induce EMT in varying cell types and processes. However, these EMT inducers seem to converge on three specific families of transcription factors that drive EMT: Snail, Zeb, and Twist (Duband, 2010; Xu et al., 2009). Furthermore these transcription factors all result in down-regulation of epithelial program genes (previous paragraph), especially E-cadherin, and increased expression of mesenchymal genes. This mesenchymal program includes genes associated with a migrational phenotype and required for invasion and ECM remodeling including the mesenchymal cell-cell adhesion protein N-cadherin, the intermediate filament vimentin, the ECM proteins

fibronectin and collagen, and matrix metalloproteases (Duband, 2010). In addition, the three polarity machineries described above must reorganize to establish front-back polarity. The front or leading edge of a migrating cell probably originates from its basal surface since this is what is in contact with the underlying basement membrane. Therefore reorientation of the trafficking machinery to the front-back axis, likely involves reorienting the Golgi network from the apical side (back) to the basal side (front) of the nucleus. However, whether or how this reorientation of the trafficking machinery occurs during EMT is unclear. The Par and Scribble polarity complexes and PtdIns(3,4,5)P3 lipids are at the front of migrating cells while PtdIns(3,4)P2 is at the back of the cell. Polarity proteins further signal localization of GTPases Cdc42 and Rac1 to the cell front and RhoA to the cell back (Nelson, 2009; Tanos and Rodriguez-Boulan, 2008). While the cell front maintains characteristics of the basal surface and the cell back resembles the apical, how these polarity proteins and GTPases are regulated during EMT is not well understood.

II. Cytoskeleton in epithelial remodeling

Ultimately the transcriptional and signaling changes that take place in epithelial remodeling drive dynamic reorganization of the cytoskeleton, leading to cell shape changes and migration. However, the underlying molecular mechanisms are incompletely understood. In apical-basal polarized epithelial cells, filamentous actin and non-muscle myosin II form a network at the cell cortex. In addition, cortical actin bundles maintain cell-cell adherens junctions that form a belt just under the tight junctions and encircle the cell. Actin filaments are joined

between cells through cadherins and anchor proteins, which allows transmission of force across the apical surface (Skoglund et al., 2008; Ratheesh and Yap, 2012; Etienne-Manneville, 2012; Mège et al., 2006; Maruthamuthu et al., 2010). Similarly, actin filaments maintain basal interactions through integrin-mediated focal adhesion contacts with the ECM (Geiger and Yamada, 2011; Maruthamuthu et al., 2011; Calderwood et al., 2000). Dense networks of cross-linked actin filaments form the structural core of microvilli on the apical surface, which accounts for the strong filamentous actin (F-actin) positive staining found in immunofluorescence images (Nelson, 1991; O'Brien et al., 2002; Drenckhahn and Dermietzel, 1988). Microtubule cytoskeleton organization is also complex and highly regulated in apical-basal polarized cells. A mesh-like network of microtubules is present near the apical and basal surfaces and few microtubules radiate from the apically localized centrosome (Müsch, 2004; Bacallao et al., 1989; Bré et al., 1990). In polarized epithelial cells, most microtubules are not associated with the centrosome as in non-polarized cells, but are anchored near the apical surface and organized in bundles parallel to the apical-basal polarity axis. This transverse microtubule array is proposed to be established by delivery of short microtubules from the centrosome to the cell-cell junctions where they can then grow toward the basal surface. The proteins ninein and nehza cap the minus end of these short microtubules, preventing depolymerization, and are recruited to desmosomes via desmoplakin and dynein motors or to adherens junctions (Mogensen et al., 2000; Abal et al., 2002; Lechler and Fuchs, 2007; Moss et al., 2007; Meng et al., 2008; Bellett et al., 2009). Although some

microtubules growing toward the apical surface may be important for apical transport, most microtubules grow towards the basal surface where they are stabilized by cortical interactions (Jaulin et al., 2007; Reilein, 2005; Hotta et al., 2010). This unique organization of microtubules is required for maintenance of cell polarity in differentiated epithelia *in vivo* (Achler et al., 1989). Microtubules may also regulate the position of the apical surface in epithelial cells during establishment of polarity and delivery of apical or basal proteins to the correct location (Müsch, 2004; Cohen, 2004; Kreitzer et al., 2003).

Only recently has actin remodeling during the process of EMT been directly observed (Haynes et al., 2011). Most of what is known about cytoskeleton organization and function during cell migration comes from studies of cells on a 2D surface. During directional migration, actin organization is very different than in apical-basal polarity, with a highly dynamic, dendritic actin network providing the protrusive force at the leading edge. Migrating cells assemble focal adhesions at the ventral surface in contact with the underlying ECM typically near the lamella. Integrins at the cell surface bind to extracellular ligands, initiate assembly of focal adhesion proteins including vinculin, talin and FAK which then anchor thick bundles of actin stress fibers to the cell cortex. Tension mediated by actomyosin contractility facilitates growth and maturation of focal adhesions. As the cell moves forward, rear focal adhesions disassemble and let go of the substratum and actomyosin contractility allows the retraction of the rear of the cell to allow for net forward movement (Etienne-Manneville, 2004; Stehbens and Wittmann, 2012; Vicente-Manzanares et al., 2009). Although the

role for the microtubule cytoskeleton is incompletely understood, dynamic microtubules are required for the establishment and maintenance of directional cell polarity and migration in many cell types and is associated with focal adhesion turnover (Akhmanova et al., 2009; Stehbens and Wittmann, 2012). However, microtubule function and organization during migration can vary depending on the cell type. Fibroblasts, epithelial, and endothelial cells require an intact microtubule array- they stop migrating and lose directionality when microtubules are depolymerized (Liao et al., 1995; Goldman, 1971; Gotlieb et al., 1983). Neutrophils continue to migrate after microtubule depolymerization, but lose control of direction. Neuronal migration in the brain during embryogenesis requires microtubules and the motor protein dynein, for the forward translocation of the cell body and nucleus (Tanaka et al., 2004). Microtubules are also required for the elongation and retraction of nerve growth cones during axon formation (Bamburg et al., 1986). Microtubule organization in fibroblasts, epithelial, and endothelial cells is similar, with the centrosome polarized in front of the nucleus in the direction of migration and microtubules radiating from the centrosome with plus-ends oriented toward the plasma membrane (Gundersen et al., 2004; Palazzo et al., 2001a). In these cells, microtubule polymerization dynamics are spatiotemporally regulated with the stabilization of microtubules in the lamella at the cell front (Komarova et al., 2002). However, in neutrophils, the centrosome is located behind the nucleus, with most microtubules oriented toward the back of the migrating cell (Xu et al., 2005). The lamella in fish keratocytes is exclusively formed by actin filaments, while the lamella in mammalian astrocytes and

neurons are long extensions that are filled with microtubules (Etienne-Manneville, 2004). Although it is clear that microtubules can be organized very differently in these different cell types, it is unclear what molecular roles microtubules play during migration in each case.

The extracellular environment also largely influences cell shape and cytoskeleton organization. For example, fibroblasts on a 2D surface are spread flat with prominent actin stress fibers that prevent cell motility, while the same cells in a 3D collagen matrix are spindle-shaped, polymerize actin filaments at a leading edge, and migrate (Walpita and Hay, 2002). In addition gene expression, intracellular signaling and regulation of cell growth in 3D cell culture is more similar to *in vivo* than 2D cell culture (Yamada and Cukierman, 2007; Even-Ram and Yamada, 2005). For example, Rac1 activity is relatively low in 3D migrating cells resulting in more persistent direction of migration as compared to 2D (Pankov et al., 2005; Yamada and Cukierman, 2007; Petrie et al., 2012; 2009). Matrix compliance and composition influence integrin activation, focal adhesion assembly, and myosin II-dependent contractility (Doyle et al., 2009; Caswell et al., 2008; Petrie et al., 2012; Geraldo et al., 2012). More recent studies have directly implicated a role for microtubules in 3D migration through regulation of GTPase signaling, stabilizing protrusions and cell shape (Heck et al., 2012; Yamada and Cukierman, 2007; Martins and Kolega, 2012; Kim and Matthew Petroll, 2007). It has become increasingly clear, especially over the last 5-10 years, that 3D culture models are an important step toward a more physiological model for the complex *in vivo* environment (Even-Ram and Yamada, 2005;

Yamada and Cukierman, 2007; Doyle et al., 2009; Meyer et al., 2012; Friedl et al., 2012). Therefore analyzing the role of microtubules in epithelial remodeling in a 3D environment is essential to understanding cell behavior in a tissue relevant context.

III. Organization and Regulation of the Microtubule Cytoskeleton

Microtubules (MTs) are highly dynamic cytoskeletal polymers with important functions in cell physiology. MTs are required for proper attachment and segregation of chromosomes during mitosis (Wittmann et al., 2001; Walczak et al., 2010), establishing polarity by local stabilization of MTs toward the front of migrating cells (Wittmann and Waterman-Storer, 2001; Kumar et al., 2009; Wu et al., 2008; Kaverina and Straube, 2011), positioning of organelles (Miller et al., 2009; Lomakin et al., 2009; Grigoriev et al., 2008), providing tracks for intracellular transport (Prigozhina and Waterman-Storer, 2006; de Forges et al., 2012), and supporting cell shape (Brangwynne et al., 2006; Stamenović et al., 2002; Bonetta, 2005). Polymerization dynamics allow MTs to rapidly reorganize, probe the intracellular environment for specific targets and provide pushing and pulling forces within a cell and are thus highly regulated (Kirschner and Mitchison, 1986; Inoué and Salmon, 1995). MTs are composed of α/β-tubulin heterodimer subunits that assemble into linear protofilaments of which 13 protofilaments further form a stiff, hollow tube. The head-to-tail association of α/β tubulin dimers results in an inherent polarity to the MT and different polymerization rates at the two ends with the β-tubulin monomer pointing toward the fast-growing “plus end” and the α-tubulin monomer toward the slow-growing

"minus end." In cells, a third form of tubulin called γ–tubulin forms the γ-tubulin ring complex γTurc, that functions as a template for MT nucleation and a cap of the MT minus end to prevent depolymerization (Wiese and Zheng, 2006; Aldaz et al., 2005; Kollman et al., 2010). Other protein complexes can contribute to capping and anchoring of MT minus ends at both centrosomal and non-centrosomal sites. For example, the minus end binding protein, ninein, can anchor MTs to the centrosome or adherens junctions (Jiang and Akhmanova, 2011; Mogensen et al., 2000).

MTs in cells and *in vitro* stochastically switch between phases of growth and shortening. This non-equilibrium polymerization behavior has been termed dynamic instability (Mitchison and Kirschner, 1984), and is driven by different structural states of the MT end, which are ultimately the result of polymerization-coupled GTP hydrolysis in the MT lattice (Fig. 1.1) (Nogales and Wang, 2006). GTP-bound tubulin dimers initially polymerize as a relatively flat open sheet at the plus end of a growing MT, which subsequently closes into a tube. Shortly after polymerization, the GTP on the β-tubulin subunit within the MT lattice is hydrolyzed to GDP, leaving a GTP-tubulin cap at the tip of the MT. More recent studies suggest that there is also a unique structure between the new GTP end and the "aged" GDP lattice of the MT. This structure likely results from the GDP/Pi transition state of tubulin during GTP hydrolysis (Kumar and Wittmann, 2012; Gardner et al., 2011; Maurer et al., 2011; 2012). The GTP-cap stabilizes the growing end and supports further addition of GTP-bound tubulin subunits, resulting in a stable growth phase. In contrast, loss of the GTP-cap results in

catastrophic depolymerization and highly curved protofilaments seem to peel away from the depolymerizing MT end as established by electron microscopy. These frayed MT ends reflect the high intrinsic curvature of GDP-bound tubulin dimers in comparison to the more straight conformation of GTP-bound dimer, and no longer support addition of new GTP-bound tubulin dimers. Thus, this large structural difference between polymerizing and depolymerizing MT ends is sufficient to explain the high persistency and abrupt switching between growing and shortening that characterizes MT dynamic instability *in vitro* (Kueh and Mitchison, 2009).

Four parameters are generally measured to describe MT polymerization dynamics: the rates of growth (polymerization), shortening (depolymerization), and the transition frequencies between these two states. The transition from growth to shortening is referred to as 'catastrophe', and the transition from shortening to growth is referred to as 'rescue' (Fig. 1.1). These parameters can be determined quite easily in *in vitro* polymerization reactions with purified components because MT growth and shortening rates are relatively constant and transitions occur infrequently. In cells, however, MT polymerization dynamics are spatiotemporally highly regulated by a large number of accessory proteins (van der Vaart et al., 2009) as well as physical interactions with other intracellular structures (Dogterom et al., 2005). In addition, even the length of the MT GTP cap may be as much as 60x longer in cells than in *in vitro*, providing a longer opportunity for the MT to be rescued during depolymerization (Seetapun et al., 2012). As a result intracellular MT polymerization dynamics are significantly more

complex and more difficult to quantify. *In vivo*, only MT plus ends exhibit dynamic instability while free minus ends are either stabilized or depolymerize. Both growth and shortening rates are highly variable, and rates of individual MTs fluctuate significantly over relatively short time periods. In addition, MT polymerization dynamics in cells often include relatively long periods of pause during which MT ends do not appear to grow or shorten within the resolution limit of the light microscope. Furthermore, intracellular MTs are subject to pulling and pushing forces, which result in MT buckling, breakage and movements of MT ends that are not due to polymerization dynamics (Brangwynne et al., 2007; Waterman-Storer and Salmon, 1997; Wittmann et al., 2003).

In cells, tubulin can acquire post-translational modifications (PTMs) by specific enzymes. These modifications include tyrosination, detyrosination, acetylation, poly-glutaylation, poly-glycylation, deglutamylation of detyrosinated tubulin (delta2 modification), phosphorylation and palmylation (Hammond et al., 2008; Verhey and Gaertig, 2007). While tyrosination occurs on soluble α-tubulin, most other modifications are added on polymerized MTs. Although these PTMs are not believed to directly affect MT polymerization rates, they do correlate with the lifetime of MTs so that stable MTs acquire more PTMs in a time-dependent manner (Hammond et al., 2008). MT acetylation has also been proposed to protect against depolymerization, resulting in higher MT stability (Matov et al., 2010; Tran et al., 2007). For these reasons, acetylation or glutamylation is often used to identify the population of stable MTs in a MT network. Although the function of PTMs of MTs are not well understood, it has been proposed that it is a

way of defining subpopulations of MTs for specific functions. This “tubulin code” can then be read by MT associated proteins by affecting their MT affinity, thus indirectly affecting MT dynamics, intracellular trafficking, polarity and cellular organization (Verhey and Gaertig, 2007; Kaverina and Straube, 2011; Conde and Cáceres, 2009; Janke and Kneussel, 2010).

Spatiotemporal regulation of MT dynamics and asymmetric polarization of the MT cytoskeleton are critical for cell migration, epithelial remodeling and differentiation of cells. In addition to the inherent dynamic instability of tubulin polymers, MT dynamics and organization are further regulated by various MT-associated proteins (MAPs). Structural MAPs (MAP2, MAP4, tau, doublecortin) directly bind and stabilize the MT lattice by preventing catastrophes and reducing shrinkage speeds (Dehmelt and Halpain, 2005; Moores et al., 2006). XMAP215 is a MT polymerase that processively tracks the growing plus ends of MTs where it catalytically feeds tubulin dimers to the polymer (Howard and Hyman, 2007; Brouhard et al., 2008). In contrast, kinesin-8, -13 (MCAK) and -14 destabilize MTs, probably by inducing a curvature to the GTP-bound dimers at the plus end, resulting in depolymerization in slightly different enzymatic processes (Hertzer and Walczak, 2008; Howard and Hyman, 2007; Gardner et al., 2011). Furthermore MT-severing enzymes such as spastin and katanin can break the MT and expose the minus end, resulting in MT depolymerization (Roll-Mecak and McNally, 2010). Polymerization dynamics can also be influenced by modulating the concentration of functional tubulin. The MT-depolymerizing factor Stathmin/Op18 binds to tubulin dimers and changes the conformation so that it

cannot be incorporated into MTs, thus effectively decreasing the concentration of functional tubulin (Cassimeris, 2002). Association of many of these proteins with tubulin or MTs is further modified by phosphorylation (Wittmann et al., 2004a; Matenia and Mandelkow, 2009) allowing for more precise spatial and temporal resolution.

A special class of MAPs, called plus end interacting proteins (+TIPs), is a heterogeneous group of proteins that accumulate specifically at the growing plus ends of MTs (Kumar and Wittmann, 2012; Akhmanova and Steinmetz, 2008). In cells, these +TIPs appear as a characteristic comet at the growing plus end of MTs, a behavior termed plus-end-tracking (Perez et al., 1999; Mimori-Kiyosue et al., 2000; Kumar and Wittmann, 2012). This category of proteins has grown dramatically over the past decade with now over 50 proteins identified to have plus-end-tracking capability (Akhmanova and Steinmetz, 2008; Kumar and Wittmann, 2012; Jiang et al., 2012). Despite a shared plus-end-tracking characteristic, these proteins are structurally and functionally diverse, playing roles in cell differentiation, cell polarity, migration, adhesion and mitosis (Wittmann and Waterman-Storer, 2005; Akhmanova and Steinmetz, 2010; Mimori-Kiyosue, 2011; Kumar and Wittmann, 2012; Stehbens and Wittmann, 2012).

The formation of MT +TIP complexes is largely dependent on their recruitment by a central adapter, EB family proteins (end-binding protein 1,2, and 3). EBs form homo- or heterodimers and bind directly to MTs through N-terminal calponin homology domains (Seetapun et al., 2012; De Groot et al., 2010; Bieling

et al., 2007; 2008; Dixit et al., 2009; Komarova et al., 2009). How EBs recognize only the growing MT plus end has been a matter of debate with proposals such as co-polymerization with tubulin dimers (Folker et al., 2005), transport on plus-end directed kinesins, binding along MT seam during tubulin-sheet closure (Sandblad et al., 2006) and recognition of the MT GTP cap (Lampert et al., 2010; Zanic et al., 2009). However, the most strongly supported and emerging consensus in the field is that EBs can bind to a specialized structure near the newly polymerized MT end that is different from the "aged" lattice of the MT (Kumar and Wittmann, 2012; Gardner et al., 2011). EBs bind between protofilaments so they are in contact with four different tubulin dimers and precisely in a position to recognize the nucleotide state of the tubulin (Maurer et al., 2012). In vitro studies have also shown that EB1 binds most strongly to BeF3- MTs that mimic the GDP/Pi transition state of tubulin after GTP hydrolysis over GDP or GTP-tubulin (Dimitrov et al., 2008; Zanic et al., 2009; Maurer et al., 2011; 2012). Taken together, this evidence suggests that EBs likely recognize a relatively slow conformational change that takes place during or after GTP hydrolysis and thus bind not at the extreme plus end of the MT, but to a slowly decaying region of intermediate conformation just behind the GTP cap (Kumar and Wittmann, 2012).

EBs can regulate MT dynamics directly, in cells by promoting persistent growth and suppressing catastrophes and *in vitro* by promoting catastrophes (Komarova et al., 2009). Depletion of EB1 in melanoma cells results in less persistent motility, potentially through an imbalance of filopodia to lamellipodia

(Schober et al., 2009) and may disrupt signaling to actin protrusions (Schober et al., 2012). EB dimers recruit other +TIPs to the growing MT plus end via two different mechanisms. The C-terminal EB homology domain (EBH) contains an EEY/F motif, which binds proteins with CAP/Gly domains, including Clip170 and $p150^{Glued}$. Additionally, the EBH domain contains two hydrophobic grooves that recognize a Ser-x-Ile-Pro (SxIP) motif on +TIPs (Honnappa et al., 2009; Kumar and Wittmann, 2012). Regions around SxIP motifs are typically predicted to be disordered, however molecular dynamics simulations with one +TIP, CLASP, shows extensive salt-bridge networks which likely contribute to binding to EB1 (Honnappa et al., 2005; 2009; Kumar et al., 2012). Binding of +TIPs to EB1 can be regulated by phosphorylation of serine residues near the SxIP motif (Honnappa et al., 2009; Kumar et al., 2009; Watanabe et al., 2009; van der Vaart et al., 2011; Moore et al., 2005; Kumar et al., 2012), and detyrosination of tubulin disrupts CAP-Gly binding (Bieling et al., 2008; Peris et al., 2006). SxIP containing proteins comprise the large majority of +TIPs, a list that has grown significantly over last year (Table 1.1) (Jiang et al., 2012; Kumar and Wittmann, 2012).

Complexes of different +TIPs formed at MT plus ends can control MT organization and function through regulation of MT dynamics and interactions with other cellular components (Galjart, 2010). Proteins localized at the plus ends of MTs are prime candidates for mediating the “search and capture” of MTs in attachment to the cell cortex, interactions with the actin cytoskeleton and distribution of organelles. Three types of +TIPs have been established to mediate stabilization of MTs toward the leading edge and are required for directed

migration: CLASPs, spectraplakins MACF/ACF7, and APC. A fourth, Amer2/FAM123A has recently emerged as a regulator of MT stabilization at the plasma membrane and is required for cell migration. CLASP demonstrates a unique spatiotemporal organization of binding to growing MT plus ends in the cell body and binding along the MT lattice in MTs near the leading edge. This differential binding is regulated by phosphorylation: inactivation of GSK3b in the lamella results in dephosphorylation of CLASP and increased lattice binding, resulting in MT stabilization (Kumar et al., 2009; Watanabe et al., 2009). Additionally CLASP has been shown to interact independently of MTs with the cortex protein LL5B around focal adhesions at the front of a migrating cell and basal surface of an apical/basal polarized cell, thus acting as a cortical adaptor between MTs and the cortex (Kumar et al., 2009; Lansbergen et al., 2006). Spectraplakins are known as cross-linkers of the MT and actin cytoskeletons. Like CLASP, GSK3b phosphorylation of MACF1/ACF7 regulates its MT binding activity and its localization to the cortex (Wu et al., 2011). MACF1/ACF7 has been proposed to guide MT growth along actin filaments, through its interactions with EB1, to focal adhesions (Wu et al., 2011). Both CLASP and MACF1/ACF7 mediated capture of MTs is required for coordinated focal adhesion turnover and directed cell migration, though whether or how these two +TIPs coordinate in these processes is not yet understood. APC can be transported along MTs by the kinesin KIF17 and accumulates at the plus ends of MTs that grow into cell edges and protrusions. This localization correlates with increased growth and stability of this MT subset (Mimori-Kiyosue et al., 2000; Kita et al., 2006) and

further regulates directional migration. APC accumulations can also occur near focal adhesions and may regulate focal adhesion assembly and capture of MTs near the leading edge (Matsumoto et al., 2010; Barth et al., 2008; Etienne-Manneville, 2009). Amer2/FAM123A has recently been identified to stabilize MTs in a complex with EB1 and APC. Overexpression of both EB1 and Amer2 resulted in bundling of stable MTs at the cell cortex close to the plasma membrane (Pfister et al., 2012). Amer1 can be membrane associated in a PIP2 dependent manner, similar to LL5B, and is primarily found at the plasma membrane as opposed to +TIP tracking. Some +TIP proteins were identified to track MT plus ends when overexpressed or when expressed as truncation mutants, but do not track plus ends under physiological conditions. Therefore this plus-end-tracking phenotype may just reflect the strong binding interaction to EB1 (Jiang et al., 2012; Pfister et al., 2012). These proteins likely provide capture points at the cortex or other intracellular structures where they are normally localized for EB1 and EB1-recruited +TIP complex coated MT plus ends (Jiang et al., 2012; Pfister et al., 2012; Stehbens et al., 2012).

In addition to actin-MT crosstalk mediated by spectraplakins, dynamic MTs have been proposed to directly regulate Rho GTPase signaling involved in migration (Waterman-Storer et al., 1999; Wittmann and Waterman-Storer, 2001; Birkenfeld et al., 2008). In some cases this is achieved by MT-mediated delivery or concentration of Rho guanine nucleotide exchange factors (GEFs) that spatially activate Rho or Rac. Tiam1 and STEF1 (Tiam2) activate Rac1 in a MT-dependent manner and may be important in actin organization, focal adhesion

turnover and in neuronal cell polarity (Rooney et al., 2010; Pegtel et al., 2007; Montenegro Gouveia et al., 2010; Montenegro-Venegas et al., 2010). GEF-H1 binds directly to MTs and can activate RhoA and downstream actomyosin contractility when locally released at the leading edge (Ren et al., 1998; Krendel et al., 2002; Chang et al., 2008; Birkenfeld et al., 2008; Nalbant et al., 2009). RhoGEF2, a drosophila protein, displays EB1-mediated plus-end-tracking and is delivered to the cell cortex, resulting in cell contraction. However, a mammalian homologue or its role in migration has not been determined (Rogers et al., 2004). The actin-nucleating formin, mDia, has been implicated in stabilization of MTs in a RhoA feedback loop through interactions with the +TIP complex of EB1 and APC (Palazzo et al., 2001b; Wen et al., 2004). IQGAP, thought to coordinate actin nucleation, also interacts with +TIPs APC and CLASPs and potentially mDia, further linking stable MTs to actin regulation (Watanabe et al., 2009; Brandt and Grosse, 2007; White et al., 2012).

+TIPs are also important in distribution and organization of organelles within migrating and apical/basal polarized cells. For example, syntabulin is required for mitochondrial transport in neuronal processes. It mediates interactions with the MT motor KIF5B and mitochondria and accumulates at sites of MT plus end/mitochondrial interaction suggesting a role in mitochondrial loading (Ma et al., 2009; Jiang et al., 2012). In *S. pombe* the CLASP homologue regulates mitochondrial distribution (Chiron et al., 2008). CLASP has also been shown to organize the Golgi apparatus and regulate polarized post-Golgi trafficking in migrating cells (Miller et al., 2009; Efimov et al., 2007). Dystonin is a

cytoskeletal linker protein (plakin) important in MT stability and Golgi and ER structure and function in neurons (Ryan et al., 2012a; c; 2012b). The ER protein STIM1 binds EB1 directly and mediates ER extension via MT growth (Grigoriev et al., 2008). The +TIP $p150^{Glued}$ and doublecortin along with dynein and Lis1 are required for nuclear positioning in migrating neurons (Tanaka et al., 2004; Dupin and Etienne-Manneville, 2011; Kuijpers and Hoogenraad, 2011). Finally, many +TIPs, including EB1, CLASP, APC, Dynein/Dynactin/Lis1, CLIP-170, and Tastin, have been implicated in mitosis, from MT attachment to the cortex, centrosome and kinetochores to spindle assembly and orientation (Tamura and Draviam, 2012).

As the list of EB1-recruited +TIPs grows, it has become increasingly clear the function, regulation and interaction of this group of proteins is highly complex. Other than the SxIP motif, protein structures are diverse. Some complexes of +TIPs have been found to interact in certain functions (Akhmanova and Steinmetz, 2008) but what other complexes exist and how these complexes interact in a broader +TIP network is the subject of ongoing research in many different labs. Though several +TIPs have been implicated in cell migration in a 2D environment (Table 1.1), whether EB1-recruited +TIP complexes function in epithelial remodeling in a more physiological 3D environment is an outstanding and important question that we begin to address in this dissertation research.

Table 1.1: EB1-recruited +TIPs that contain confirmed or potential SxIP motifs.

Protein	SxIP motifs	Phosphorylation near SxIP motifs	Uniprot Identifier	Proposed functions
+TIPs with confirmed SxIP motifs				
CLASP1 CLASP2	SKIP SRIP (Honnappa et al., 2009; Kumar et al., 2012)	CDKs, GSK3 (Kumar et al., 2012; 2009; Watanabe et al., 2009)	Q7Z460 O75122	Microtubule capture (Kumar et al., 2009; Lansbergen et al., 2006; Mimori-Kiyosue et al., 2005), dynamics (Al-Bassam et al., 2010), and nucleation at the Golgi apparatus (Efimov et al., 2007)
MACF1/ACF7	SKIP (Honnappa et al., 2009)	GSK3 (Wu et al., 2011)	Q9UPN3	Microtubule capture (Wu et al., 2008; Kodama et al., 2003; Zaoui et al., 2010)
APC	SQIP (Honnappa et al., 2009)	CDKs, GSK3 (phosphorylation not confirmed *in vivo*) (Honnappa et al., 2009; 2005)	P25054	Microtubule capture (Barth et al., 2008; Kita et al., 2006; Etienne-Manneville et al., 2005; Reilein and Nelson, 2005); mutated in colon adenocarcinoma (Näthke, 2004)
STIM1	TRIP (Honnappa et al., 2009)	Mitotic phosphorylation (Smyth et al., 2009), mass spectrometry	Q13586	ER-microtubule interactions (Grigoriev et al., 2008); activator of store-operated Ca^{2+} entry; mutated in certain immunodeficiencies (Feske et al., 2010)
MCAK	SKIP (Honnappa et al., 2009)	Aurora B (Moore et al., 2005; Andrews et al., 2004)	Q99661	Microtubule depolymerase (Howard and Hyman, 2007)
Kif18B	SFLP SSLP (Stout et al., 2011; Tanenbaum et al., 2011)	Probable, mass spectrometry	Q86Y91	Microtubule depolymerase (Howard and Hyman, 2007)
SLAIN2	GGIP SAIP SGLP GGIP RSLP (van der Vaart et al., 2011)	Mitotic phosphorylation (van der Vaart et al., 2011)	Q9P270	Microtubule dynamics; recruits XMAP215/ch-TOG to microtubule plus ends (van der Vaart et al., 2011)
Sentin/SSP2 (*Drosophila*)	TGIP (Li et al., 2011)	Not determined	Q9VUA5	Microtubule dynamics; recruits XMAP215/ch-TOG homologue to microtubule plus ends (Li et al., 2011; 2012)
CDK5RAP2	SRLP (Fong et al., 2009)	Not determined	Q96SN8	Centrosome maturation; mutated in autosomal recessive primary microcephaly (Megraw et al., 2011)

Kebab (*Drosophila*)	TKIP TCIP (Meireles et al., 2011)	Not determined	Q9VQ69	Kinetochore component; unknown function (Meireles et al., 2011)
Ipl1 (*S. cerevisiae*)	SKIP SKIP (Zimniak et al., 2012)	CDK1 (Zimniak et al., 2012)	P38991	Yeast Aurora kinase homologue
Eg5	xxIP (Jiang et al., 2012)	Not determined	P52732	Spindle bipolarity by sliding antiparallel microtubules (Ferenz et al., 2010)
AMER2/FAM123A	SKIP (Pfister et al., 2012; Siesser et al., 2012) TKIP (Pfister et al., 2012; Jiang et al., 2012)	Not determined	Q8N7J2	Regulates distribution of APC between MTs and plasma membrane (Grohmann et al., 2007; Jiang et al., 2012); recruits EB1 to plasma membrane and stabilizes MTs, regulates cell migration and gastrulation (Pfister et al., 2012); inhibits ARHGEF2, decrease actomyosin contractility (Siesser et al., 2012)
Shot (*Drosophila*)	SNLP SRIP SSIP (Alves-Silva et al., 2012)	Not determined	AIZ9J0	Homolog of ACF7 spectraplakin; microtubule organization/stabilization and axonal outgrowth (Alves-Silva et al., 2012)
GTSE1	SALP SGLP (Jiang et al., 2012; Scolz et al., 2012)	Ser435 Plk1 gives nuclear accumulation (Liu et al., 2010; Bublik et al., 2010) Hyperphosphorylated during mitosis, probably by cdk1 (Scolz et al., 2012)	Q9NYZ3	Modulates stabilizes p21 levels, resistance to paclitaxel (Bublik et al., 2010); negative regulator of p53 required for G2 checkpoint recovery (Liu et al., 2010); cell migration and focal adhesion turnover (Scolz et al., 2012)
+TIPs with probable SxIP motif				
Melanophilin (Grigoriev et al., 2008)	SNLP	Not determined	Q9BV36	Melanosome transport; mutated in Griscelli syndrome (Van Gele et al., 2009)
p140CAP (Jaworski et al., 2009)	TSIP	Not determined	Q9C0H9	Microtubule interactions in dendritic spines (Jaworski et al., 2009); Src kinase regulator
MTUS2/TIP150 (Jiang et al., 2009)	SRLP SNLP SRLP SLLP	Probable, mass spectrometry	Q5JR59	Microtubule dynamics; recruits MCAK to microtubule plus ends (Jiang et al., 2009)
FOP (Yan et al., 2006)	SKIP	Probable, mass spectrometry	Q95684	Centrosome microtubule anchoring (Yan et al., 2006); mutated in certain myeloid cancers (Popovici et al., 1999)
NAVIGATOR 1 (2, 3) (Martínez-López	SRIP SGIP SLIP	Not determined	Q8NEY1 (Q8IVL1, Q8IVL0)	Neurite outgrowth (van Haren et al., 2009)

et al., 2005; van Haren et al., 2009)				
DRhoGEF2 (*Drosophila*) (Rogers et al., 2004)	SKIP	Not determined	Q44381	Rho GTPase signaling (Rogers et al., 2004)
PSRC1/DDA3 (Hsieh et al., 2007)	SAIP	Not determined	Q6PGN9	Mitotic regulator of MCAK (Jang et al., 2008; Jiang et al., 2012)
Tastin, Trophinin-associated protein (Jiang et al., 2012)	SKIP	Phosphorylated in mitosis, motifs for CDK1, PLK1, MAPK, but sites not identified (Yang et al., 2008)	TROAP	Bipolar spindle assembly and centrosome integrity (Yang et al., 2008)
CEP104 (Jiang et al., 2012)	SKIP	Not determined	O60308	Centrosomal protein; regulates function of CP110-CEP97 complex during cilia outgrowth (Jiang et al., 2012)
SLAIN1 (Jiang et al., 2012)	SALP	Not determined	Q8ND83	Microtubule dynamics; recruits XMAP215/ch-TOG to microtubule plus ends (assumed because of homology to SLAIN2) (van der Vaart et al., 2011)
Syntabulin (Jiang et al., 2012)	SRIP	Not determined	Q9NX95	Transport of mitochondria and synaptic cargo in neurons (Ma et al., 2009)
TTBK1 TTBK2 (Jiang et al., 2012)	SRIP SKIP	Not determined	Q5TCY1 Q6IQ55	Tau kinase involved in phosphorylation and aggregation of Tau; associated with spinocerebellar ataxia type 11 (Sato et al., 2006; Houlden et al., 2007)
RasL11B (Jiang et al., 2012)	SLIP	Not determined	Q9BPW5	Mesoderm development in zebrafish (Pézeron et al., 2008)
Gas2L1 Gas2L2 (Jiang et al., 2012)	SRIP	Not determined	Q99501 Q8NHY3	Spectraplakin-like, promotes interaction with microtubules and actin (Goriounov et al., 2003)
FILIP1 (Jiang et al., 2012)	TRIP	Not determined	Q7Z7B0	Shape and migration of neurons (Sato and Nagano, 2005); regulates cortical cell migration from ventricular zone (Nagano et al., 2002); actin/microtubule crosslinking? (Jiang et al., 2012)
Cortactin binding protein 2 (Jiang et al., 2012)	SFLP	Not determined	Q8WZ74	Actin crosslinking through cortactin; role in neuronal function (Ohoka and Takai, 1998); actin/microtubule crosslinking? (Jiang et al., 2012)

Sickle tail (Jiang et al., 2012)	SKIP	Not determined	Q5T5P2	Development of intervertebral disc (Semba et al., 2006)
FAM190A (Jiang et al., 2012)	SRLP	Not determined	Q9C0I3	Expressed in cerebellum; SNPs associated with ADHD (Lantieri et al., 2010); Gene rearrangements associated with cancers (Scrimieri et al., 2011)
FAM190B (Jiang et al., 2012)	SKLP	Not determined	Q9H7U1	Homolog of FAM190A encoded by different gene
Nck-associated protein 5 (Jiang et al., 2012)	SKLP	Not determined	O14513	Homolog of Nck-associated protein 5-like encoded by different gene
Nck-associated protein 5-like (Jiang et al., 2012)	SKLP	Not determined	Q9HCH0	Homolog of Nck-associated protein 5 encoded by different gene
Inhibitor of ASPP protein (Jiang et al., 2012)	SRIP	Not determined	Q8WUF5	Inhibits p53-independent apoptosis by inhibiting transcription of pro-apoptotic genes (Cai et al., 2012); prevents senescence, required for epithelial stratification (Notari et al., 2011)
Cytospin-B (Jiang et al., 2012)	TGIP	Not determined	Q5M775	
Potential SxIP motif-containing EB-binding proteins; unconfirmed plus-end-tracking activity				
Dystonin (Jiang et al., 2012)	SKIP	Not determined	Q03001	Plakin that interacts with Map1B, Clip170, clathrin, regulates microtubule organization; loss of function associated with neurodegeneration (Bhanot et al., 2011; Ryan et al., 2012c; b); may link Golgi/ER/microtubules (Ryan et al., 2012a)
MAP2 (Jiang et al., 2012)	SSLP	Not determined	P11137	Stabilizes and bundles microtubules (mostly in dendrites) (Conde and Cáceres, 2009)
MACF1, isoform 4 (Jiang et al., 2012)	SKIP	Not determined	Q96PK2	Microtubule capture (assumed because isoform of MACF1) (Wu et al., 2008; Kodama et al., 2003; Zaoui et al., 2010)
APC2 (Jiang et al., 2012)	SRLP	Not determined	O95996	Microtubule capture (Barth et al., 2008; Kita et al., 2006; Etienne-Manneville et al., 2005; Reilein and Nelson, 2005); mutated in colon adenocarcinoma (Näthke, 2004)
Plexin-B3 (Laht et al., 2012)	SGIP	Not determined	Q9ULL4	Axon guidance

CHAPTER 1: Analysis of microtubule polymerization dynamics in live cells

I. Abstract

Intracellular microtubule polymerization dynamics are spatiotemporally controlled by numerous microtubule-associated proteins and other mechanisms, and this regulation is central to many cell processes. Here, we give an overview and practical guide on how to acquire and analyze time-lapse sequences of dynamic microtubules in live cells by either fluorescently labeling entire microtubules or by utilizing proteins that specifically associate only with growing microtubule ends, and summarize the strengths and weaknesses of different approaches. We give practical recommendations for imaging conditions, and we also discuss important limitations of such analysis that are dictated by the maximal achievable spatial and temporal sampling frequencies.

II. Introduction

Microtubules (MTs) are highly dynamic cytoskeletal polymers composed of α/β-tubulin dimers, and precise regulation of intracellular MT dynamics is important for many biological processes ranging from proper attachment and segregation of chromosomes during mitosis (Wittmann et al., 2001) to local stabilization of MTs toward the front of migrating cells (Wittmann and Waterman-Storer, 2001). MTs in cells and in vitro stochastically switch between phases of growth and shortening. This non-equilibrium polymerization behavior has been termed dynamic instability (Mitchison and Kirschner, 1984), and is driven by different structural states of the MT end, which are ultimately the result of

polymerization-coupled GTP hydrolysis in the MT lattice (Fig. 1.1) (Nogales and Wang, 2006). GTP-loaded tubulin dimers initially polymerize as a relatively flat open sheet at the plus end of a growing MT, which subsequently closes into a tube. Shortly after polymerization GTP is hydrolyzed to GDP within the MT lattice, which is thought to leave a short GTP-tubulin cap at the tip of the MT. This remaining GTP-cap stabilizes the growing end and supports further addition of GTP-loaded tubulin subunits, resulting in a stable growth phase. In contrast, loss of the GTP-cap results in catastrophic depolymerization, and by electron microscopy highly curved protofilaments seem to peel away from the depolymerizing MT end. These frayed MT ends reflect the high intrinsic curvature of GDP-loaded tubulin dimers, and do not support addition of new GTP-loaded tubulin subunits. Thus, this large structural difference between polymerizing and depolymerizing MT ends is sufficient to explain the high persistency and abrupt switching between growing and shortening that characterizes MT dynamic instability *in vitro* (Kueh and Mitchison, 2009).

Four parameters are generally measured to describe MT polymerization dynamics: the rates of growth (polymerization), shortening (depolymerization), and the transition frequencies between these two states. The transition from growth to shortening is referred to as ‘catastrophe’, and the transition from shortening to growth is referred to as ‘rescue’ (Fig. 1.1). These parameters can be determined quite easily in *in vitro* polymerization reactions with purified components because MT growth and shortening rates are relatively constant and transitions occur infrequently. In cells, however, MT polymerization dynamics are

spatiotemporally highly regulated by a large number of accessory proteins (van der Vaart et al., 2009) as well as physical interactions with other intracellular structures (Dogterom et al., 2005). As a result intracellular MT polymerization dynamics are significantly more complex and more difficult to quantify. *In vivo*, only MT plus ends exhibit dynamic instability. Free minus ends are either stabilized or depolymerize. Both growth and shortening rates are highly variable, and rates of individual MTs fluctuate significantly over relatively short time periods. In addition, MT polymerization dynamics in cells often include relatively long periods of pause during which MT ends do not appear to grow or shorten within the resolution limit of the light microscope. Furthermore, intracellular MTs are subject to pulling and pushing forces, which result in MT buckling, breakage and movements of MT ends that are not due to polymerization dynamics (Brangwynne et al., 2007; Waterman-Storer and Salmon, 1997; Wittmann et al., 2003).

III. Rationale

The objective of this chapter is to give an overview of different techniques to observe and analyze intracellular MT dynamics either by continuous MT labeling or by the expression of fluorescently labeled proteins that specifically recognize growing MT ends. We aim to emphasize the strength and limitations of each approach, and discuss the theoretical boundaries of intracellular MT dynamics analysis that are imposed by the spatial and temporal resolution limits of light microscopy. Finally, it is important to note that these fundamental

limitations similarly impact other intracellular tracking problems such as for example vesicular trafficking.

IV. Imaging and Analysis of Homogeneously Labeled MTs

A. Probes to Visualize Dynamic MTs

Conventional analysis of intracellular MT dynamics involves homogenous labeling of the entire MT network. This was initially achieved by microinjection of tubulin in which surface amino groups that are exposed in polymerized MTs are chemically labeled using N-hydroxysuccinimide-derivatized fluorescent dyes (Sammak and Borisy, 1988; Shelden and Wadsworth, 1993). Several protocols are published describing tubulin labeling and microinjection procedures (Hyman et al., 1991; Waterman-Storer, 2002; Wittmann et al., 2004b), and fluorescently labeled tubulin is also available commercially (e.g. from Cytoskeleton Inc.). Because microinjection is technically difficult, time-consuming, and only very few cells are available for analysis per experiment, this has mostly been replaced by the exogenous expression of tubulin tagged with fluorescent proteins (FPs). However, it should be noted that fluorescent dye-conjugated tubulin has some advantages over FP-tagged tubulin. Synthetic fluorescent dyes are generally brighter than FPs due to a higher extinction coefficient and better quantum yield, and because fluorescent dyes are small, dye-conjugated tubulin appears to be more efficiently incorporated into MTs. Together, this results in a higher MT to cytoplasm fluorescence ratio than FP-tagged tubulin. Finally, photobleaching of synthetic fluorophores is largely oxygen-dependent and can be efficiently

inhibited by oxygen depletion from the tissue culture medium (Waterman-Storer, 2002; Wittmann et al., 2003; 2004b).

Nevertheless, we and others have successfully used FP-tagged α- or β-tubulin to image and analyze intracellular MT polymerization dynamics (Rusan et al., 2001; Kumar et al., 2009). Although a growing toolbox of fluorescent proteins is now available, EGFP-tagged tubulin still appears to be the brightest and most photostable variant. For dual-color imaging we have also successfully used mCherry-tagged tubulin (Fig. 1.2 A). In addition, recent advances in elucidating the mechanisms of FP photobleaching indicate that FP photostability can be significantly improved by using riboflavin-free media (Bogdanov et al., 2009). Plasmid vectors suitable for transient transfections encoding different FP-tubulin fusion proteins are available from a variety of sources. We also routinely use adenovirus particles to transiently introduce FP-tagged tubulin and other cytoskeleton proteins into difficult to transfect cells (Kumar et al., 2009). However, because the correct folding of α/β tubulin dimers relies on a complex pathway involving several specific chaperones (Szymanski, 2002), care should be taken not to overwhelm the cells biosynthetic machinery by using too much virus. Too rapid expression of tagged tubulin results in poor incorporation into the MT cytoskeleton and excessive cytoplasmic background.

While stable mammalian cell lines expressing FP-tubulins have been made and are viable (Rusan et al., 2001), it has so far not been possible to generate whole animals expressing FP-tagged tubulin, indicating that the FP-tag does disrupt developmentally important tubulin functions. In an alternative

approach, mice expressing the MT-binding domain of a MT-associated protein, ensconsin, display homogeneously labeled MTs and are viable (Lechler and Fuchs, 2007). In addition, the MT signal can be increased by attaching up to five GFP moieties to ensconsin (Bulinski et al., 2001). Although GFP-ensconsin does not appear to modify intracellular MT dynamics, appropriate controls should be included when expressing exogenous MT-binding domains.

B. Preparation of Purified, Concentrated Adenovirus Particles

Although extensive adenovirus methods are published (Luo et al., 2007), we include a short reference protocol for the preparation of concentrated, purified adenovirus particles that we routinely use to prepare virus stock to introduce FP-tagged proteins in many different cell types. AdEasy-based viral genomes for the expression of EGFP-tubulin and EB1-EGFP from our lab are available through AddGene. Although these viruses are replication-deficient and new virus can only be produced in the packaging cell line, the experimentalist should be aware that these are infectious particles. At all times adhere to the required BSL-2 safety precautions, and sterilize and dispose infectious material according to the appropriate local regulations.

Required materials:

PacI-linearized and purified AdEasy viral plasmid containing the gene of interest

Transfection reagent (e.g. Lipofectamine 2000, Invitrogen Cat. No. 11668-027)

Adenovirus packaging cell line (AD-293, Stratagene)

Dulbecco's Modified Eagle Medium (DMEM, Invitrogen Cat. No. 10313)

supplemented with 10% Fetal Bovine Serum (FBS, Invitrogen Cat. No. 26140),

10 mM $MgCl_2$, 2 mM L-glutamine (Invitrogen Cat. No. 25030), 1x Penicillin/Streptomycin (Invitrogen Cat. No. 15140)

10 mM Tris-Cl pH 8.0

Low density CsCl buffer (ρ = 1.2 g/ml): Dissolve 35 g CsCl in a final volume of 100 ml 10 mM Tris-Cl pH 8.0

High density CsCl buffer (ρ = 1.45 g/ml): Dissolve 53 g CsCl in a final volume of 100 ml 10 mM Tris-Cl pH 8.0

ARCA buffer: 10 mM Tris-Cl, pH 8.0, 1 mM $MgCl_2$, 5% sucrose, 1% glycine, 0.05% Tween-80

Beckman ultracentrifuge and tubes: 38.5 ml (Beckman Cat. No. 41103909 for SW 28 Ti rotor) and 13.2 ml (Beckman Cat. No. 41103909 for SW 41 Ti rotor)

Econo-Pac 10DG Desalting Columns (Bio-Rad Laboratories Cat. No. 732-2010)

Adenovirus production and amplification:

1. Transfect a 6 cm dish of ~50% confluent AD-293 cells with the linearized AdEasy viral genome according to the manufacturer's instructions in antibiotic-free DMEM. We commonly use Lipofectamine 2000. AD-293 cells do not adhere well to tissue culture plastic and care should be taken not to disrupt the monolayer after transfection.
2. Grow transfected cells until the cytopathic effect (CPE) of virus production becomes visible. At this point, cells start to round up and lift off from the bottom of the plate. Depending on transfection efficiency, this will take approximately 1-2 weeks. Gently change medium when it turns too acidic without disrupting the cell monolayer. Transfection efficiency can also be

estimated by fluorescence microscopy because transfected cells will express the EGFP-tagged fusion protein.

3. Harvest all cells and media by gently tapping the plate and pipetting up and down into a 15-ml centrifuge tube. Centrifuge at 4°C, 1200 rpm, 5 minutes. Discard supernatant and resuspend pellet in 1 ml sterile 10 mM Tris-Cl pH 8.0.
4. Lyse cells by freezing for 5-10 min in a dry ice/EtOH bath, then thaw completely in a 37°C water bath. Repeat freeze/thaw cycle three times. Centrifuge to remove cell debris at 4000 rpm for 20 min, 4°C. The supernatant now contains first generation virus, which is used for all subsequent amplifications. Remove 200 µl for the next step and freeze the rest at -80°C.
5. For subsequent virus amplification, infect a 10 cm dish of ~80% confluent AD-293 cells: Remove medium from cells, and gently add 200 µl of the first generation virus diluted to 2 ml in DMEM. After 1 hour add additional 8 ml DMEM. Harvest cells as in Step 3 as soon as CPE becomes evident.
6. Repeat the infection and amplification cycle (Step 3-5) until CPE is visible within 48 hours post-infection. This should take a total of 2-3 cycles.

Large-scale adenovirus production:

7. Prepare twenty large plates (15 cm diameter or similar) of AD-293 cells. To ensure that cells are plated evenly, prepare cell suspension in a media bottle, mix, and plate 20 ml into each dish. At this point, DMEM with 5% FBS can be used to conserve serum.

8. Grow cells to ~90% confluency. Dilute 0.5 ml virus from Step 6 into 100 ml DMEM. Infect each plate with 5 ml of the diluted virus, mix gently, and return plates to incubator. After 48 hours the virus-induced CPE should be clearly visible.
9. Harvest the cells and medium by pipetting up and down or by using a cell scraper. Centrifuge at 1200 rpm, 10 min, 4°C. Discard supernatant and resuspend pellet in 13 ml of 10 mM Tris-CL pH 8.0.
10. Lyse cells with three freeze/thaw cycles (as in Step 4), and vortex for 30 seconds after each thaw. Centrifuge at 4000 rpm, 20 min, 4°C. Collect and keep supernatant on ice. It is very important for the subsequent purification step that all cell debris is removed.

Adenovirus purification by cesium chloride density gradient centrifugation:

11. Prepare two CsCl step gradients in 38.5-ml Beckman Ultraclear centrifuge tubes: First, slowly pour 10 mL of low density CsCl buffer into centrifuge tube. Then gently underlay 10 mL of high density CsCl by carefully inserting and pipetting to the bottom of the tube. Gently overlay virus supernatant on top of the step gradient. Fill tube completely with 10 mM Tris pH 8.0 to avoid collapse during ultracentrifugation. The second CsCl gradient tube is filled with 10 mM Tris pH 8.0 and used as balance. Make sure the tubes are well balanced, and that everything is kept sterile in a BSL-2 laminar flow tissue culture hood.
12. Centrifuge at 20,000 rpm in an SW 28 Ti swinging bucket rotor with slow acceleration and no brakes, for 2 hours at 4°C. Unload tubes in tissue culture

hood, and place tube in ring stand near eye level. A bluish band about halfway down the tube contains purified, concentrated virus. Just above there is usually a second, fainter band containing defective virus particles. During extraction of the virus band, care should be taken to avoid contamination from this upper band.

13. Remove some of the excess liquid from above the virus, being extremely careful not to disturb the band. Wipe the outside of the tube with ethanol to sterilize. Stick a piece of adhesive tape on the side of the tube where it is to be punctured to avoid leakage. Carefully pierce the tube with a hypodermic syringe with an 18-gauge needle slightly below the bluish virus band. Be sure to use as little force as possible in order not to pierce through both sides of the tube. Remember that the band contains highly concentrated virus particles. Thus, keep hands out of the way, and make sure to wear appropriate personal protective equipment. Tilt the needle upward into the virus band and draw approximately 3 ml of the virus slowly into the syringe. Leave the syringe with needle in the tube, and pipet liquid from the tube until it is below the needle. Now remove the syringe and expel the virus into a sterile 15-ml polypropylene tube.
14. Dilute virus to 4 ml with 10 mM Tris pH 8.0. This is essential to reduce the density to below 1.2 g/ml. Prepare a smaller step gradient with 4 ml of each CsCl buffer as in Step 11, but in smaller 13.2-ml tubes. Overlay with the diluted virus and fill tube with 10 mM Tris pH 8.0. Centrifuge at 20,000 rpm at 4°C in an SW 41 Ti rotor, and isolate virus band as in Step 13.

15. Desalt virus on a 10DG column: Equilibrate column with 30 ml ARCA buffer. Load 3 ml of the virus, and collect 0.5 ml fractions on ice. Concentrated virus should start eluting in the third fraction. Concentrated, opaque fractions can be pooled, aliquoted, and stored at –80°C. This procedure yields highly infectious adenovirus particles, and we generally use less than 1 µl adenovirus stock to infect cells for microscopy. Virus titer can be estimated by measuring optical density at 260 nm in PBS containing 1% SDS (1OD ~ 1.1 x 10^{12} virus particles per ml).

C. Imaging of Intracellular MT Dynamics

Analysis of intracellular MT dynamics relies on time-lapse imaging of fluorescently labeled proteins. Different modalities of fluorescence microscopy including widefield epifluorescence, confocal and total internal reflection (TIRF) microscopy can and have been used to image MT dynamics although each has its limitations. In widefield images, out-of-focus blur severely limits the ability to observe MTs in thicker cell regions and only works reasonably well in flat, peripheral cell areas (Wittmann et al., 2003). Although TIRF microscopy produces superior contrast, it only allows imaging of MTs in very close proximity of the bottom cell membrane (Krylyshkina et al., 2003) *[Akhmanova chapter this book]*. We mostly use spinning disk confocal microscopy as a versatile method to image dynamic MTs because it combines thin optical sectioning, which largely eliminates out-of-focus blur, with better sample penetration compared with TIRF. Independent of the exact microscopy modality used, it is important to acquire images at the best possible spatial resolution. At the emission wavelength of

EGFP of about 510 nm, the resolution limit of a fluorescence light microscope with a 1.4 NA objective lens under optimal conditions is ~250 nm. Because tubulin dimers are about 8 nm long and are thus small compared to this approximate diameter of the microscope point spread function, any discernible MT length change represents the addition or removal of several hundred tubulin subunits. In order to be able to image changes as close to the molecular scale as possible, it is important that the digital camera used to acquire images is of sufficiently high resolution to oversample the optical resolution to fulfill the Nyquist sampling criterion (Wittmann et al., 2004b). This means that the effective pixel size of the captured image should be ~2-3 fold smaller than the resolution limit. On a microscope system with no intermediate magnification this can be achieved with a 60x or 100x objective and a high-resolution scientific grade charge-coupled device (CCD) camera. Such cameras from different manufacturers typically use a Sony Interline CCD sensor with 6.45 x 6.45 µm pixels resulting in an effective pixel size of ~107 nm in object space at 60x magnification. Electron multiplying CCD (EMCCD) cameras have much larger pixels up to 16 x 16 µm (effective pixel size of 266 nm at 60x), which is insufficient for optimal sampling of the optical resolution without additional magnification[1]. For similar reasons, the use of two-photon microscopy (which halves the optical resolution) or binning (which halves the detector resolution) is not optimal for MT dynamics imaging. Finally, it is important to remember that optimized imaging conditions are only achieved when cells are grown in two

[1] Up-to-date information and excellent tutorials about many aspects of light microscopy can also be found online, for example at www.microscopyu.com.

dimensions preferably on #1.5 cover glasses. We typically use glass-bottom tissue culture dishes (e.g. from MatTek Corporation), or custom-made sealed cover glass chambers (Wittmann et al., 2004b). The imaging system should also be environmentally controlled because, as any biochemical reaction, the rate of microtubule polymerization is temperature-dependent. Imaging at high resolution becomes significantly more challenging for more physiological, three-dimensional samples.

Our lab uses a Yokogawa CSU-10 spinning disk confocal head with 200 mW 488 nm and 561 nm solid-state lasers in an LMM5 laser launch (Spectral Applied Research). In combination with 60x or 100x 1.49 NA TIRF objective lenses (Nikon) and a high-resolution CoolSNAP cooled CCD camera (Photometrics), we can achieve the highest spatial resolution possible with conventional light microscopy. Image acquisition is controlled by Nikon NIS-Elements software. With this setup we have been able to achieve frame rates of up to 4 frames per second at below 200 ms exposure times, although as outlined below manual tracking of continuously labeled MTs becomes highly error-prone at time intervals shorter than 2 to 5 seconds between frames. Thus, slightly longer exposure times (~500 ms) combined with lower illumination intensities are usually acceptable.

Because MT polymerization dynamics analysis requires long time-lapse sequences, it is crucial to minimize sample exposure and photodamage. There are relatively simple aspects in the design of an imaging system that are often overlooked, but significantly improve the performance of fluorescent live-cell

microscopy. Excitation shutters should be hardware-controlled and triggered directly from the camera so that shutters are only open when an image is actually acquired. In contrast, software shutter control typically adds several hundred milliseconds of sample exposure before and after image acquisition, which results in significantly faster photobleaching especially at low exposure times. In addition, it is important to use optimized emission filter sets. For example, for single-channel EGFP imaging, we use a long-pass dichroic mirror and emission filter (Semrock) with edge wavelengths of ~500 nm. This allows maximum detection over most of the EGFP emission spectrum, and results in a greater than 50% signal increase at the same exposure settings compared to high quality multi-band pass filter sets.

D. Semi-manual Tracking and Analysis of Dynamic MTs

Accurate, automatic detection of the ends of continuously labeled MTs is a highly challenging computational problem. Although substantial progress is being made to develop computer vision algorithms to detect and track movement of continuously labeled MTs (Altinok et al., 2007; Hadjidemetriou et al., 2008) *[Rose chapter this book]*, a robust solution is not currently available. However, computer-assisted hand-tracking in which the user manually selects MT ends in a time-lapse sequence can be done with a variety of available software packages (Fig. 1.2 B). We now mostly use the tracking function in NIS-Elements (Nikon), but similar functions are available in other image analysis software packages including MetaMorph (Molecular Dynamics) and ImageJ.

The output of such semi-manual tracking is a list of positions or displacements of the MT end as a function of time. It is important to remember that this list does not include information on whether an end displacement represents MT growth or shortening, and after the initial tracking we go through the list a second time to designate shortening events by negative numbers. MT end displacement can then be plotted (Fig. 1.2 C), and analyzed in different ways to calculate growth and shortening rates, transition frequencies, and the percent time MTs spend in growth, shortening, or pause phases. Because of the large variations of intracellular MT growth rates, we find it difficult to a priori designate phases of constant growth or shortening velocities in such life-history plots (Walker et al., 1988). Instead, we calculate instantaneous growth and shortening rates on a frame-to-frame basis. Because of the positional uncertainty introduced by image formation in the microscope and the error introduced by hand-clicking on the image, we then set a lower threshold of MT end displacement in the range of the optical resolution (Kumar et al., 2009; Wittmann et al., 2003). Growth or shortening events below this threshold are classified as a pause.

A drawback of this method is that the positional error becomes dominant if sequences are analyzed that are acquired at very short time intervals, which results in completely different measurements of microtubule dynamics parameters depending on the frame rate. In the example in Fig. 1.2, images were acquired at 1.6 frames per second (625 ms between images). Assuming a localization error of 1 pixel, which is about half the diameter of the point spread function and probably an overestimation of hand-clicking accuracy, any growth or

shortening event below 10 μm/min is classified as a pause, overestimating the time MTs spend in a pause state (Fig. 1.3 A). This also truncates the lower end of the true growth and shortening rate populations, and results in a gross overestimation of the average rates (Fig. 1.3 B). At lower frame rates, this threshold becomes much more reasonable, and the measured growth and shortening rates better approach true intracellular rates. Nevertheless, because of this positional detection limit, slow MT polymerization events cannot be distinguished from bona fide pauses during which no polymerization or depolymerization occurs. Thus, the threshold below which an event is considered a pause is relatively arbitrary and largely depends on the imaging conditions.

Transition frequencies are defined as follows: The catastrophe frequency is the number of transitions from growth to shortening divided by the time MTs spend growing. This is mathematically identical to the inverse of the average time MTs spend in an uninterrupted growth phase. Because true pauses cannot be clearly defined, we allow growth phases preceding a catastrophe to be interrupted by apparent pauses. Importantly, because events that occur between two acquired images are not observable, the imaging frame rate also defines an upper boundary for transition frequencies, and faster frame rates will result in the measurement of higher transition frequencies (Fig. 1.3 C). For example, at a slower time resolution of 0.2 frames per second (i.e. an image acquired every 5 seconds), the shortest observable growth interval is 5 seconds. Thus, the maximal observable catastrophe frequency is identical to the frame rate. Similarly, pauses shorter than 5 seconds cannot be observed contributing to the

apparent increase in the time MTs spend in growth at lower frame rates (Fig. 1.3 A). Likewise, the rescue frequency is defined as the number of transitions from shortening to growth divided by the time MTs spend shortening, and the same limitations as for catastrophe frequencies apply.

In conclusion, because of the inevitable MT end localization error semi-manual analysis of MT dynamics is best performed on time-lapse sequences with images acquired every 2-5 seconds at high spatial resolution, which represents the range of frame rates used most frequently in published analysis of MT dynamics. These conditions are a good compromise to minimize the error introduced by positional inaccuracy, while still maintaining a relatively high time resolution for the quantification of transition frequencies. However, one should be aware of the inherent limitations of this analysis, and it is imperative to only compare quantifications obtained from time-lapse sequences acquired at identical magnification and frame rate (Shelden and Wadsworth, 1993). In addition, because semi-manual tracking is extremely time-consuming, the number of MTs analyzed is often low and it is challenging to obtain statistically sufficiently large data sets. Nevertheless, growth and shortening rates can be determined with good accuracy. Relatively large standard deviations on rate measurements reflect the variability of intracellular MT polymerization dynamics rather than measurement errors. In contrast, the number of observed catastrophes or rescues tends to be low, and care should be taken in interpreting differences in transition frequencies in different conditions. For any meaningful

quantification, we would recommend to track 5-10 MTs per cell in at least five cells, and an observation time of around 5-10 minutes per MT.

V. MT Fluorescent Speckle Microscopy

In time-lapse sequences of continuously labeled MTs it is not possible to distinguish between MT polymerization dynamics and MT translocation. However, fluorescent speckle microscopy (FSM) can be used to test whether MT end displacements are due to movements of the entire MT. The principle underlying MT FSM is simple and relies on the stochastic incorporation of fluorescently labeled tubulin subunits along the MT. At low intracellular ratios of fluorescently labeled to unlabeled tubulin, convolution with the microscope's point spread function results in intensity variations (fluorescent speckles) along the MT (Waterman-Storer and Salmon, 1998; Wittmann et al., 2004b). Although best speckle contrast is achieved at labeling ratios of below 1% labeled tubulin, intensity variations along MTs can be observed at much higher labeling ratios and are often evident in cells expressing low to moderate levels of FP-tagged tubulin. Simple image processing such as low pass filtering to remove camera pixel noise, and sharpening with an unsharp mask filter can be used to greatly increase speckle contrast (Wittmann et al., 2004b). Because MTs only exchange subunits at the ends, the pattern of intensity variations along the MT is stable and can be used as a direct read-out for MT translocation (Fig. 1.4).

VI. Imaging and Analysis of Growing MT Ends

A. Probes to Visualize Growing MT Ends

Analysis of MT dynamics in time-lapse sequences of continuously labeled MTs suffers from a fundamental limitation. Even in cell areas in which MTs are only moderately dense, it quickly becomes impossible to clearly observe growing ends. Thus, conventional analysis of intracellular MT dynamics is subjective and regionally biased because it is limited to a small subpopulation of MTs near the cell periphery, where MT ends can be observed clearly over sufficient periods of time (Wittmann et al., 2003).

An alternative strategy to visualize intracellular MT dynamics utilizes fluorescently tagged proteins that specifically recognize growing MT plus ends (Akhmanova and Steinmetz, 2008; Salaycik et al., 2005). Because these proteins, commonly referred to as +TIPs, bind only weakly along MTs, growing MT ends are clearly visible in more central cell areas in which MTs are too dense to visualize MT ends directly (compare images of the same cell in Fig. 1.2 A and Fig. 1.5 A).

End Binding Proteins, EBs, are the +TIP prototype and are thought to directly recognize the structurally distinct GTP-tubulin cap at growing MT ends (Fig. 1.1). EBs are small dimeric proteins containing an N-terminal MT-binding domain, and a C-terminal cargo-binding domain, and most if not all other +TIPs associate with growing MT ends through interactions with this C-terminal domain (Akhmanova and Steinmetz, 2008; Bieling et al., 2008; Honnappa et al., 2009). Because N-terminal FP-tags interfere with EB localization to MT ends (Skube et al., 2010), C-terminally tagged EB1- or EB3-EGFP constructs have been predominantly used to highlight growing MT ends in cells. The exponential decay

of available binding sites results in the characteristic comet-like fluorescence profiles of EGFP-tagged EBs on MT ends. In addition, rapid binding kinetics of EBs (Dragestein et al., 2008) causes rapid loss of EB fluorescence from non-polymerizing MT ends, and rapid appearance of EB comets when MTs start growing. However, because EBs are central adaptor proteins that recruit many other +TIPs to growing MT ends, concerns have grown that EB-EGFP constructs may disrupt endogenous localization of other +TIPs and thus alter MT polymerization dynamics and cell behavior (Skube et al., 2010). Nevertheless, low level EB-EGFP expression appears relatively benign and we and others have made multiple stable EB1-EGFP-expressing cell lines that appear to behave normally. Similar to FP-tagged tubulin we also use adenovirus to introduce EB1-EGFP into difficult to transfect cells.

One way to increase EB-EGFP signal at growing MT ends without increasing the overall expression level and background along MTs is to add multiple EGFP tags. Alternatively, EB-binding domains of other +TIPs such as CLIP-170 or CLASPs can be used to visualize intracellular MT polymerization dynamics (Komarova et al., 2009; Kumar et al., 2009; Wittmann and Waterman-Storer, 2005). Thus, different types of +TIPs can be used to validate experimental results and help eliminate potential +TIP overexpression-induced artifacts. Most importantly, a minimal EB-binding motif has recently been identified that is sufficient for plus end localization (Honnappa et al., 2009). It should therefore be possible to engineer artificial +TIPs that only minimally interfere with intracellular

MT dynamics. The same considerations about high-resolution fluorescent live cell imaging as outlined in section II.C also apply for FP-tagged +TIPs.

B. Computational Tracking and Analysis of +TIP Dynamics

Because +TIPs specifically associate with growing MT ends, it is straightforward to determine growth rates from time-lapse sequences of FP-tagged +TIPs. For example, computer-assisted hand tracking as described above for continuously labeled MTs can be used. Alternatively, maximum intensity projections of +TIP comet time-lapse sequences can be used to calculate growth rates directly from the comet-to-comet distance (Wittmann and Waterman-Storer, 2005).

However, one immediately obvious challenge in using +TIPs to analyze MT polymerization dynamics is that MT ends are not visible during pause and shortening phases. Thus, only growth rates can be measured directly. To extract additional parameters of MT dynamic instability, a computational framework has recently been developed that breaks down the analysis of +TIP time-lapse sequences into three steps (Matov et al., 2010): First, a band-pass filter is used to detect objects of the size scale of +TIP comets. Second, these objects are tracked by single particle tracking. Such automated tracking is highly accurate (Fig. 1.5 C and D), and yields statistically large populations of MT growth rates (Jaqaman et al., 2008). For example, over 400 individual EB1-EGFP growth tracks were detected in the one-minute sequence shown in Fig. 1.5. To eliminate tracks that result from detection errors, we generally only consider tracks for further analysis that have a lifetime of at least 4 frames. In order to achieve good

EB1-EGFP comet correspondence between subsequent frames and minimize the number of tracking errors, computational tracking approaches generally require higher frame rates (~1-2 frames per second) as compared to manual analysis. We have successfully used this approach to demonstrate spatial gradients of MT polymerization dynamics in migrating cells (Kumar et al., 2009).

Finally, +TIP growth tracks are linked by geometrical cluster analysis. This analysis relies on a priori knowledge of the physical characteristics and behavior of MTs. Intracellular MTs are laterally relatively immobile, and are stiff and bend very little over the short time window used to record +TIP dynamics. As a result, MT shortening, rescues and pauses predominantly occur in very close proximity to the path defined earlier by the growing end of the same MT (Fig. 1.2 B). A global combinatorial optimization algorithm that utilizes a cost function based on geometrical and temporal constraints between the beginning and the end of +TIP growth tracks can be used to determine those tracks that most likely belong to the same MT (Matov et al., 2010). Because of the statistical nature of this algorithm, it will make errors and clearly has some fundamental limitations. For example, terminal shortening phases are hidden because a shortening phase has to be followed by a growth phase in order to be detected by the clustering algorithm. In addition, to minimize the number of clustering errors, the constraints for linking individual growth tracks have to be kept quite stringent only allowing the search for a rescue event ~10-20 frames in the future. Thus, long shortening phases such as the one in MT #2 are frequently missed by the algorithm (compare Fig. 1.2 B and Fig. 1.5 B). Finally, the tracking algorithm misses growth

phases if they are too slow and too short to produce a sufficient +TIP signal such as the short growth phases at the end of MT #1.

Thus, data derived by geometrical clustering of +TIP growth tracks cannot be directly compared to conventionally determined MT dynamics parameters. Nevertheless, because statistically large MT numbers can be analyzed relatively quickly using this approach, we expect this algorithm to be extremely useful to compare different experimental conditions on a relative basis. plusTipTracker, a Matlab-based open source software package enabling +TIP comet detection, growth track reconstruction, visualization, sub-cellular regional analysis, and MT subpopulation analysis will soon be available from http://lccb.hms.harvard.edu (Applegate et al., 2011).

VII. Conclusion

Because spatiotemporal regulation of intracellular MT dynamics is important in many aspects of cell biology, the interest in generally applicable methods for quantitative analysis of MT dynamics is high. In this chapter, we give a brief overview and practical guide on how to acquire and analyze time-lapse sequences of dynamic MTs in cells by either fluorescently labeling entire MTs or by utilizing proteins that specifically associate only with growing MT ends. Because of the optical resolution limit it is not possible to measure the 'true' position of a MT end with conventional light microscopy. Therefore, quantification of intracellular MT polymerization dynamics depends to a very large extent on the imaging conditions, sampling frequencies and analysis methods used, which define theoretical limits of rates and transition frequencies that can be

determined from a particular data set. Thus, absolute MT dynamics parameters are only of very limited value, and measurements should only be used to compare different experimental conditions for which time-lapse sequences were recorded identically. It will be exciting to see if and how modern super-resolution techniques will be used to more precisely observe MT polymerization dynamics in cells. In addition, because of the structural and biochemical processes, and nanoscale fluctuations of polymerization dynamics that occur on MT plus ends (Schek et al., 2007; Kerssemakers et al., 2006), the conventional definition of MT growth and shortening rates and transition frequencies is most likely not sufficient to accurately capture the complexity of MT polymerization dynamics. This problem is further aggravated in cells, where MT polymerization dynamics are even more variable as a result of regulation by associated proteins. Novel methods to analyze MT dynamics are needed, and we provide an outlook on one such method that utilizes computational clustering of MT growth tracks defined by the association of fluorescently labeled +TIPs with growing MT ends. It will be interesting to see how such new computational approaches will impact our future understanding of intracellular MT function and dynamics.

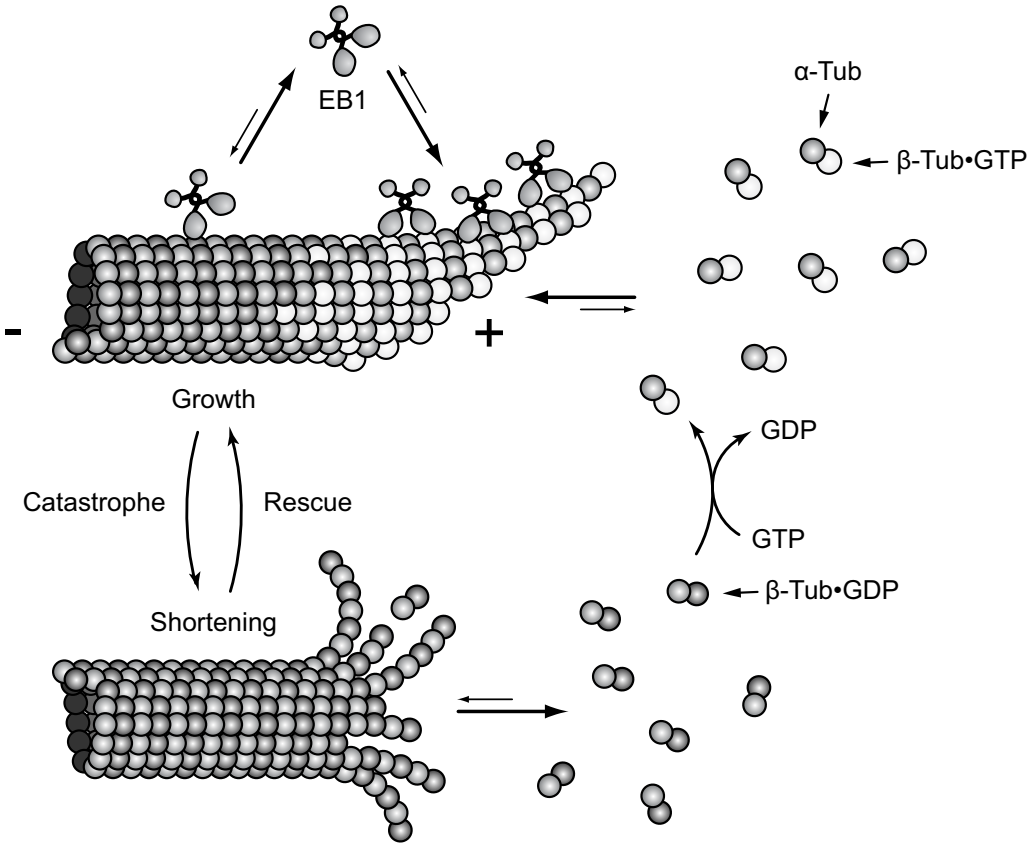

Figure 1.1. Diagram of different phases of MT polymerization dynamics. MT growth is thought to be accompanied by a protective cap of GTP-loaded tubulin at growing MT ends. The structurally distinct GTP-tubulin cap also provides a platform for the binding of MT plus-end-tracking proteins, +TIPs (Akhmanova and Steinmetz, 2008) that can be used as indirect reporters of intracellular MT polymerization dynamics.

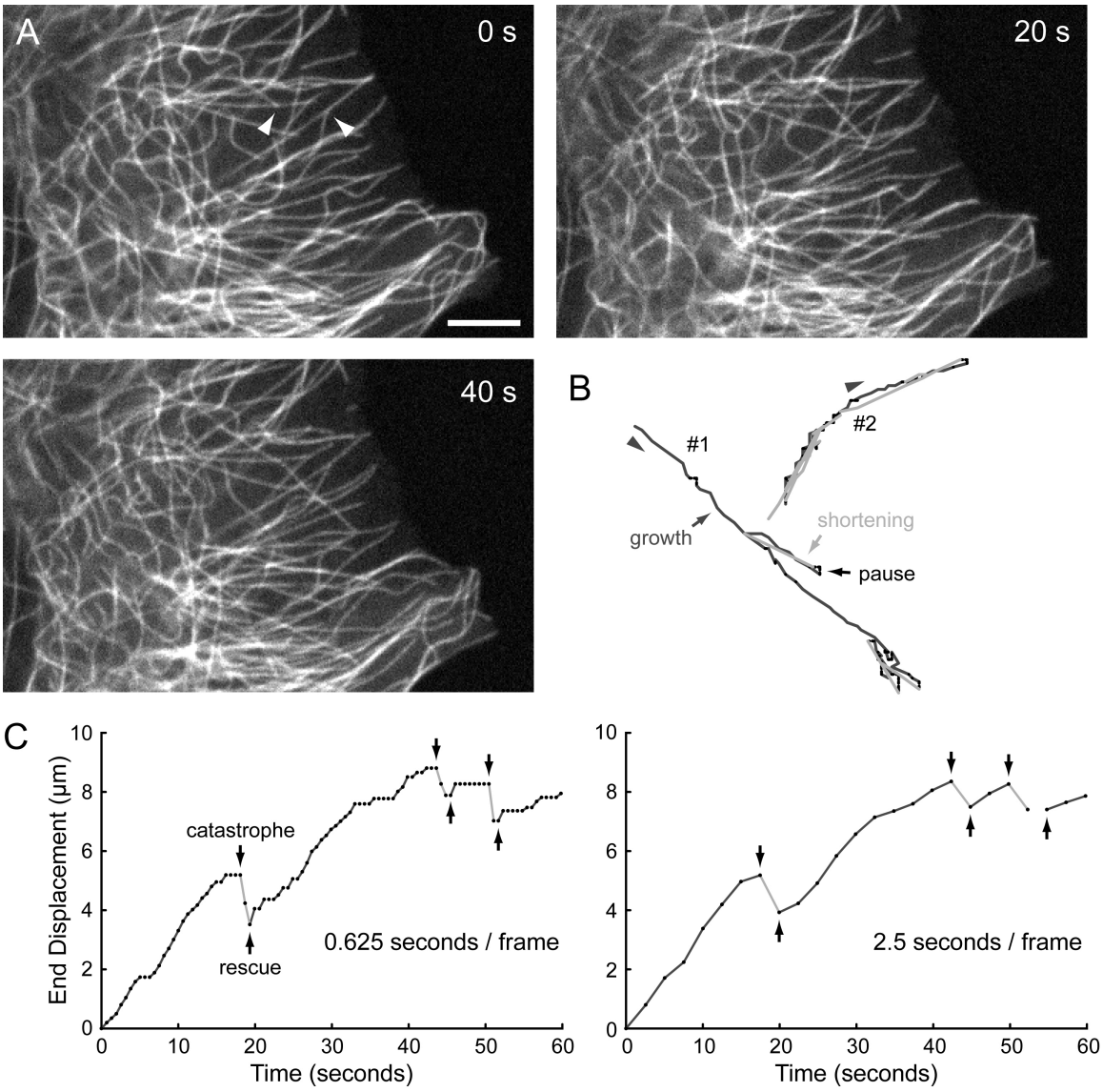

Figure 1.2. Semi-manual analysis of continuously labeled MTs. (A) Images from a time-lapse sequence of mCherry-tagged tubulin. Images were acquired every 625 milliseconds (1.6 frames per second) for 1 minute. Scale bar, 5 µm. (B) Traces of the two MT ends indicated by arrowheads in A obtained by computer-assisted hand-clicking. (C) Life-history plots of MT #1 at the original time resolution, and at a simulated frame rate of 0.4 frames per second by only analyzing every 4th image. This demonstrates the averaging of the high variability of intracellular MT polymerization dynamics at slower frame rates.

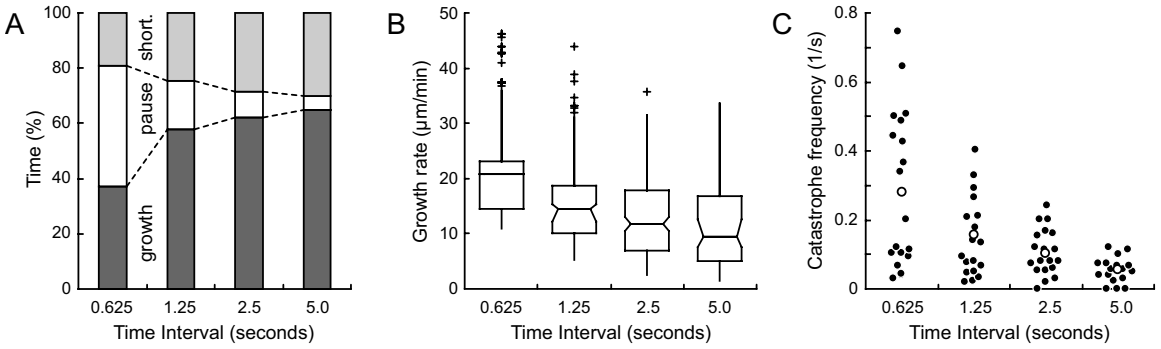

Figure 1.3. Dependence of MT polymerization dynamics quantification on temporal resolution. (A) Time MTs spend in different phases, (B) Growth rates, and (C) Catastrophe frequencies as a function of frame rate. 19 MTs from the sequence in Fig. 1.2 were analyzed, and simulated frame rates were obtained by temporal sub-sampling.

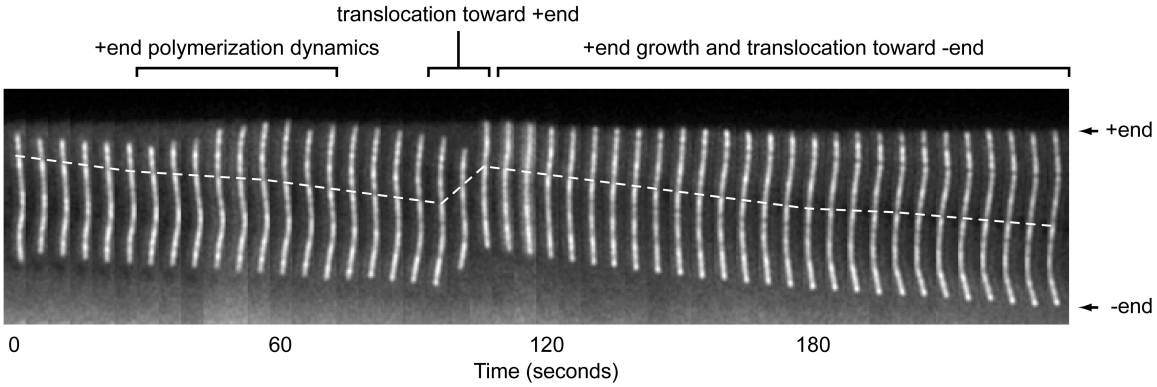

Figure 1.4. MT fluorescent speckle microscopy. Montage of a time-lapse sequence of a MT fragment in a cell expressing constitutively active Rac1 (Wittmann et al., 2003) injected with X-rhodamine-labeled tubulin. One bright speckle is followed over time and highlighted by the dashed line. The speckle pattern reveals different types of MT movement that would be misinterpreted as polymerization dynamics if the MT were homogenously labeled. For example, in the second half of the sequence, the MT plus end remains in close contact with the cell edge and is apparently stationary. However, the appearance of new speckles is evidence for polymerization at the plus end and translocation of the speckle pattern demonstrates movement of the MT polymer.

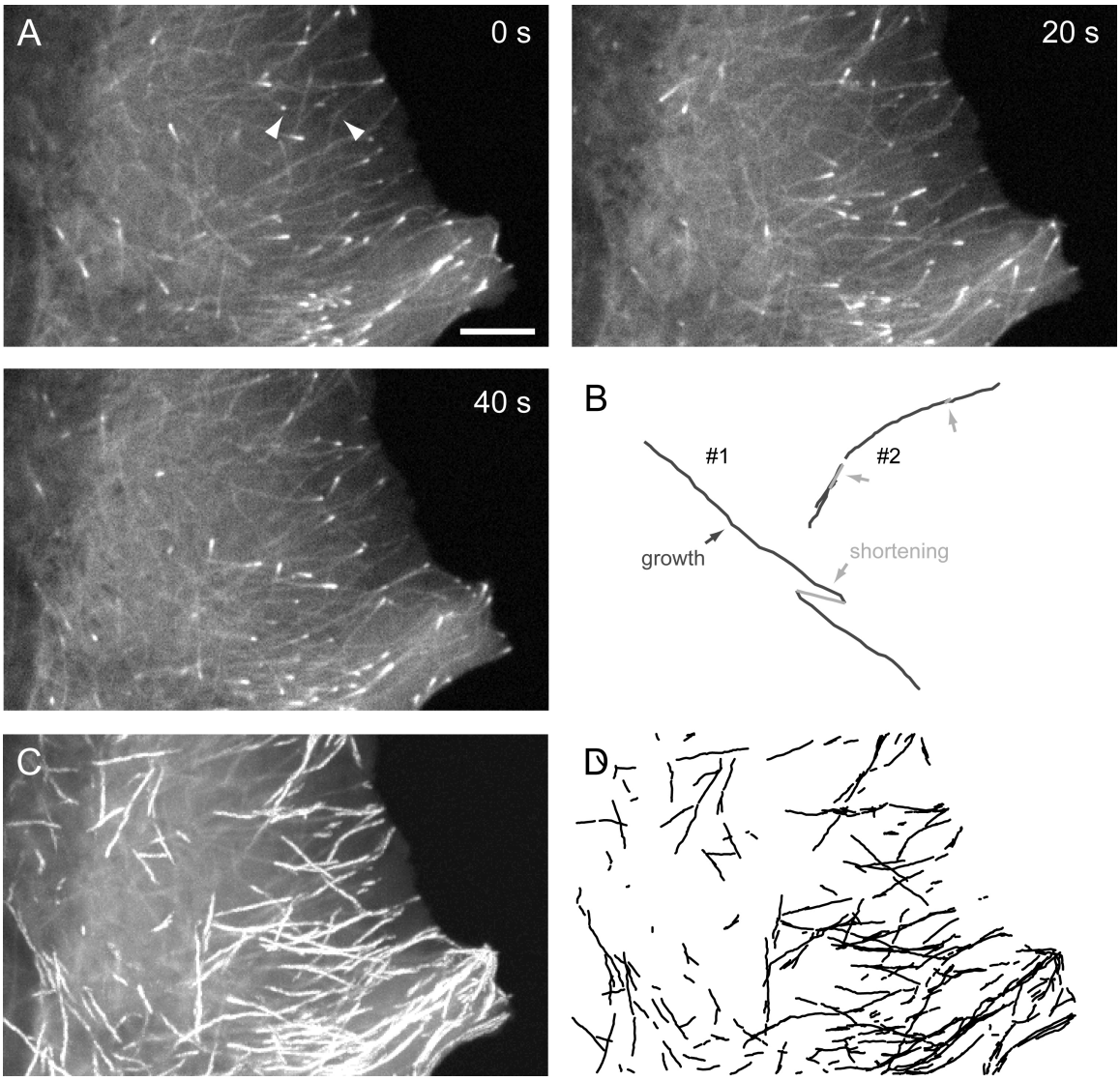

Figure 1.5. +TIPs as reporters of MT polymerization dynamics. (A) Images of EGFP-tagged EB1 from the same dual-wavelengths time-lapse sequence as in Fig. 1.2. Scale bar, 5 um. (B) Computer-generated growth tracks of the same two MTs as in Fig. 1.2 with shortening events (light grey arrows) inferred by geometrical cluster analysis. (C) Maximum intensity projection of the entire image sequence directly showing EB1-EGFP growth tracks. (D) Computer-generated growth tracks with a minimum lifetime of four frames demonstrating high tracking fidelity.

CHAPTER 2: CLASP function in epithelial cell migration

During my rotation and at the start of my thesis work, the lab was investigating the regulation and function of the microtubule +TIP CLASP in migrating epithelial cells. In many cell types, including epithelial cells, a large population of microtubules is oriented toward the leading edge and is required for directional migration. CLASP was proposed to help organize microtubules and mediate microtubule attachment to the cell cortex in the lamella and near focal adhesions (Drabek et al., 2006; Lansbergen et al., 2006; Wu et al., 2008). But how lamella microtubules, specifically, are stabilized by CLASP was not understood. CLASP is uniquely spatiotemporally regulated so that it decorates the growing plus ends of microtubules in the cell body and binds along the microtubule lattice in the lamella of the migrating epithelial cell (Wittmann and Waterman-Storer, 2005). Dr. Praveen Kumar, a postdoc in the lab, investigated the role of the kinase glycogen synthase kinase 3β (GSK3β) in regulating CLASP microtubule-binding activity and identified multiple residues on CLASP that were directly phosphorylated by GSK3β. This regulation of CLASP localization was required for stabilization of peripheral microtubules and directed migration. Furthermore, it was found that CLASP clustered around focal adhesions and that dynamic turnover of CLASP and focal adhesion structures is spatiotemporally coordinated in migrating epithelial cells (Kumar et al., 2009).

During my rotation, I investigated the role of CLASP in microtubule organization and cell polarity in migrating human keratinocytes (HaCaTs). To first describe the effects of CLASP on microtubule organization, CLASP1 and 2 were

depleted by siRNA. HaCaT monolayers were wounded once the monolayer was confluent, to induce cells to polarize and migrate. Monolayers fixed and stained for microtubules and CLASP showed that in control cells, a dense array of microtubules were oriented toward the leading edge (Fig. 2.1 A, top). CLASP decorated the microtubule lattice in the lamella of the polarized cell. When CLASP was depleted, microtubules became disorganized, more curled and less dense. Staining for acetylated tubulin showed a trend of a decreased amount of stable microtubules in the CLASP-depleted cells although this was difficult to quantify (Fig. 2.1 A, bottom). Next I tested if CLASP depletion affects EB1 localization to microtubule plus ends. Staining for EB1 in control and CLASP-depleted cells showed that EB1 plus-end-tracking activity is independent of CLASP (Fig. 2.1 B). This suggests that that microtubule stabilization phenotype is CLASP specific and not due to a more general disruption of +TIPs. These data were repeated by Dr. Kumar and included in supplementary Figure S2 of the article published in Journal of Cell Biology (Kumar et al., 2009).

In epithelial cells, the centrosome (microtubule organizing center) typically orients toward the direction of migration with microtubules radiating from the centrosome toward the leading edge (Gundersen et al., 2004; Palazzo et al., 2001a). I tested whether the CLASP siRNA-mediated disruption of microtubule organization could be a result of a defect in centrosome reorientation. Control HaCaT monolayers were wounded then fixed at increasing time intervals to determine the amount of time required for centrosome orientation. The angle of the centrosome from the direction of migration was measured and I found that

after 8 hours nearly all centrosomes were oriented in the front half of the cell (>90 degree angle) (Fig. 2.2 A). Next I compared centrosome localization in control siRNA and CLASP-depleted cells. Cells were fixed 14 hours after wounding for more complete reorientation in the control condition and were measured for centrosome orientation. Centrosome reorientation did not appear to be affected by CLASP depletion (Fig. 2.2 B). This suggests that the decrease in microtubule density toward the leading edge in CLASP-depleted cells is due to a defect in stabilization near the front of the cell, rather than a lack of nucleation or reorganization of growth toward the leading edge.

I also started to investigate the relationship between microtubules and focal adhesions. Co-staining of microtubules and paxillin in migrating HACAT cells showed a close association, but not colocalization, near the leading edge. Furthermore, co-staining of CLASP and paxillin showed that CLASP surrounded focal adhesions and appeared to also be associated with microtubules there. I attempted to test whether CLASP depletion affects focal adhesions but siRNA depletion was inefficient and focal adhesions were too variable to determine an effect. This project was taken up later by a postdoc, Dr. Samantha Stehbens, and is currently in review at Nature Cell Biology.

Finally, after joining the lab, I tested how phosphorylation affects CLASP interactions with EB1. Previous work had shown that CLASP binds EB1 through the same domain required for plus-end-tracking (Mimori-Kiyosue et al., 2005). To test if phosphorylation affects this interaction I performed an immunoprecipitation of the CLASP microtubule-binding domain (aa 512-650) and two mutant

constructs and tested the interaction with EB1. CLASP2 (512-650) and a non-phosphorylatable mutant (9xS/A) efficiently immunoprecipitated EB1, while a GFP control or pseudophosphorylated construct did not. This showed that the CLASP-EB1 interaction is regulated by phosphorylation in the same way as the CLASP-microtubule interaction. This result, reprinted here in Figure 4, was published in the Journal of Cell Biology article for which I was a co-author (Kumar et al., 2009).

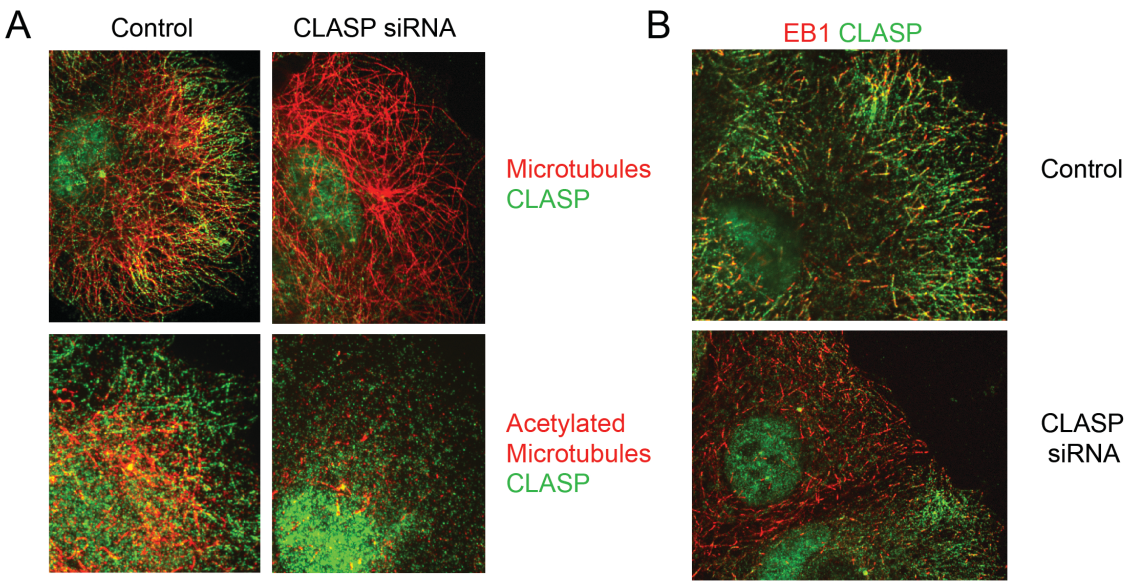

Figure 2.1. CLASP depletion by RNAi in HaCaT cells. HaCaT cell monolayer was transfected with a mixture of SMARTpool siRNA oligonucleotides directed against human CLASP1 and CLASP2 (Thermo Fisher Scientific). Cells were grown until confluent then wounded. Cells were fixed in 20C methanol about 72 hrs after transfection and stained for endogenous CLASP and microtubules (A, top), CLASP and acetylated microtubules (A, bottom) or CLASP and EB1 (B).

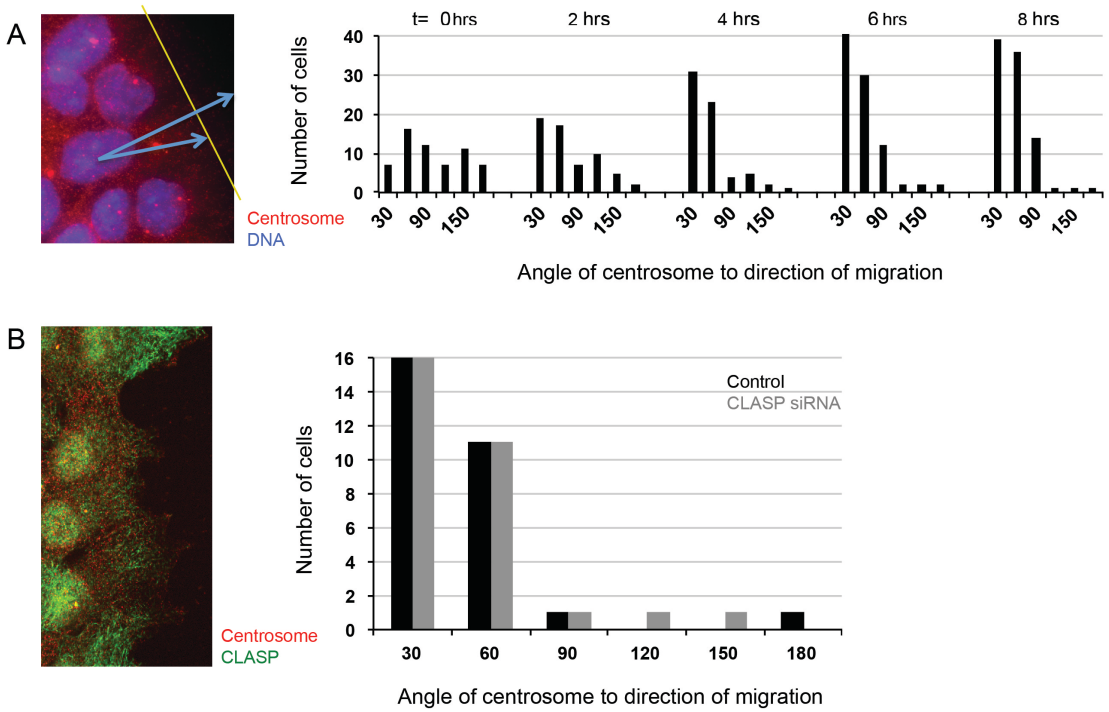

Figure 2.2. Centrosome orientation in wounded HaCaT cell monolayer. (A) HaCaT cell monolayer was wounded and then fixed with -20C methanol at increasing time intervals. Cells were stained for nuclei and centrin to locate centrosome. To measure centrosome orientation, a line was drawn from the center of the nucleus to the leading edge in the direction of migration (perpendicular to the leading edge, yellow line). A second line was drawn from the center of the nucleus through the centrosome and the angle formed by these two lines was measured. (B) HaCaT monolayer was transfected with CLASP siRNA oligos as described in Fig. 2.1. Cells were fixed 14hrs after wounding and stained for CLASP to identify knockdown cells and centrin to locate centrosome. Centrosome location was measured as in A.

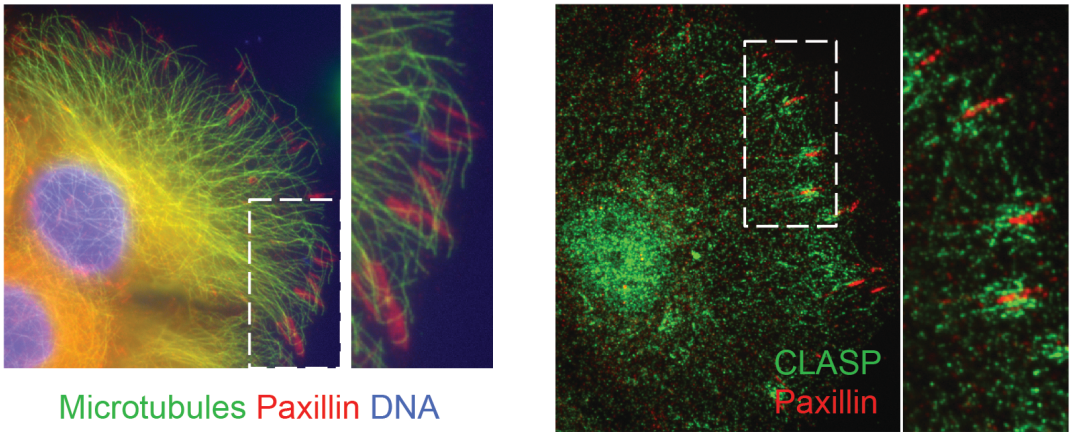

Figure 2.3. Focal adhesion and microtubule organization in migrating HaCaT wound layer. HaCaT cell monolayer was wounded and fixed with 0.25% gluteraldehyde after 20 hrs and stained for microtubules and paxillin to identify focal adhesions (left) or methanol and stained for CLASP and paxillin (right).

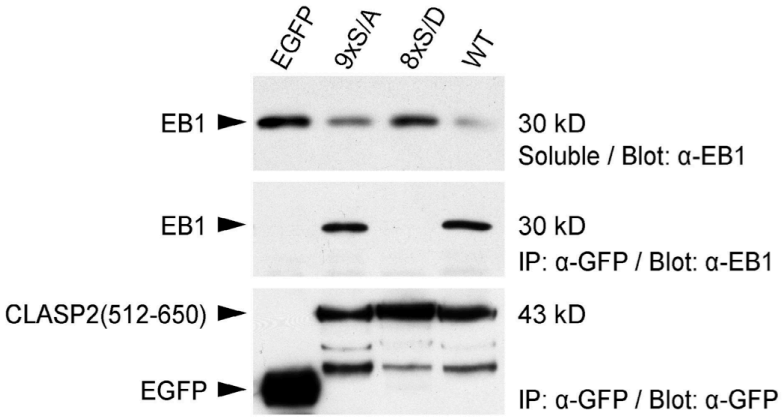

Figure 2.4. Binding of the CLASP2 plus-end-tracking domain to EB1 is directly inhibited by GSK3β phosphorylation. Immunoprecipitation (IP) using GFP antibodies from HeLa cells expressing EGFP-tagged CLASP2-MT plus-end-tracking domain constructs. Endogenous EB1 only immunoprecipitates with WT EGFP-CLASP2(512-650) and the nonphosphorylatable mutant 9xS/A but not with pseudophosphorylated 8xS/D or GFP alone.

CHAPTER 3: Madin Darby Canine Kidney cell tubulogenesis assay as a model for epithelial remodeling

As discussed in the introduction, relatively little is known about how the actin and microtubule cytoskeletons function and are regulated during the very important processes of EMT and epithelial remodeling. For this reason I chose to investigate the regulation and dynamics of the cell cytoskeleton during cell shape changes and migration in a 3D environment, a more physiological culture model than previously studied 2D cultures. Previous studies on the cytoskeleton in apical-basal polarized cells had been mostly done on polycarbonate filters (Bacallao et al., 1989; Reilein, 2005; Bellett et al., 2009). This allows for formation of a true apical-basal polarization of an epithelial monolayer, but has the disadvantage that it cannot be used for live imaging, as the filter would get in the way. Monolayers have to be fixed, stained and then flipped onto a coverslip. Alternatively, cells may be plated directly on coverslips and grown until confluent. This allows for live-cell inverted microscopy, however, it is unclear whether the cells establish full polarity as in filter-grown cells. With both methods, imaging of the apical-basal axis is achieved through z-stack reconstructions, which can give an estimation of intracellular organization but has relatively poor resolution compared to xy images (Reilein, 2005; Bowen et al., 2011). Studies of cell migration in a 3D ECM have steadily increased since I began my project in 2007, but have focused on single cell migration and very few have achieved imaging of intracellular protein dynamics (Fischer et al., 2009; Petrie et al., 2012; Geraldo et al., 2012; Meyer et al., 2012). We therefore decided to use the Madin-Darby

canine kidney (MDCK) cell culture model, a widely established *in vitro* system for studying epithelial morphogenesis. Extracellular-matrix-embedded MDCK cells develop into spherical cysts with a central lumen and distinct apical-basal polarity. Stimulation of cysts with Hepatocyte Growth Factor (HGF), results in 3D epithelial remodeling into tubules in a characteristic multi-step process. Some “pioneer” cells in the cyst undergo a partial epithelial-to-mesenchymal transition (pEMT), sending out long dynamic extensions into the ECM. These cells migrate out of the cyst, divide and eventually form chains of cells, while retaining cell-cell contacts. Cells continue to divide resulting in multilayer cords, which then transition back to apical/basal polarity and form a lumen along the tubule (Fig. 3.1) (O'Brien et al., 2002; Zegers et al., 2003). This model has two major advantages. The first is that cells can be stimulated to undergo shape changes under temporal control, which allows us to image the process of epithelial remodeling in real time. The second is that because of the spherical nature of the cyst, we can image the apical-basal axis in the xy-plane, resulting in the highest resolution images of this epithelial axis that have been published (Fig. 4.1).

The first goal was to optimize the MDCK tubulogenesis system for high-resolution imaging. The major technical difficulty with imaging cells in a 3D environment is the issue of working distance of the objectives and the fact that spherical aberration increases with distance from the coverslip. The highest numerical aperture oil objectives (1.49NA) that give the best resolution also have a relatively short working distance. Therefore, our goal was to grow cysts as close as possible to the objective while still embedding the cyst in a 3D ECM gel.

I started with an overlay technique used by members of the Mostov Lab (Kwon et al., 2011) and tested many modifications before settling on an optimized protocol (Appendix protocols A,B). Glass bottom dishes were coated with a very thin layer of gelled Matrigel (BD biosciences). Coverslips used were #1 thickness to minimize distance across the glass. A single cell suspension of MDCK cells were plated onto coated dishes in media containing 2% Matrigel. Cells adhere to the dish and are coated by the basement membrane matrix that sinks to the bottom of the dish. Cysts that develop over about 4-5 days are in a relatively even plane and close to the coverslip. However, epithelial remodeling does not properly and completely proceed in Matrigel (Williams and Clark, 2003). I attempted some HGF experiments in Matrigel instead of collagen and found very different results between the two conditions in the early extension phases of tubulogenesis (Fig 3.2). We therefore treated cells with a short trypsinization to remove some of the Matrigel on the cysts and replaced it with a collagen I gel (Fig 3.3). Treatment of collagen embedded cysts with HGF resulted in cell ruffling, extension formation and eventually migration from the cyst wall (Fig 3.4). Although cysts can grow from cells embedded in collagen in the first place, this usually results in a monolayer of cells that have sunk onto the coverslip before collagen has gelled and cysts in all different z-planes resulting in too great of a working distance. Although more laborious and technically difficult, the Matrigel to collagen switch allows for more superb imaging in a 3D matrix. Most high-resolution imaging of intracellular proteins was performed with 60x or 100x TIRF objectives. These have a spherical aberration collar to correct for coverslip thickness and changes

caused by using temperature controlled chambers at 37C. Collars were adjusted to correct for combined thickness of coverslip, Matrigel layer and cyst structure. Independent of the distance from the coverslip, image quality of the upper half of cysts degraded severely. This seemed to be caused by the spherical, lens-like nature of the cysts. To image through the cyst at further distances from the coverslip we used a 60x water lens that provides lower resolution but longer working distance. Although the majority of my studies were on cytoskeleton dynamics during epithelial remodeling, I believe this MDCK tubulogenesis system will be useful in the future for studies on other intracellular dynamics during epithelial remodeling. For example, understanding how organelles are reorganized and distributed through live imaging of ER and mitochondria markers (Fig. 3.6)

To initially test whether dynamic microtubules are required for cyst development and epithelial remodeling we tested the effects of low concentrations of nocodazole. Cysts were treated with 100 nM nocodazole on day 3 and were fixed after 24hrs. Nocodazole treated cysts appeared to maintain cell-cell contacts but the lumen either was not developed/cleared or was collapsed (Fig 3.5 A). Control HGF-induced extensions grew out and retracted repeatedly, and the leading edge pulled and aligned collagen fibers (Fig. 3.5 B, frames 1-3). Following three hours of imaging, extensions were treated with 200 nM nocodazole. This resulted in loss of cell contact with the ECM and retraction to the cell body. These data supported the hypothesis that dynamic microtubules play an important role in epithelial remodeling and further

supported our investigation into this process. The results of these studies, the main work of my dissertation, were published in Current Biology and are presented here in Chapter 4.

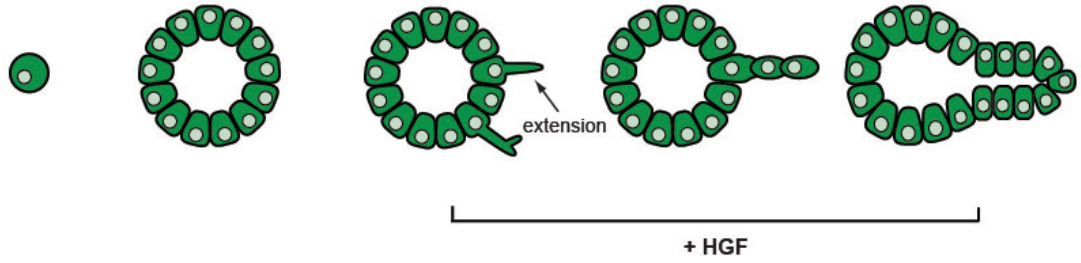

Figure 3.1. Steps in MDCK tubulogenesis. MDCK cells form cysts when cultured in extracellular matrix. Upon stimulation with HGF, some cells send out long dynamic extensions into the ECM. These cells migrate out of the cyst, divide and eventually form chains of cells, while retaining cell-cell contacts. Cells continue to divide resulting in multilayer cords, which then transition back to apical-basal polarity and form a lumen along the tubule.

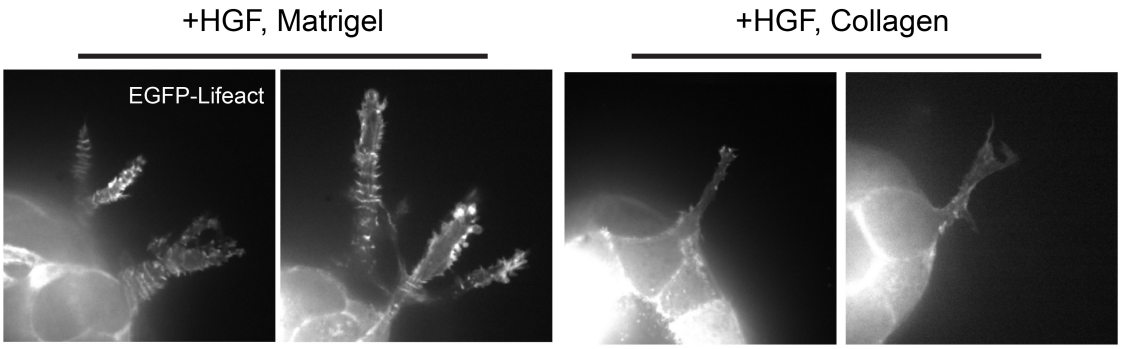

Figure 3.2. HGF-induced extensions in Matrigel or collagen. Extensions formed in Matrigel have relatively stable actin-rich ring-like structures along the length of the extension (two left examples). In contrast to collagen embedded cysts, these extensions in Matrigel do not get much longer than shown here or migrate from the cyst (data not shown). Extensions formed in collagen usually maintain actin rich ruffles near the tip of the extension, while the length of the extension is smooth and lined with cortical F-actin (right two examples).

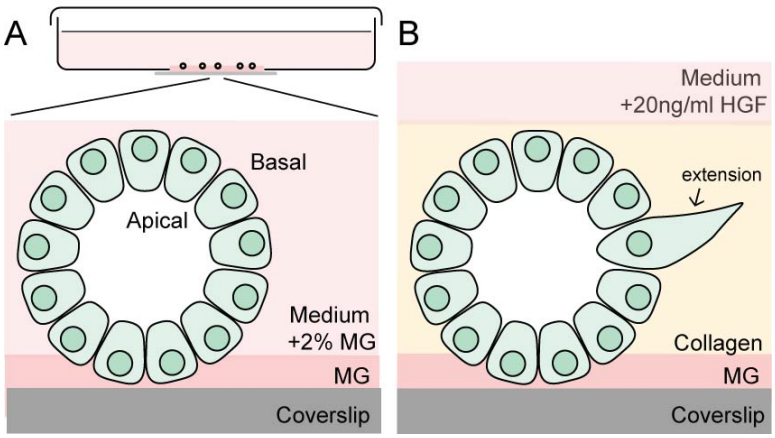

Figure 3.3. Three-dimensional MDCK epithelial culture system for live imaging. (A) Polarized cyst grown in Matrigel (MG). (B) HGF-induced epithelial remodeling in collagen.

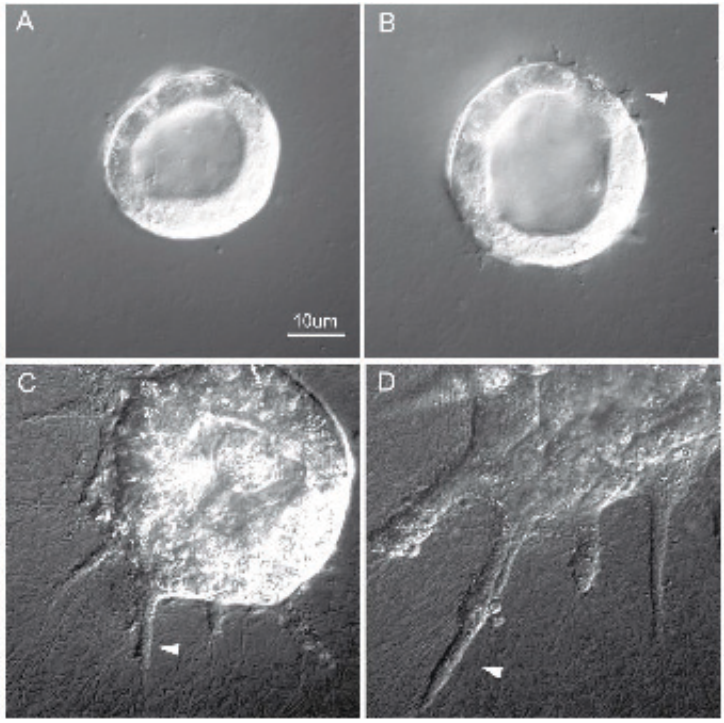

Figure 3.4. Differential Interference Contrast (DIC) imaging of MDCK cells in early stage of HGF-induced epithelial remodeling. (A) Cyst before morphological changes. (B) Approximately 5 hours after HGF addition membrane ruffles begin forming at basal surface (C) Dynamic extensions pull on collagen and align fibers (D) Some cells eventually migrate from cyst wall while maintaining contact with other cells (arrow).

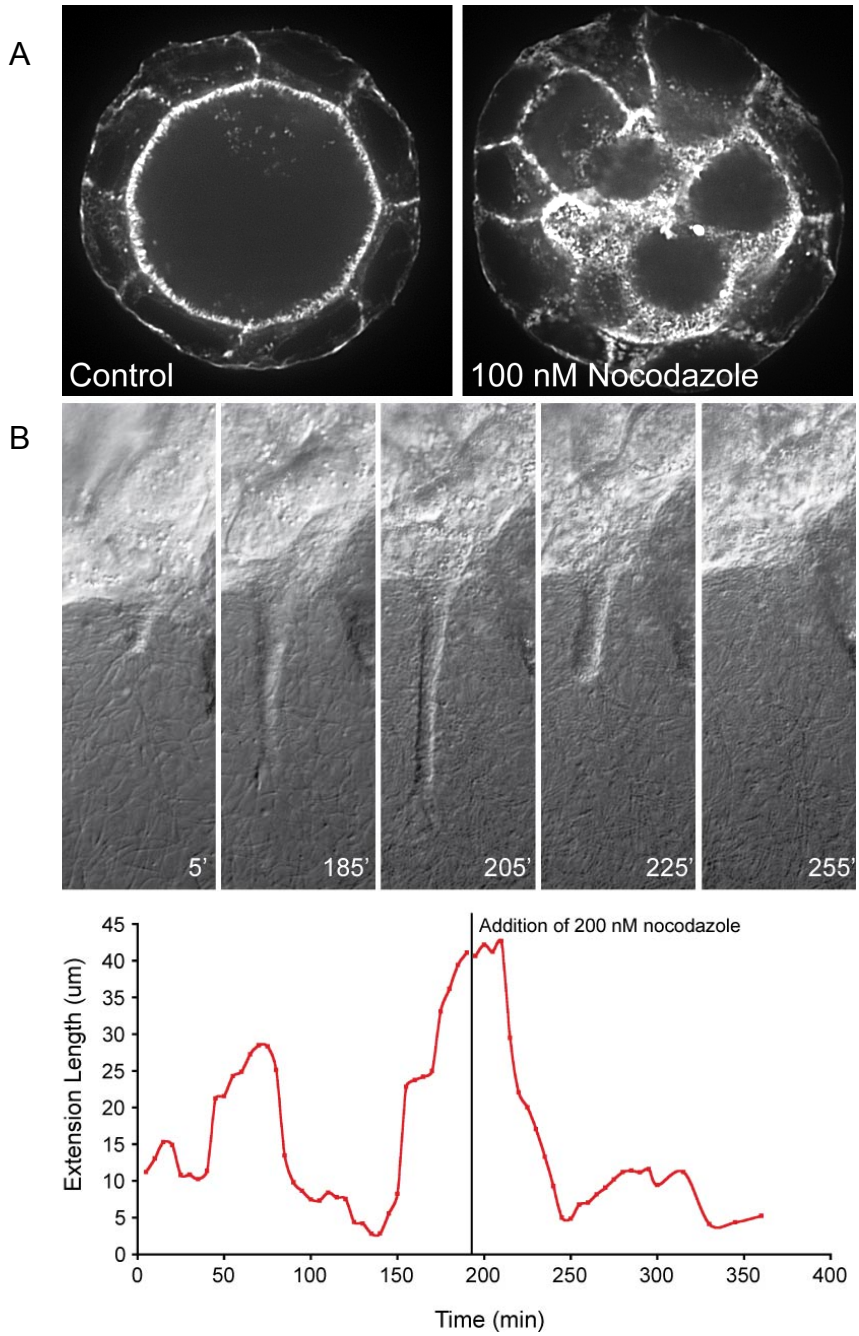

Figure 3.5 Nocodazole treatment of cysts and HGF-induced cysts (A) Cysts grown for 3 days in Matrigel were treated with DMSO or 100 nM for 24hrs before fixation with 4% paraformaldehyde. Fixed cysts were stained for F-actin with rhodamine-phalloidin to identify cyst organization and apical surface. (B) Cysts treated with HGF overnight were imaged every 5 min by DIC. Extensions grew out and retracted repeatedly, and the leading edge pulled and aligned collagen fibers (frames 1-3). Following 3hrs of imaging, 200nM nocodazole was added. After 30 min, extensions lost connections with the matrix (frame 4) and slowly retracted back to the cell body. Extensions grew back for short periods, but never recovered longer extensions in later time points (up to 10hrs).

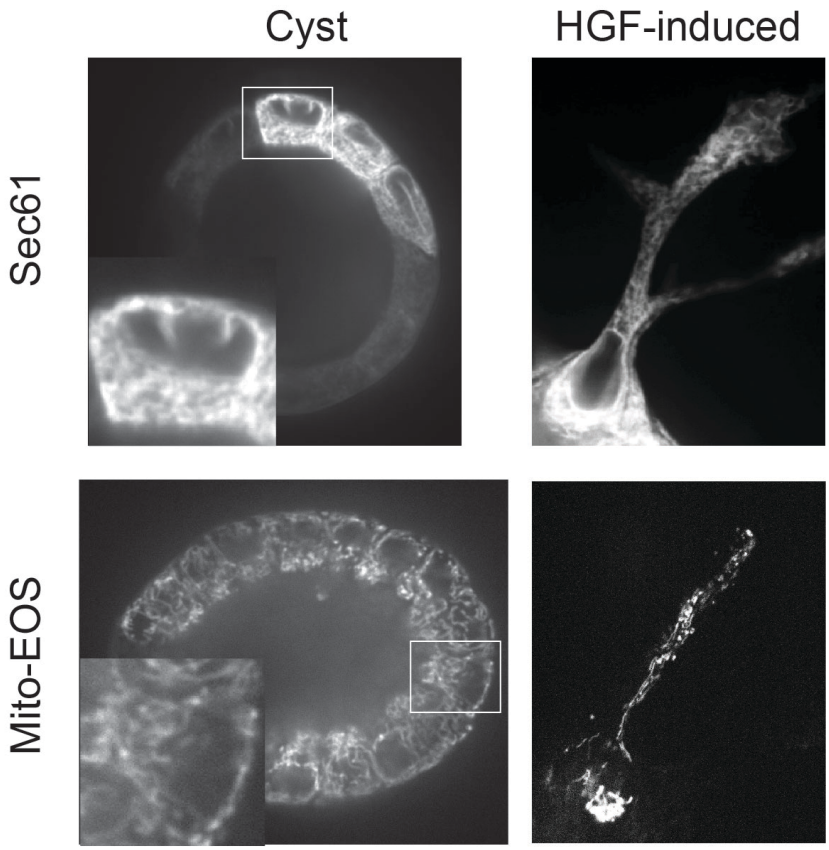

Figure 3.6 Organelles during epithelial remodeling. GFP-Sec61 labeled ER network is densely distributed throughout cytoplasm in apical-basal polarized cells and in HGF-induced extensions. Mito-EOS labeled mitochondria are less dense and more motile. Mitochondria reach tip of the extension and appear to be shorter rods near the tip compared to longer tubules in the extension.

CHAPTER 4: EB1-recruited microtubule +TIP complexes coordinate protrusion dynamics during 3D epithelial remodeling

I. Abstract

Epithelial remodeling, in which apical-basal polarized cells switch to a migratory phenotype, plays a central role in development and disease of multicellular organisms. Although dynamic microtubules (MTs) are required for directed migration on flat surfaces, how MT dynamics are controlled or contribute to epithelial remodeling in a more physiological three-dimensional (3D) environment is not understood. We use confocal live cell imaging to analyze MT function and dynamics during 3D epithelial morphogenesis and remodeling of polarized Madin-Darby canine kidney (MDCK) epithelial cells that undergo partial epithelial-to-mesenchymal transition (EMT) in response to hepatocyte growth factor (HGF). We find that HGF treatment increases MT growth rate before morphological changes are evident, and that large numbers of MTs grow into HGF-induced cell extensions independent of centrosome reorientation. Using lentivirus-mediated shRNA, we demonstrate that EB1, an adaptor protein that mediates recruitment of numerous other +TIP proteins to growing MT plus ends, is required for this HGF-induced MT reorganization. We further show that protrusion and adhesion dynamics are disorganized, and that vesicular trafficking to the tip of HGF-induced cell extensions is disrupted in EB1-depleted cells. We conclude that EB1-mediated interactions with growing MTs are important to coordinate cell shape changes and directed migration into the surrounding

extracellular matrix during epithelial remodeling in a physiological 3D environment. In contrast, EB1 is not required for the establishment or maintenance of apical-basal cell polarity, suggesting different functions of +TIPs and MTs in different types of cell polarity.

II. Introduction

Epithelial cells are typically polarized with a basal surface connecting to the underlying extracellular matrix (ECM), and an apical domain facing the topological outside of the organism. Although apical-basal polarity is critical to normal epithelial function and homeostasis, epithelial tissue architecture is remodeled during many developmental processes (Bryant and Mostov, 2008). For example, branching morphogenesis during mammary gland or kidney tubule development requires that individual cells lose apical-basal polarity, change shape and acquire a more mesenchymal, migratory phenotype (Affolter et al., 2009). Such migratory cell shape changes are ultimately driven by reorganization of the cytoskeleton, a process that has been studied predominantly in cells migrating on flat and rigid 2D surfaces. In 2D, directed cell migration is primarily motored by actin polymerization that is required for leading edge protrusion. Adhesion turnover and myosin-mediated contractility further facilitate net forward movement. In many cell types, dynamic MTs are required to establish and maintain 2D directed migration. MT dynamics are spatiotemporally controlled with most growing MT ends facing toward the direction of migration (Kaverina and Straube, 2011; Wittmann and Waterman-Storer, 2001). However, to what extent MT dynamics are regulated or MTs contribute to cell shape changes in

more physiologically relevant 3D environments is not known largely because of the technical challenges associated with high resolution microscopy of live cells embedded in a 3D matrix.

MTs are highly dynamic polymers that stochastically switch between phases of growth and shortening, and complex relationships exist between the regulation of MT growth dynamics and extracellular matrix properties in a 3D environment (Myers et al., 2011). +TIPs, a heterogeneous group of proteins that reversibly bind to growing MT ends, have been proposed to control MT dynamics and interactions with other intracellular structures (Akhmanova and Steinmetz, 2008). Specifically, the Adenomatous Polyposis Coli protein (APC), spectraplakins (ACF7), and CLASPs mediate MT interactions with cortical structures and signaling factors at the leading edge of migrating cells (Etienne-Manneville, 2009; Kumar et al., 2009; Wu et al., 2011), and may be important regulators of cell architecture. Most +TIPs do not directly bind to growing MT ends, but are recruited by end-binding proteins (EBs) that have emerged as central components of +TIP protein interaction networks. EBs are small dimeric proteins consisting of an N-terminal calponin homology domain that directly recognizes a structural feature of growing MT ends, and a C-terminal EB homology domain that mediates localization of other +TIPs (Honnappa et al., 2009).

Here, we use a physiological 3D epithelial tissue culture system to address MT dynamics and function during epithelial morphogenesis and remodeling. ECM-embedded Madin-Darby canine kidney (MDCK) cells develop

into spherical cysts with a central lumen and distinct apical-basal polarity. Stimulation with hepatocyte growth factor (HGF) results in 3D epithelial remodeling in which cells undergo a partial epithelial-to-mesenchymal transition (EMT) and send out dynamic cell extensions into the surrounding extracellular matrix (Bryant and Mostov, 2008; Leroy and Mostov, 2007). Using spinning disk confocal microscopy we resolved the challenge of imaging real-time cytoskeleton behavior in 3D at high spatial and temporal resolution. We examine MT dynamics in both polarized MDCK cells and during epithelial remodeling by computational tracking, and we report extensive reorganization of the MT cytoskeleton and MT dynamics during HGF-induced cell shape changes. We further demonstrate that EB1 and +TIPs recruited to growing MT ends by EB1 are critically important for coordinated protrusion and cell-matrix adhesion dynamics during the early stages of HGF-induced epithelial remodeling.

III. RESULTS

A. Microtubule reorganization during epithelial remodeling in a 3D environment

In order to analyze MT function and dynamics during epithelial remodeling in a physiological 3D environment, we adapted an organogenesis model system for high-resolution spinning-disk confocal microscopy. Briefly, single MDCK cells seeded on coverslips coated with a thin Matrigel basement membrane matrix layer were overlaid with diluted Matrigel to allow development of polarized epithelial cysts. To induce partial EMT, cell outgrowth, and migration into the surrounding matrix, polarized cysts were treated with HGF after replacing the

Matrigel overlay with collagen (Fig. 4.1B) (O'Brien et al., 2006; Kwon et al., 2011).

We first compared polarized and HGF-treated cysts by immunofluorescence to determine how the cytoskeleton is reorganized during this morphological change. As expected, prior to HGF treatment, filamentous actin (F-actin) predominantly localized to cell-cell junctions and microvilli at the apical surface (Fig. 4.1A). The spherical geometry of MDCK cysts allowed direct observation of apical, basal, and lateral MT arrays in different optical sections. MTs formed a dense network just below the apical microvilli and a less dense network at the basal surface. Cross-sections of perinuclear MT and F-actin bundles above the basal surface were consistent with MT organization typical for polarized epithelial cells (Bacallao et al., 1989), and MTs in medial sections were resolved much more clearly compared with z-axis reconstructions (Fig. 4.1A, bottom panel). HGF treatment resulted in extensive cytoskeleton reorganization. After 24 hours, individual cells had formed long extensions from the basal surface into the surrounding collagen matrix that often terminated in lamellipodia-like, F-actin-rich ruffles (Fig. 4.1C). In contrast to the relatively sparse basal MT network in polarized cysts, HGF-induced cell extensions contained numerous bundled MTs that extended into the distal extension tips (Fig. 4.1C, inset). MT acetylation was increased in HGF-induced extensions indicating increased MT stability compared with apical-basal polarized cells in which acetylated MTs were mostly localized to the apical surface and primary cilia (Fig. 4.S1A) (Jaulin and Kreitzer, 2010).

To test whether HGF-induced MT reorganization was mediated by centrosome reorientation toward the cell front as occurs in many cell types migrating on a 2D surface (Wittmann and Waterman-Storer, 2001), we analyzed centrosome dynamics in HGF-induced extensions. In contrast to polarized cells in which both EGFP-γ-tubulin-marked centrosomes remained in close proximity near the apical surface, the two centrosomes often moved significantly apart in HGF-induced cell extensions (Fig. 4.1D,E). Typically, one centrosome remained close to the apical surface while the other one appeared to be pulled away, suggesting the presence of intracellular forces that may be unique to cell shape changes in a 3D environment. Nevertheless, both centrosomes remained behind the nucleus in the apical domain in >98% of cells with HGF-induced extensions (*n* = 50). Although centrosome reorientation may occur after cells lose their apical surface (Yu et al., 2003), it is not required for HGF-induced MT reorganization.

To directly visualize MT reorganization and dynamics in 3D epithelial structures, we expressed EB1 tagged with two EGFP moieties, EB1-2xEGFP, that yielded consistently bright signals on growing MT ends after optimization of imaging conditions (Fig. 4.S1B,C). In both polarized and HGF-treated cells, the density of growing MT ends was highest in the apical domain, consistent with apical MT nucleation (Fig. 4.1F). Kymograph analysis indicated predominant MT growth toward the basal surface. In HGF-treated cysts, MTs continued to grow into cell extensions with increased growth rate and persistency. Growing MT ends also frequently bumped into and deformed the HGF-induced extension tip suggesting that MTs may mechanically contribute to protrusion or extension

stability (Movie 1). Together these results suggest that MT reorganization during HGF-induced extension formation is mediated through regulation of MT growth dynamics.

B. EB1 is required for HGF-induced epithelial remodeling in 3D

EB1 is a central adaptor protein linking most +TIPs to growing MT ends, and EB1-recruited +TIP complexes likely play important roles in MT plus end dynamics and interactions (Akhmanova and Steinmetz, 2008; Honnappa et al., 2009). To determine +TIP function during epithelial morphogenesis and remodeling, we targeted EB1 in MDCK cells by RNA interference. Because the canine genome contains predicted EB1 genes on over ten different chromosome loci, we developed eight short-hairpin RNA (shRNA) lentivirus constructs to target different combinations of homologous sequences. shRNA constructs #1 and #3 resulted in >95% depletion of EB1 protein (Fig. 2A). Although redundancy between EB1 and EB3 has been reported in other mammalian cell types (Komarova et al., 2009), plus-end-tracking of three different EGFP-tagged +TIP proteins, CLASP2 (Kumar et al., 2009; Mimori-Kiyosue et al., 2005), MCAK (Honnappa et al., 2009; Moore et al., 2005), and APC (Honnappa et al., 2009; Slep et al., 2005) was reduced ~5-fold in EB1-depleted cells (Fig. 4.2B; Fig. 4.S2A), indicating that EB1 shRNA is an efficient tool to disrupt +TIP protein complexes at growing MT ends in MDCK cells.

We next tested how EB1 depletion affected epithelial cyst morphogenesis and HGF-induced remodeling. While most EB1-depleted cysts developed normally, there was a modest increase in the number of cysts with abnormally

small or collapsed lumen (Fig. 4.S2B,C,E). In addition, apical localization of podocalyxin (GP135) (Ojakian and Schwimmer, 1988) indicated normal establishment of apical-basal polarity (Fig. 4.S2D). In contrast, HGF-induced epithelial remodeling was markedly affected in EB1-depleted cells. After 16 hours in HGF, extensions formed by EB1-depleted cysts were significantly shorter, more branched, and appeared to retract and change direction more frequently than extensions and multicellular chains formed by control cysts (Fig. 4.2C,D; Movie 2). EB1 depletion also resulted in significant morphological differences in later stages of HGF-induced epithelial remodeling (Fig. 4.S2F). Both shRNAs #1 and #3 produced identical defects in HGF-induced extension formation, indicating that the phenotype is EB1 specific (Fig. 4.2C,D). In addition, expression of a dominant negative EB1 fragment (EB1C, Fig. 4.S1B) (Komarova et al., 2009) similarly inhibited HGF-induced extension formation (Fig. 4.S2G). Together these data indicate that EB1 plays an important role during epithelial remodeling in 3D.

C. EB1 is required for microtubule organization in HGF-induced cell extensions

To investigate the mechanism by which EB1 contributes to HGF-induced epithelial remodeling, we analyzed how EB1 depletion affected MT organization and dynamics in polarized and in HGF-treated cysts. Because MT growth is directed toward the basal surface (Fig. 4.1F) and EB1 is associated with basal MT arrays (Reilein and Nelson, 2005), we predicted that EB1 is required for MT interactions with the basal surface in polarized cells. Time-lapse microscopy of

EGFP-α-tubulin confirmed that EB1-depleted cells had fewer, more curled MTs that displayed increased, rapid lateral movements consistent with a lack of cortical MT attachment (Fig. 4.S3A; Movie 3) (Kumar et al., 2009). MT density was also decreased in EB1-depleted HGF-induced extensions, and MTs appeared laterally mobile (Fig. 4.S3B, Movie 3). MT arrays did not reach the cell tip in contrast to straight, highly organized bundles in control cell extensions, further suggesting a defect in the stabilization of MT growth and organization toward the leading cell tip (Fig. 4.S3C).

The high MT density and optical aberrations in the 3D system made it impossible to quantify MT dynamics using EGFP-α-tubulin. We therefore developed a double EGFP-tagged, shRNA#3-resistant, EB1 construct truncated at amino acid 248, EB1ΔC-2xEGFP (Fig. 4.S1B). Although EB1ΔC-2xEGFP may rescue EB1-intrinsic effects on MT dynamics (Komarova et al., 2009), it is not expected to restore EB1-dependent recruitment of other +TIPs to growing MT ends, and it did not rescue the EB1-depletion phenotype (Fig. 4.2E). We used computational tracking of EB1ΔC-2xEGFP to analyze MT dynamics (Applegate et al., 2011; Matov et al., 2010). Taking advantage of the spherical geometry of polarized MDCK cysts, we first compared apical, medial and basal optical sections (Fig. 4.3A,D; Fig 4.S3D; Movie 4). In both control and EB1-depleted cysts, MTs in medial sections grew significantly faster than MTs in apical or basal sections. Analysis of MT growth rates as a function of track lifetime indicated that these differences are not an artifact of differing geometries of these MT networks

(Fig. 4.S3E,F). In contrast, differences between control and EB1-depleted cysts were small and mostly not statistically significant (Fig. 4.3D; Table S1).

MT growth dynamics were significantly changed in HGF-treated cells. MTs in the cell body and the bulk of HGF-induced extensions grew considerably faster than in polarized cells, although the growth rate decreased as MT ends approached the leading extension tip (Fig. 4.3B,E; Table 4.S1; Movie 5). Strikingly, the MT growth rate was already significantly increased at the basal surface of HGF-treated cells prior to extension formation (Fig. 4.3F; Fig. 4.S3G,H), indicating that HGF signaling directly stimulates MT growth, and that this increase is not solely due to cell shape changes. However, MT growth rates in HGF-induced extensions of EB1-depleted cells were indistinguishable from control cells, and a gradient in growth rates between cell body and extension tip remained statistically significant (Fig. 4.3E). Nevertheless, MT growth tracks in EB1-depleted HGF-induced extensions were less organized and less directional than those of control extensions (Fig. 4.3B,C,G).

In addition, EB1-depleted HGF-induced cell extensions displayed a highly unusual MT behavior. EB1ΔC-2xEGFP-labeled MT ends often exhibited rapid and extensive retrograde movements (Fig. 4.3H; Movie 5). Because EB1 only associates with growing MT ends (Akhmanova and Steinmetz, 2008; Matov et al., 2010), these movements reflect retrograde translocations of growing MTs and are not due to MT depolymerization. Although some retrograde MT movements occurred in control HGF-induced extensions and average rates of these movements were similar in control (40 +/- 11 μm min^{-1}) and EB1-depleted

cells (57 +/- 23 μm min^{-1}), they were much more frequent in EB1-depleted cells and covered significantly longer distances (Fig. 4.3I). Together these data demonstrate that during HGF-induced epithelial remodeling, EB1-recruited +TIP complexes do not appear to control spatial or HGF-induced differences in MT growth rates, but instead are required for proper reorganization and stabilization of the cell extension MT array.

D. EB1-depleted cells display uncoordinated protrusion and adhesion dynamics, and disrupted vesicle trafficking

To further characterize epithelial remodeling defects in EB1-depleted cells, we analyzed HGF-induced cell extension dynamics by imaging of mEGFP-Lifeact, a small yeast peptide that binds F-actin (Riedl et al., 2008; Haynes et al., 2011). Control HGF-induced cells elongated persistently with a small F-actin-rich lamellipodia-like structure near the tip of the cell extension (Fig. 4.4A; Movie 6). In contrast, actin dynamics were increased and delocalized in EB1-depleted cells. Highly dynamic, short-lived F-actin-rich ruffles formed along the length of the extension resulting in multiple branched protrusions and a lack of productive forward movement. These mislocalized actin dynamics were particularly evident in maximum intensity projections of mEGFP-Lifeact time-lapse sequences. Cells in control cysts mostly protruded directionally whereas EB1-depleted cysts had a fractal-like appearance indicative of extensive protrusion and retraction in many different directions (Fig. 4.4B).

The inability of EB1-depleted cells to stabilize a dominant protrusion indicated a failure to productively interact with the extracellular matrix. To

investigate this we expressed paxillin-EGFP to visualize focal adhesion dynamics in HGF-induced cell extensions. Despite controversy over whether focal adhesions are relevant during cell migration in 3D (Harunaga and Yamada, 2011), control cells formed pronounced focal adhesions at the distal end of the extension that appeared to mature and turn over in a coordinated manner as the extension tip advanced (Fig. 4.5A; Movie 7). This was severely disrupted in EB1-depleted extensions in which adhesions appeared uncoordinated with respect to protrusion advancement. Consequently, adhesions in EB1-depleted cells remained significantly less elongated, suggesting a defect in tension-mediated adhesion maturation (Fig. 4.5B).

We next analyzed HGF-treated cysts by high-resolution differential interference contrast (DIC) microscopy to test how such uncoordinated protrusion and adhesion dynamics affected cell-matrix interactions (Fig. 4.5C; Movie 8). Control extensions displayed long phases of persistent outgrowth that coincided with progressive pulling on and deformation of the collagen matrix. Pulling forces were evident by collagen fiber alignment in front of the extension as well as movement of fiduciary marks in the collagen matrix toward the extension tip (Fig. 4.5C, arrows). In contrast, EB1-depleted cells did not productively engage collagen fibers, resulting in little and non-directional net movement of the collagen matrix. To determine whether the apparent lack of focal adhesion maturation and absence of matrix pulling forces correlated with decreased actomyosin contractility, we stained HGF-treated cysts for myosin regulatory light chain phosphorylation (pMLC), the main activator of non-muscle myosin

(Vicente-Manzanares et al., 2009). As reported previously, pMLC localized along cortical actin fibers in control cell extensions (Fig. 4.5D) (Yu et al., 2003). In contrast, in EB1-depleted cells we only observed punctate pMLC staining and no enrichment along the cortical actin cytoskeleton, indicating decreased actomyosin contractility (Fig. 4.5E).

Efficient vesicular trafficking is associated with directed migration and depends on an intact MT cytoskeleton (Prigozhina and Waterman-Storer, 2006; Veale et al., 2010; Kean et al., 2009). To test whether disrupted trafficking could provide a mechanistic link between MT cytoskeleton defects and epithelial remodeling phenotypes in EB1-depleted cells, we analyzed the dynamics of VAMP3, a recycling endosome-associated SNARE that has been implicated in membrane, integrin and matrix metalloprotease transport to the leading edge (Veale et al., 2010; Kean et al., 2009). In both control and EB1-depleted HGF-induced cells, EGFP-VAMP3 localized to the plasma membrane and to highly dynamic tubulovesicular structures that displayed rapid bidirectional movement along the length of cell extensions. In control cells, VAMP3-positive vesicles were closely associated with the tip of HGF-induced extensions and rapidly moved into newly formed membrane protrusions (Fig. 4.6A). In contrast, membrane protrusions that formed in EB1-depleted extensions often remained devoid of VAMP3-positive vesicular structures, likely because they lacked MT tracks. Although it was not possible to unambiguously detect or track individual vesicles, consistent with this observation, total EGFP-VAMP3 fluorescence was significantly enriched near the tip of HGF-induced extensions in control but not in

EB1-depleted cells (Fig. 4.6B). Together these data suggest that EB1-mediated organization of the MT cytoskeleton and resulting directed vesicle delivery to the tip of HGF-induced extensions is required to coordinate cell-matrix adhesion and protrusion dynamics during 3D epithelial remodeling.

IV. DISCUSSION

We report for the first time direct analysis and comparison of MT dynamics in apical-basal polarized epithelial cells and during growth factor induced epithelial remodeling by taking advantage of the spherical geometry of ECM-embedded apical-basal polarized epithelial cysts that allows optical sectioning in different planes. Adaptation of this tissue culture system such that epithelial structures are located within 30-50 μm of the coverslip surface allows spinning disk confocal microscopy with high N.A. oil immersion objectives. Although light scattering, spherical aberration, and lens-like properties of the epithelial sphere limit image resolution and signal intensity, equivalent high-resolution imaging of MT dynamics in epithelial cells in a 3D environment has not been achieved previously. We further used advanced computational tracking to quantify MT growth rates, thus gaining important insight into the mechanisms of MT reorganization during 3D epithelial remodeling. We believe these technical advances will be instrumental in future studies of intracellular movements of cytoskeletal components, organelles and other structures in a physiological 3D environment.

In polarized epithelial cells, MT minus ends are thought to be released from the centrosome and transported to tight junctions where they become

anchored (Bellett et al., 2009). Consistent with MT minus end localization near the apical surface (Bacallao et al., 1989; Bellett et al., 2009), we found that lateral MTs almost exclusively grew from the apical toward the basal cell surface. The growth rate of these lateral MTs was slightly but significantly increased compared with the more randomly organized apical and basal MT networks, demonstrating spatial MT regulation in polarized epithelial cells. Although MT growth at steep angles to the focal plane would result in apparently decreased growth rates, differences between different MT networks remained statistically significant for longer tracks that are more parallel to the section plane. Thus, random arrangement of MT growth directions likely increases the variance of growth rate populations, but still allows conclusions about relative differences between these populations. In HGF-induced cell extensions, the MT growth rate was increased further compared with apical-basal polarized cells. In addition, we observed spatial differences in HGF-induced extensions in which the MT growth rate decreased significantly toward the extension tip similar to spatial gradients between the interior and lamella of epithelial cells in 2D cultures (Kumar et al., 2009; Matov et al., 2010).

To analyze the function of +TIP proteins during MT organization in 3D epithelial structures, we targeted the central +TIP adaptor protein EB1 (Honnappa et al., 2009), and demonstrate that EB1 depletion in MDCK cells efficiently disrupts plus-end-tracking of different +TIPs. Both in polarized and HGF-stimulated cells, MT growth rates were largely independent of the +TIP binding activity of EB1, indicating that +TIP complexes do not function as global

MT dynamics regulators. Because HGF stimulation results in sustained Pak1 activation downstream of Rac1 in MDCK cells (Royal et al., 2000), the HGF-induced growth rate increase could instead result from phosphorylation and inactivation of the MT destabilizer Op18/stathmin (Wittmann et al., 2004a). However, because we visualized growing MTs by expressing an EGFP-tagged EB1 MT-binding domain, we cannot exclude EB1-intrinsic effects on MT dynamics (Komarova et al., 2009).

Nevertheless, EB1 depletion markedly disrupted MT organization in HGF-induced cell extensions. MTs often did not reach the cell extension tip, growing MT ends were less frequent and growth trajectories were disorganized. These MT organization defects are consistent with the proposed functions of a number of EB1-recruited +TIP proteins, including CLASPs, APC, and ACF7, which link MT plus ends to the cell cortex (Etienne-Manneville, 2009; Kumar et al., 2009; Wu et al., 2011). Defects in cortical MT interactions are also consistent with the frequent rapid and extensive retrograde movements of growing MT ends in EB1-depleted cells. Maximum rates of such retrograde MT translocations exceeded 100 μm min^{-1}, which is almost two orders of magnitude more rapid than typical actin retrograde flow in epithelial cells (Waterman-Storer and Salmon, 1997; Wittmann et al., 2003). Thus, MT-actin coupling cannot explain these movements. Instead, we propose that they result from pulling forces on MTs in the cell body and sudden loss of +TIP-mediated MT interactions with the cell cortex. Although retrograde MT movements also occurred to a lesser extent in polarized EB1-depleted cysts (Movie 4), we rarely observed extensive retrograde

MT translocations in cells plated on a 2D surface, indicating that the magnitude of these movements is related to unique forces acting on MTs in migrating cells in a 3D environment.

Finally, we show that EB1-mediated reorganization of the MT cytoskeleton is important for coordinated cell extension and adhesion dynamics during HGF-induced epithelial remodeling. Although the underlying molecular mechanism is likely complex and depends on multiple integrated functions of the MT cytoskeleton, +TIP-mediated stabilization of MTs in HGF-induced extensions is likely central to all these functions (Fig. 4.6C). MT dynamics have been proposed to directly influence Rho GTPase signaling (Wittmann and Waterman-Storer, 2001; Birkenfeld et al., 2008), which may be required for lamellipodia formation in a dominant extension tip and to restrict lateral protrusions. Mechanical resistance of stiff EB1-anchored MTs to contractile forces may be particularly important in a soft 3D environment to oppose cell retraction and contribute to extension elongation (Wang et al., 2001). In addition, our data point toward a requirement of EB1-mediated stabilization of the MT cytoskeleton for efficient vesicular trafficking toward the tip of HGF-induced extensions. Reduced adhesion maturation and actomyosin contractility could be consistent with defects in integrin activation or recycling of adhesion components. Transport and recycling of integrins, and other adhesion or membrane components is likely more important during 3D cell shape remodeling and migration due to different geometrical constraints and potentially longer distances between the secretory machinery and the cell's leading edge compared with cells on a 2D surface.

Strikingly, although basal MT organization appeared disrupted in EB1-depleted polarized cells, EB1 depletion had very little effect on establishment or maintenance of apical-basal epithelial cell polarity. This may reflect incomplete EB1 knockdown or partial compensation by homologous proteins, however it does highlight different requirements for EB1 and consequently +TIP protein functions in apical-basal polarity compared with front-back polarity of migrating cells. The similarity of MT organization in HGF-induced cell extensions to that in growing neurons (Conde and Cáceres, 2009) and fibroblasts migrating on linear tracks (Doyle et al., 2009) further suggests a conserved role of +TIP complexes during cell migration in fibrillar 3D extracellular matrices. Thus, our work lays the foundation for future studies how cell shape changes are coordinated by intracellular signaling, cytoskeleton and adhesion dynamics in a physiological 3D environment.

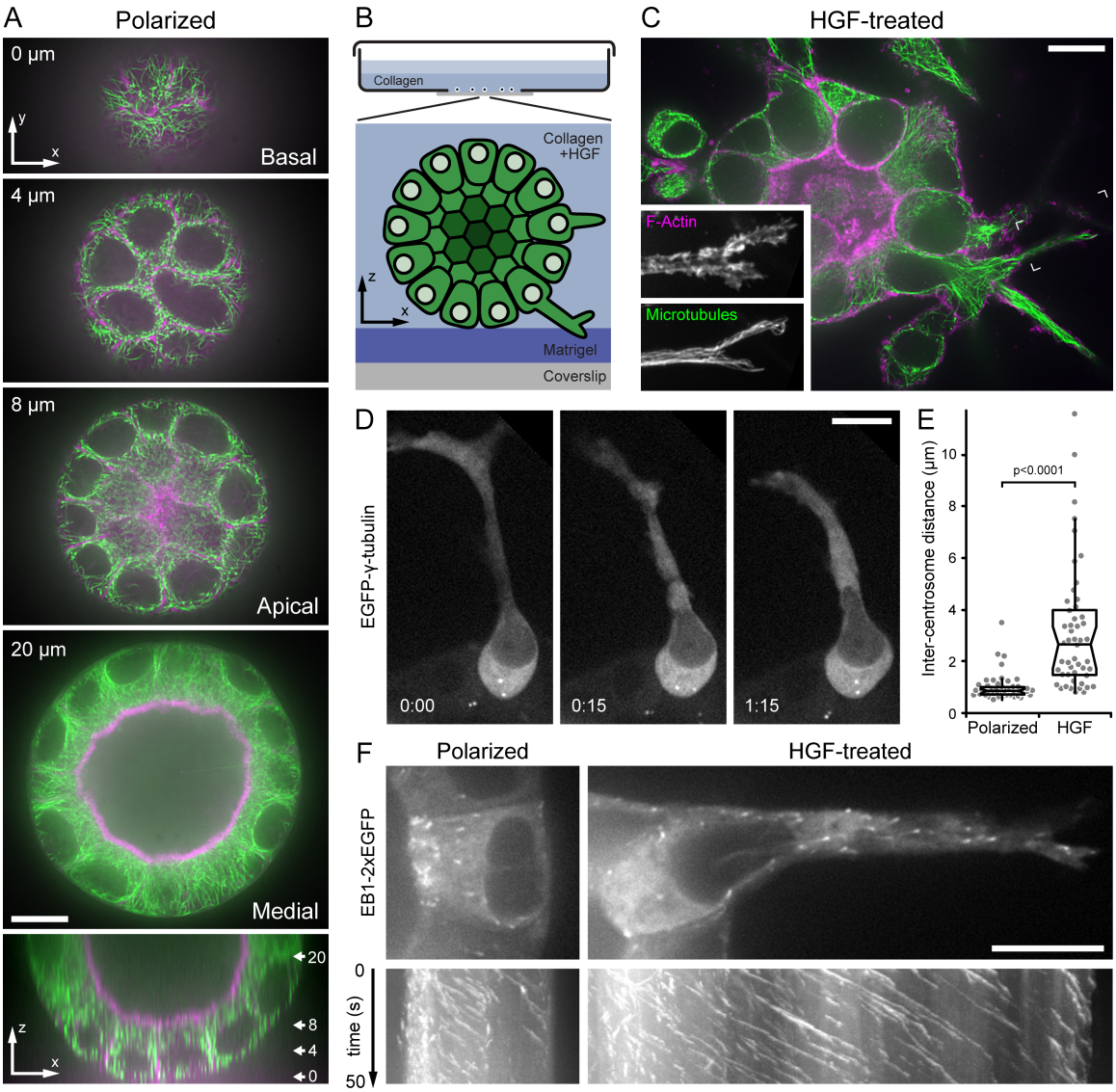

Figure 4.1. Microtubule cytoskeleton reorganization during HGF-induced epithelial remodeling. (A) Spinning disk confocal microscopy optical sections of a polarized MDCK cyst stained for F-actin (magenta) and MTs (green). Distance from the bottom of the cyst is indicated. The bottom panel is a z-axis reconstruction, and the approximate location of the optical sections shown is indicated. (B) Diagram of the 3D MDCK epithelial culture system adapted for high-resolution imaging. (C) Single optical section of F-actin (magenta) and MTs (green) 24 hours after HGF addition. Insets show a maximum intensity projection of the indicated area at higher magnification to illustrate the dense MT array extending to the extension tip. (D) EGFP-γ-tubulin time-lapse sequence in an HGF-induced extension showing centrosome separation and dynamics. Centrosomes remain close in the neighboring polarized cell that has not formed an extension. Elapsed time is indicated in hours:minutes. (E) Distance between

centrosomes in untreated polarized cells and cells with HGF-induced extensions. Gray symbols are measurements from individual cells (*n* = 50). (F) Images from medial optical sections of EB1-2xEGFP time-lapse sequences recorded at 2 frames s^{-1} with the apical surface oriented to the left. The bottom panels show kymographs perpendicular to the apical-basal cell axis. Oblique lines represent MT ends growing toward the basal surface or into the HGF-induced extension, respectively. Scale bars, 10 μm. See also Fig. 4.S1 and Movie 1.

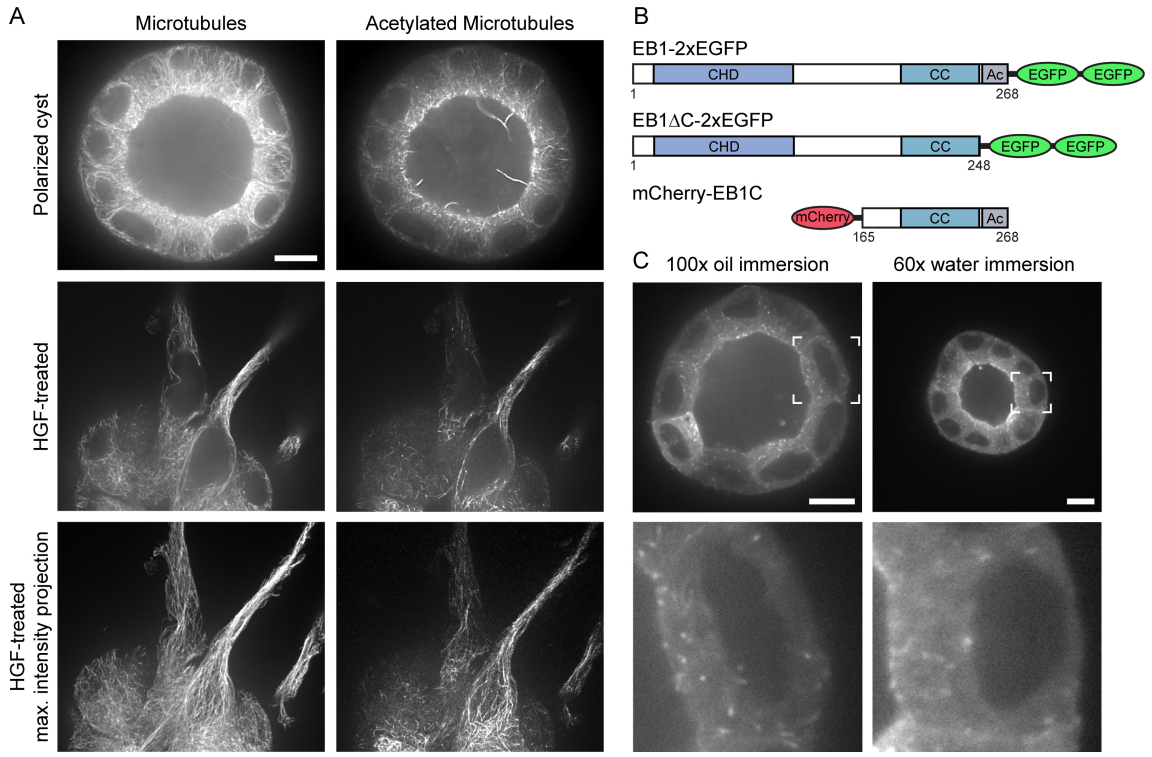

Figure 4.S1. Microtubule organization in MDCK 3D epithelial structures. (A) Microtubule acetylation in MDCK epithelial structures. Top panel shows a medial optical section of a polarized cyst stained for microtubules and acetylated tubulin, which is enriched in the apical microtubule network and primary cilia. Middle panel is a single optical section of an HGF-induced extension stained for microtubules and acetylated tubulin showing increased tubulin acetylation in the extension that originated from the basal cell surface. Bottom panel is a maximum intensity projection of multiple optical sections of the same HGF-induced extension. (B) Schematic of EB1 constructs used. (C) Spinning disk confocal images of medial optical sections of MDCK cysts expressing EB1-2xEGFP at similar levels, acquired with a 100x NA 1.49 oil immersion or a 60x NA 1.2 water immersion objective lens. No image processing was applied to these images. The 100X 1.49 NA oil immersion objective resulted in superior resolution of EB1 comets compared with the water immersion objective with theoretically better spherical aberration correction for thick specimens. Bottom panels show magnification of the insets indicated. Scale bars, 10 um.

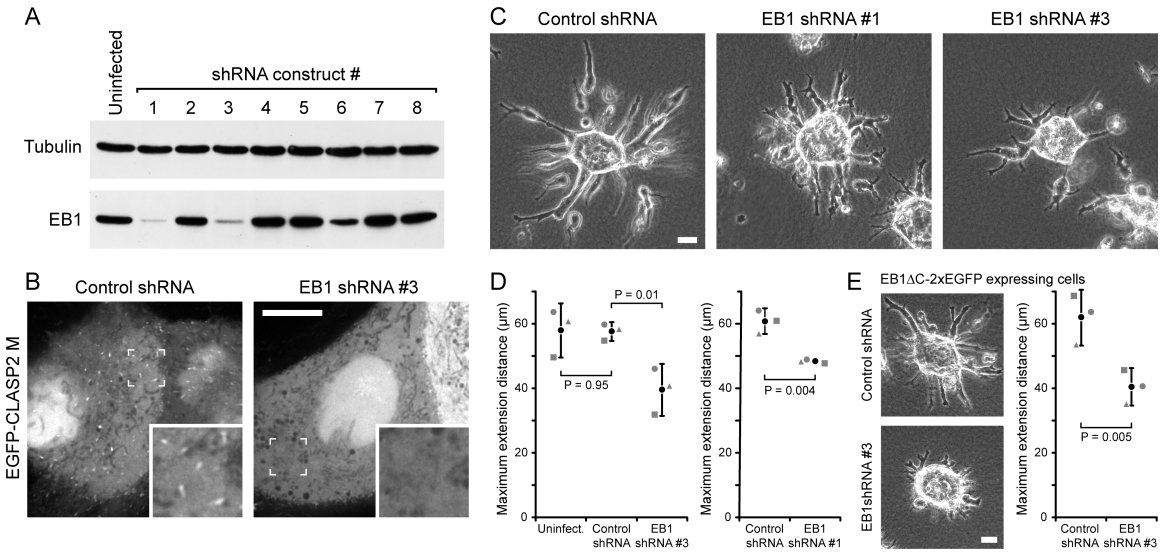

Figure 4.2. EB1 is required for HGF-induced epithelial remodeling. (A) Immunoblot of lysates from cells expressing different shRNA constructs after 7 days of puromycin selection. Tubulin was used as loading control. (B) MDCK cells stably expressing control or EB1 shRNA#3, transiently transfected with an EGFP-tagged, non-phosphorylatable construct encoding the CLASP2 EB1-binding domain (CLASP2 M) [8]. Insets show indicated region at higher magnification. Scale bar, 10 μm. (C) Phase contrast images of control and EB1-depleted HGF-treated MDCK cysts. Scale bar, 20 μm. (D) Quantification of HGF-induced cell extension into the surrounding collagen matrix. Graphs shows the average length of the three longest extensions measured from extension tip to cyst edge. Gray symbols are the average of 80-100 cysts from 3 separate experiments. Black circle represents the average of these three experiments. Error bars indicate 95% confidence interval. (E) Phase contrast images of EB1ΔC-2xEGFP-expressing control and EB1-depleted HGF-treated MDCK cysts, and quantification of HGF-induced cell extensions as in (D). Scale bar, 20 μm. See also Fig. 4.S2 and Movie 2.

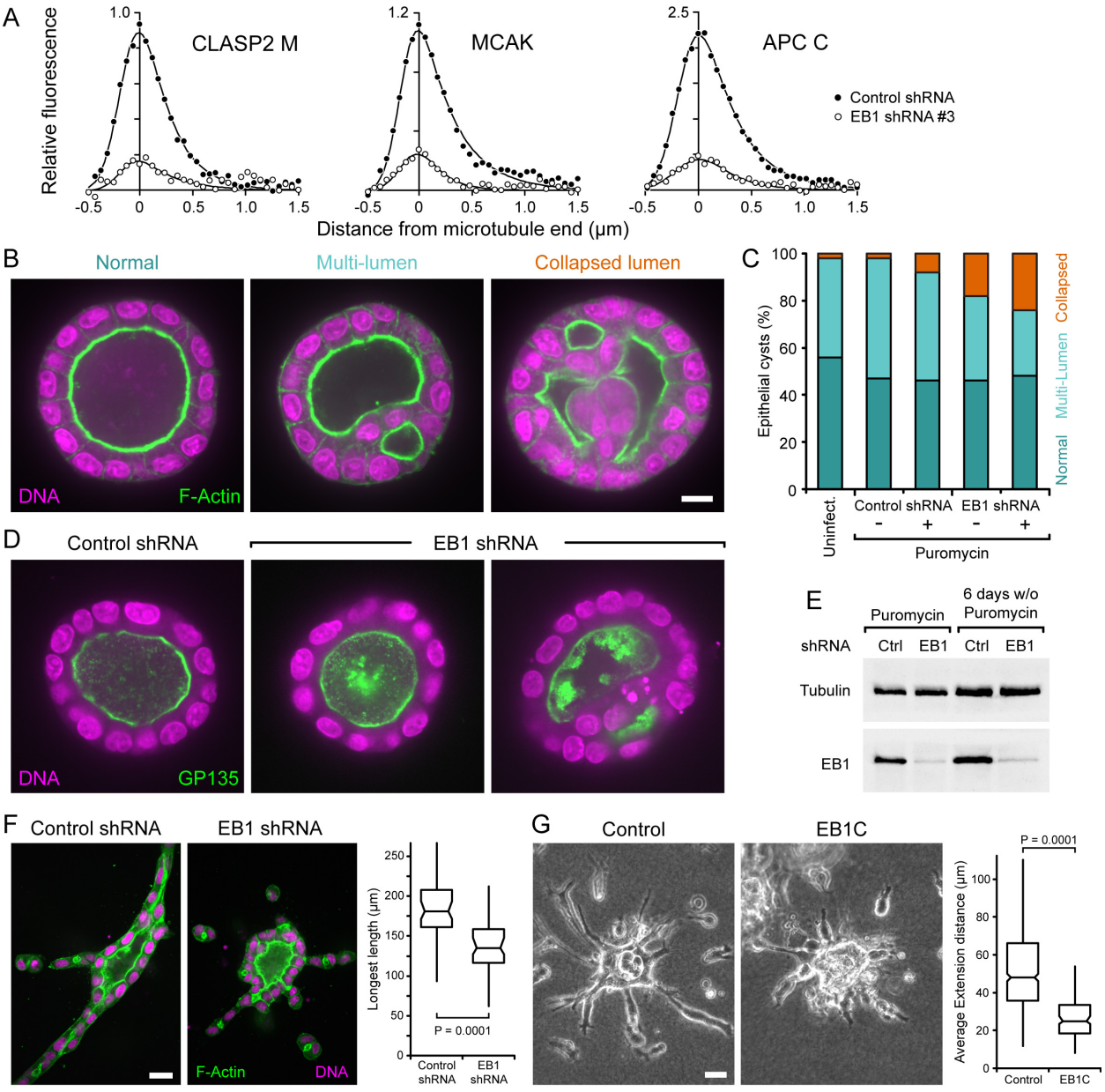

Figure 4.S2. EB1 depletion has little effect on apical-basal cell polarity, but disrupts HGF-induced tubulogenesis. (A) Quantification of MT plus-end-tracking of three different EGFP-tagged +TIPs in control (closed circles) and EB1-depleted cells (open circles). Shown are EGFP fluorescence intensity profiles along the MT end, normalized to fluorescence intensity in the cytoplasm. Data for each condition are averaged from 15 MT ends in 5 cells. Solid lines are exponentially-modified Gaussian curve fits. (B) Representative lumen morphologies in EB1-depleted cysts after 7 days of cyst development. Cysts were stained for F-actin (green) and DNA (magenta) to identify the apical surface and nuclei. Scale bar, 5 μm. (C) Quantification of lumen morphologies in cells

expressing the indicated shRNA constructs in the presence or absence of puromycin for the duration of the experiment (*n* = 50 cysts per condition). We detected a relatively high frequency of cysts with additional small lumens even in control conditions likely because cyst morphology was analyzed from z-stacks through the entire cyst. EB1-depleted cysts only have subtle defects in lumen formation, but cells are still polarized. (D) Control and EB1-depleted cysts stained for the apical marker GP135 (green) and DNA (magenta). (E) Immunoblot of lysates from cells stably expressing control shRNA or EB1 shRNA grown either in puromycin selection or after puromycin was removed for 6 days indicating that EB1 depletion was stable for a time period typically used for 3D epithelial morphogenesis experiments. (F) Immunofluorescence images of early epithelial tubule formation in control and EB1-depleted cells 48 hours after HGF treatment, stained for F-actin (green) and DNA (magenta). The graph shows length of the longest axis of epithelial structures formed (*n* = 100). EB1-depleted HGF-induced tubule structures remained markedly shorter than controls. All EB1 depletions were performed with EB1 shRNA #3 (G) Phase contrast images of HGF-treated control cysts and cysts expressing dominant-negative mCherry-EB1C. The graph shows the average length of all clearly defined extensions per cyst (*n* = 63 cysts) 18 hours after HGF addition. The phenotype of EB1C expression appeared more severe than EB1 depletion, possibly due to more complete inhibition of EB1 +TIP interactions. Scale bar, 20 μm.

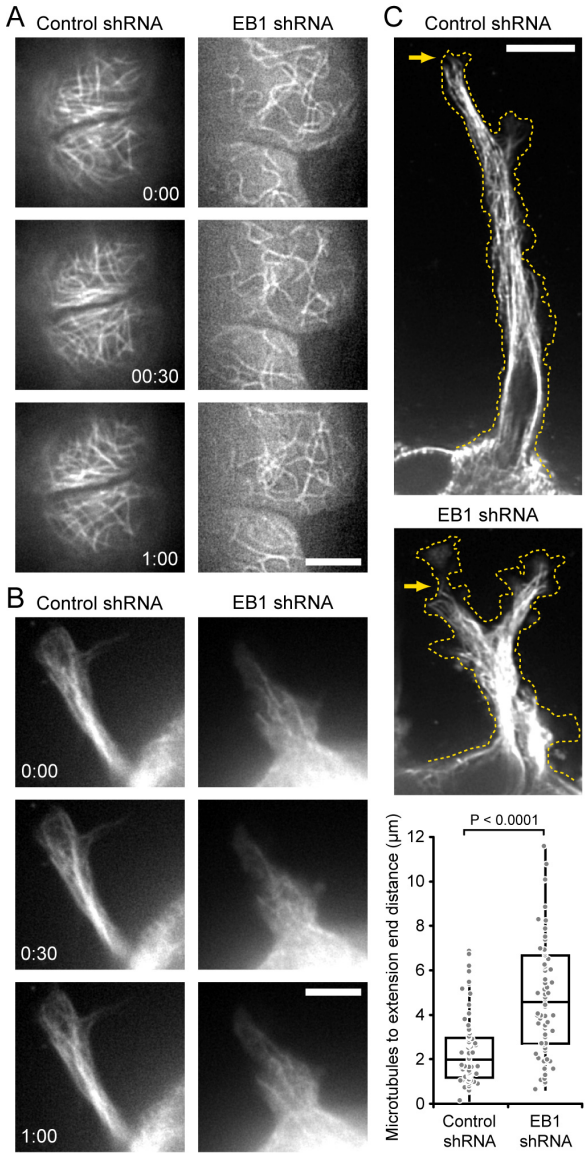

Figure 4.S3. Microtubule organization and growth rate analysis. (A-C) EB1 is required for HGF-induced microtubule reorganization**.** EGFP-α-tubulin time-lapse sequences of (A) the basal MT array in control and EB1-depleted cysts, and (B) in HGF-induced extensions. Elapsed time is indicated in minutes:seconds. See also Movie 3. (C) Representative images of MT staining in fixed HGF-induced extensions. Dashed line indicates the cell outline as determined by phalloidin staining, and arrows indicate the ends of most distal MTs. The graph shows a quantification of the distance between the most distal MT end and the tip of the cell (*n* = 70 extensions). Scale bars, 10 µm.

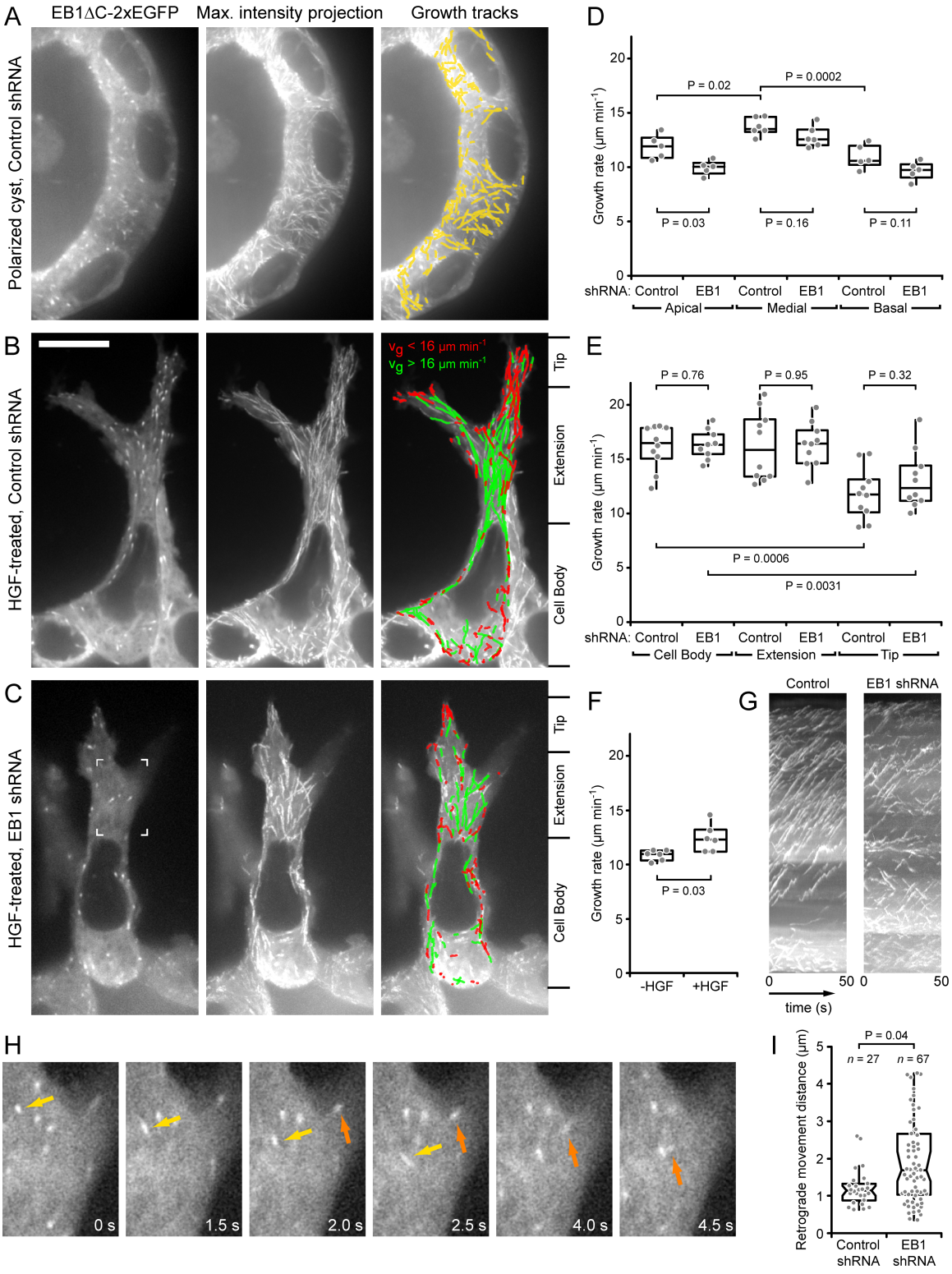

Figure 4.3. Analysis of microtubule dynamics in 3D epithelial structures. (A-C) Representative images of EB1ΔC-2xEGFP tracking in (A) a polarized, control shRNA cyst, and HGF-induced extensions of (B) control and (C) EB1-depleted cysts. Left panels are single images of the time-lapse sequence, middle panels

show maximum intensity projections over the entire sequence (100 frames recorded at 2 frames s^{-1}), and right panels show computer-generated tracks overlaid on the maximum intensity projection indicating tracking quality. Only tracks with a lifetime of >2.5 s are shown. Tracks in (B) and (C) are color-coded for growth rate. (D) MT growth rates in apical, medial, and basal optical sections in control or EB1-depleted polarized cysts. (E) MT growth rates in the cell body, extension and extension tip in control or EB1-depleted HGF-induced extensions. Division of cells into these three regions is indicated on the right of (B) and (C). (F) MT growth rates in basal optical sections in polarized cysts in Matrigel expressing EB1-2xEGFP before and 5 hrs after HGF addition. (D-F) Gray symbols represent the average growth rate of all tracks per cell and indicated condition. P-values of relevant comparisons are indicated on the graphs. (G) Kymographs of the cells shown in (B) and (C). (H) EB1ΔC-2xEGFP time-lapse sequence in an EB1-depleted HGF-induced extension. The region shown is indicated in (C). Two growing MT ends that display extensive retrograde movements are highlighted by arrows. Elapsed time is in seconds. (I) Number and distance of all retrograde MT movements in ten control and EB1-depleted HGF-induced extensions. Each gray symbol represents a retrograde movement event. Scale bar, 10 μm. See also Fig. 4.S3, Movies 3, 4 and 5.

	Number of tracks analyzed that are longer than 2.5 s (5 s)	Growth Rate ($\mu m\ s^{-1}$)
Polarized cells (EB1ΔC-2xEGFP)		
Apical (*n* = 5)		
Control shRNA	1046 (271)	11.85 +/- 1.12 (12.53 +/- 0.67)
EB1 shRNA	1132 (231)	9.91 +/- 0.67 (10.53 +/- 0.84)
Lateral (*n* = 6)		
Control shRNA	954 (194)	13.70 +/- 0.81 (14.82 +/- 2.75)
EB1 shRNA	1317 (301)	12.75 +/- 0.95 (13.66 +/- 0.95)
Basal (*n* = 5)		
Control shRNA	678 (186)	10.95 +/- 1.12 (12.78 +/- 0.76)
EB1 shRNA	810 (192)	9.64 +/- 0.85 (10.98 +/- 1.36)
HGF-induced extensions (EB1ΔC-2xEGFP)		
Cell Body (*n* = 10)		
Control shRNA	1011 (273)	16.10 +/- 2.00 (17.05 +/- 1.90)
EB1 shRNA	819 (202)	16.32 +/- 1.29 (16.59 +/- 2.57)
Extension (*n* = 10)		
Control shRNA	763 (336)	16.18 +/- 3.16 (16.91 +/- 3.30)
EB1 shRNA	605 (247)	16.28 +/- 2.02 (17.29 +/- 2.30)
Tip (*n* = 10)		
Control shRNA	416 (157)	11.78 +/- 2.37 (13.83 +/- 2.35)
EB1 shRNA	413 (130)	13.06 +/- 2.66 (14.87 +/- 2.85)
Basal microtubule array (EB1-2xEGFP) (*n* = 6)		
Polarized	1470 (452)	10.83 +/- 0.48 (12.50 +/- 0.76)
HGF-treated	2153 (753)	12.44 +/- 1.28 (13.72 +/- 1.28)

Table S4.1. Summary of measured microtubule growth rates. plusTipTracker was used to automatically track growing microtubule ends in cells expressing the indicated constructs. To control for microtubules growing through the optical section at steep angles, which would decrease the apparent growth rates, EB1 tracks were analyzed at minimum track lengths of either 5 frames (2.5 s) or 10 frames (5 s). As expected longer tracks generally display a higher growth rate. However, relative differences between conditions are similar indicating that these differences do not result from differences in overall microtubule organization. Regions in polarized cysts include several cells from one cyst measured as one region because it was difficult to accurately determine cell borders. In HGF-treated conditions, only one HGF-induced extension was quantified per cyst. Numbers represent mean +/- standard deviation.

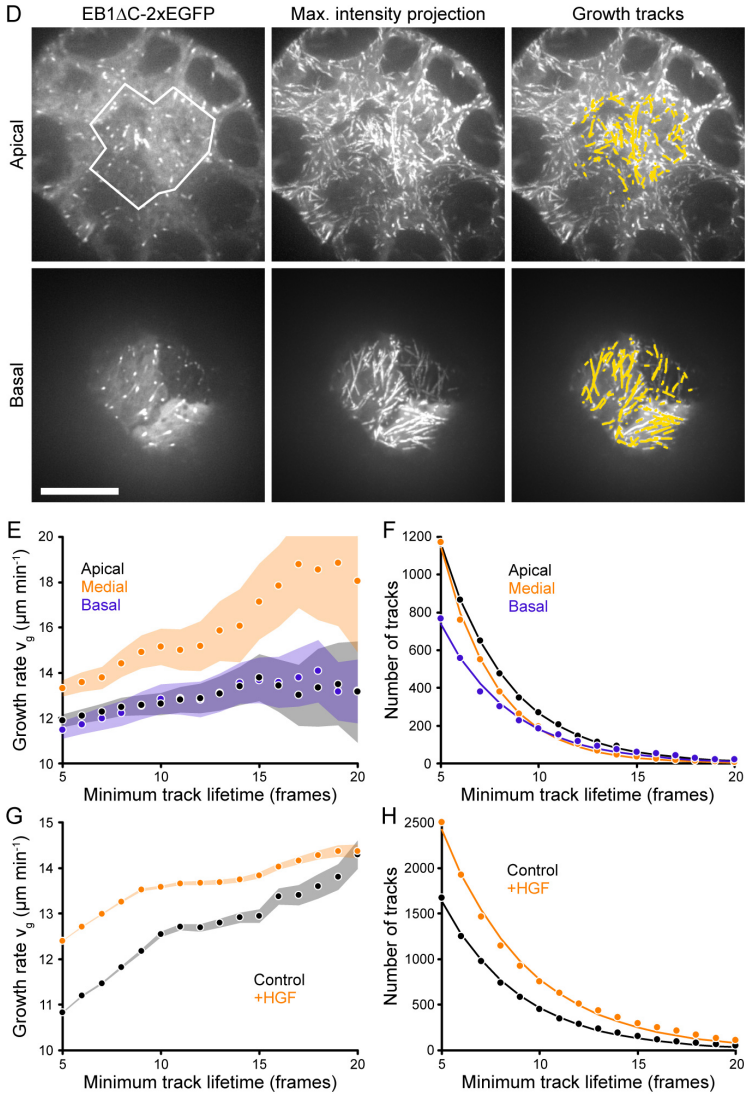

Figure 4.S3. Microtubule organization and growth rate analysis. (D-H) Validation of EB1ΔC-2xEGFP computational tracking in polarized cysts. (D) Representative images of automated EB1ΔC-2xEGFP tracking in a polarized, control shRNA cyst at the apical and basal surfaces. Left panels are single images of the time-lapse sequence, middle panels show maximum intensity projections over the entire sequence (100 frames recorded at 2 frames s^{-1}), and right panels show computer-generated tracks overlaid on the maximum intensity projection indicating tracking quality. Only tracks with a lifetime of >2.5 s are shown. (E, G) Microtubule growth rates as determined by computational tracking of EB1ΔC-2xEGFP plotted as a function of the minimum track lifetime included in the analysis in (E) apical, medial, and basal sections of control polarized MDCK cysts, or in (G) basal sections of control and HGF-treated cysts before cell extension outgrowth. Although longer tracks generally display an increased

growth rate, there is a plateau at a minimum growth rate of ~10 frames (i.e. 5 s). Shaded areas indicate 95% confidence intervals. Importantly, medial microtubule growth rates are significantly different from rates determined in apical and basal optical sections for all track lifetimes. Because longer tracks are likely more parallel to the focal plane, this indicates that these rates are truly different and differences do not result from differing geometries of the microtubule network, or microtubules growing at different angles relative to the focal plane. (F, H) Total number of tracks analyzed plotted as a function of the minimum track lifetime included in the analysis. Beyond a minimum track lifetime of ~15 frames, the total number of analyzed tracks becomes very small, and growth rates of these very long tracks are likely overestimated due to erroneous connections between tracks. Solid lines are exponential fits of the data.

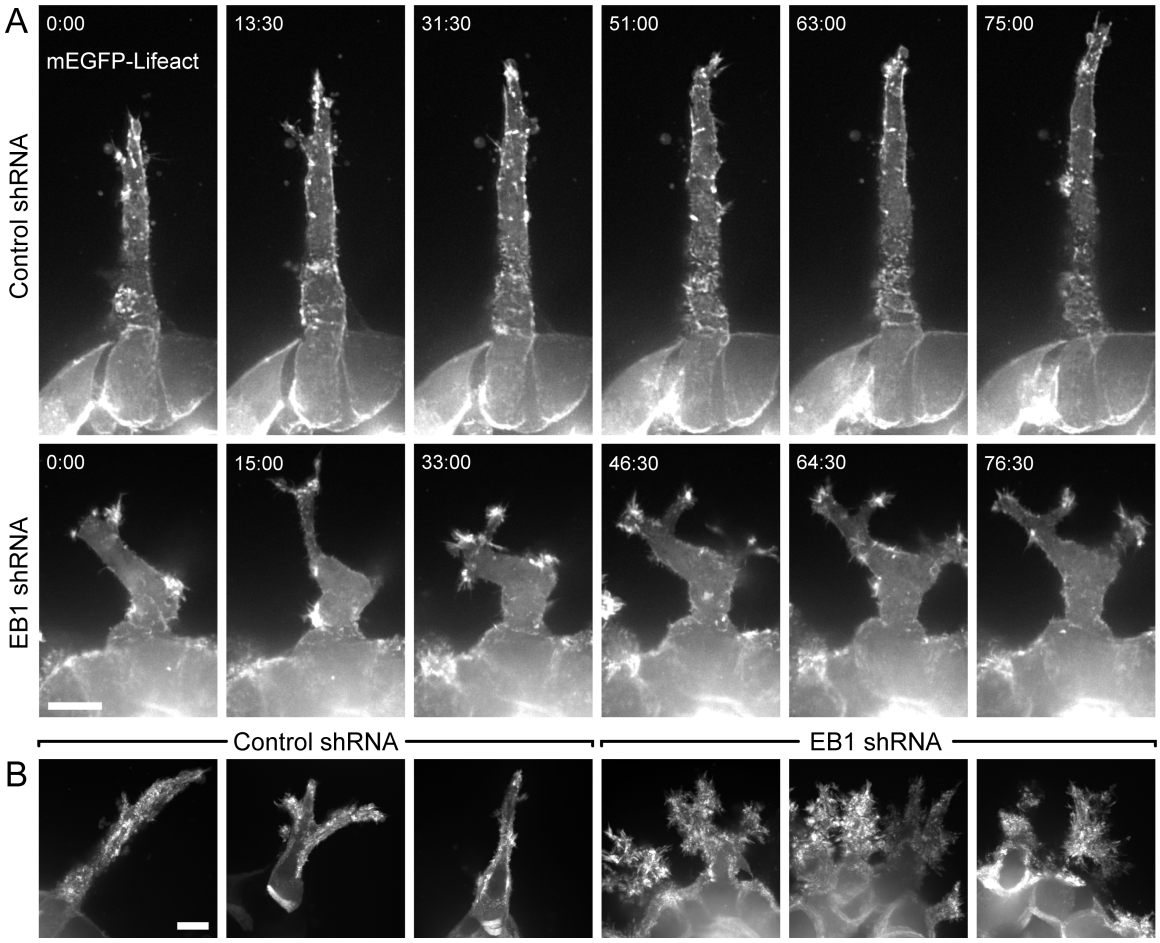

Figure 4.4. Uncoordinated protrusion dynamics in EB1-depleted cells. (A) mEGFP-Lifeact time-lapse sequences of HGF-induced extensions in control and EB1-depleted cysts. Each image is a maximum intensity projection of three optical sections (2 μm between sections) to compensate for cell movement out of the plane of focus. Elapsed time is in minutes:seconds. (B) Maximum intensity projection over two hour time-lapse sequences, which highlights increased and uncoordinated actin dynamics in EB1-depleted cells. Scale bars, 10 μm. See also Movie 6.

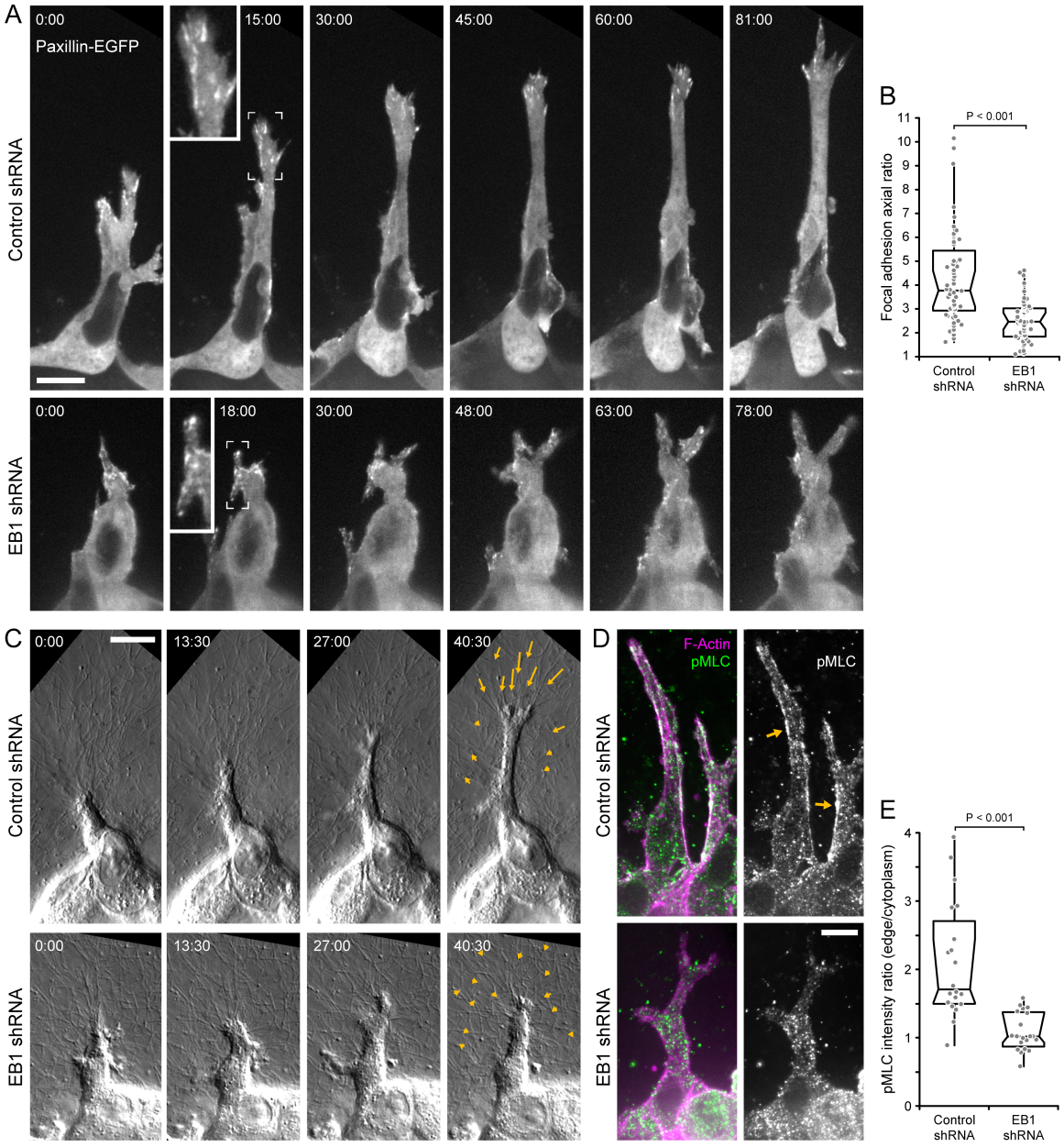

Figure 4.5. EB1 is required for productive interactions with the extracellular matrix. (A) Paxillin-EGFP time-lapse sequences of HGF-induced extensions in control and EB1-depleted cysts. Each image is a maximum intensity projection of three optical sections (1 μm between sections). Insets show higher magnification of indicated areas. (B) Axial ratio, defined as long divided by short axis, of focal adhesions in control and EB1-depleted extensions. The three longest adhesions were measured for each extension and each circle represents one adhesion (*n* = 60 adhesions in 20 cells). (C) DIC time-lapse sequences of HGF-induced extensions protruding into the surrounding fibrillar collagen matrix. Arrows indicate movement of fiduciary marks in the collagen between first and last frame shown. Elapsed time is indicated in minutes:seconds in (A) and (C). (D) pMLC

immunofluorescence in HGF-induced extensions. Each image is a maximum intensity projection of three optical sections (1 μm between sections). Arrows indicate pMLC staining along cortical actin cables in control cells. (E) Ratio of pMLC fluorescence intensity along cell extension edge and cytoplasm. (*n* = 20 cell extensions). See also Movies 7 and 8. Scale bars, 10 μm.

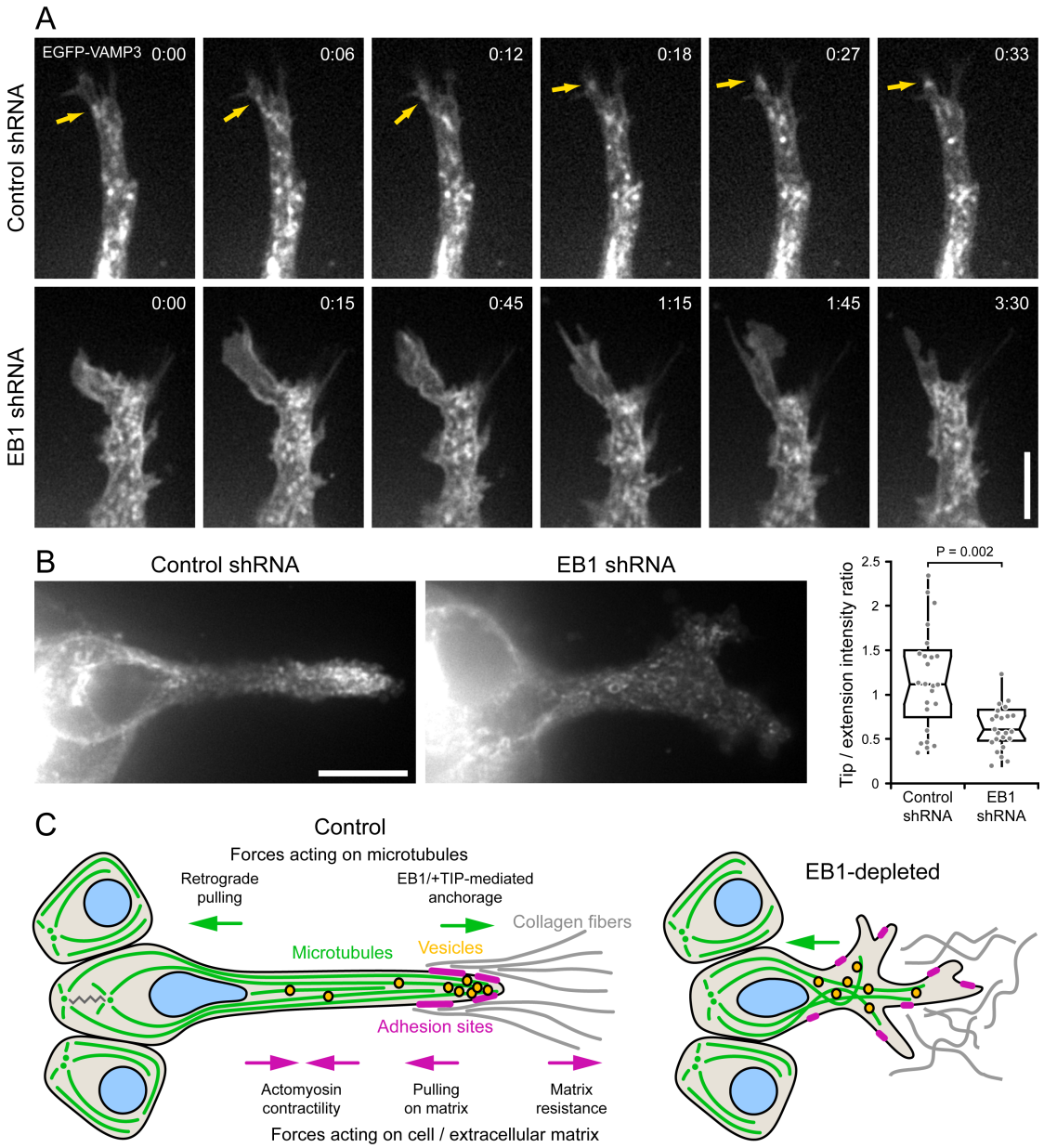

Figure 4.6. EB1 depletion disrupts VAMP3-positive vesicle trafficking to the extension tip. (A) EGFP-VAMP3 time-lapse sequences of control and EB1-depleted HGF-induced extensions. Faster time scale in control cell demonstrates the rapid movement of vesicles into the extension tip, while the membrane protrusion in the EB1-depleted cell remains vacant over a much longer time period. Arrows indicate vesicle movement into the extension tip. Elapsed time is indicated in minutes:seconds. Scale bar, 5 μm. (B) VAMP3-positive vesicles accumulate near the extension tip in control cells. The graph shows a quantification of the ratio of EGFP-VAMP3 fluorescence intensity near the extension tip and in the middle of the cell extension (*n* = 25 cells). Scale bar, 10 μm. (C) Model of EB1 contribution to cell migration in a 3D environment. EB1-

recruited +TIP complexes anchor and stabilize MTs along the HGF-induced cell extension, providing mechanical resistance to contractile forces in the cell body and establishing transport tracks toward the extension tip.

SUPPLEMENTAL MOVIES LIST

Movies can be viewed at http://dx.doi.org/10.1016/j.cub.2012.02.069

Movie 1. EB1-2xEGFP in 3D MDCK epithelial structures, related to Figure 4.1F. Left panel: Polarized cell; right panel: HGF-induced extension. Microtubules grow toward the basal domain in polarized cells. In HGF-induced extensions, microtubules persistently grow toward the extension tip, and often hit and sometimes deform the distal end of the extension. Images were acquired every 500 ms. The video plays at 12 frames s^{-1} and is thus accelerated 6 times.

Movie 2. Phase contrast time-lapse sequences of HGF-induced extension outgrowth, related to Figure 4.2C. Left panel: Control; right panel: EB1-depleted (shRNA#3) cells. Cell extensions and multicellular chains are shorter, more branched and retract more frequently in EB1-depleted cysts. Total length of sequence is 310 min. Images were acquired every 5 min. The video plays at 12 frames s^{-1} and is thus accelerated 3,600 times.

Movie 3. EGFP-α-tubulin at the basal surface of polarized cysts and HGF-induced extensions, related to supplemental Figure 4.S3A and B. Left panels: Control; right panels: EB1-depleted. Top: In EB1-depleted cysts, basal microtubules are curled and display rapid lateral movements consistent with cortical attachment defects. Bottom: HGF-induced extensions in EB1-depleted cysts display a decreased density of microtubules, and microtubules appear curled and laterally mobile. The total length of the sequence is ~4 min. Images were acquired every 10 s. The video plays at 12 frames s^{-1} and is thus accelerated 120 times.

Movie 4. EB1ΔC-2xEGFP in medial sections of polarized cysts, related to Figure 4.3A. Left panel: Control; right panel: EB1-depleted. Example of time-lapse sequences used for tracking of lateral microtubule growth. Microtubules grow toward the basal domain in both control and EB1-depleted cysts. However, growth is notably more erratic in EB1-depleted cells with frequent retrograde movements of growing microtubules. Images were acquired every 500 ms. The video plays at 12 frames s^{-1} and is thus accelerated 6 times.

Movie 5. EB1ΔC-2xGFP in HGF-induced extensions, related to Figure 4.3B,C. Left panel: Control; right panel: EB1-depleted. Example of time-lapse sequences used for tracking of microtubule growth. In the control, microtubules persistently grow to the tip of the cell. In the EB1-depleted cell, microtubule growth is disorganized and many microtubules show extensive retrograde movements. Examples of such retrograde movements are highlighted with colored dots. Images were acquired every 500 ms. The video plays at 12 frames s^{-1} and is thus accelerated 6 times.

Movie 6. mEGFP-Lifeact in HGF-induced extensions, related to Figure 4.4. Left panel: Control; right panel: EB1-depleted. The control extension persistently elongates with a small actin-rich lamellipodia-like protrusion at the tip. The EB1-depleted extension displays short-lived actin-rich protrusions all along extension, and multiple dynamic extension branches. Total length of sequence is 112.5 min. Images were acquired every 1.5 min. The video plays at 12 frames s^{-1} and is thus accelerated 1,080 times.

Movie 7. Paxillin-EGFP in HGF-induced extensions, related to Figure 4.5A. Left panel: Control; right panel: EB1-depleted. Focal adhesions form at the distal end of the control extension, elongate and turn over as the cell tip advances. Adhesions in EB1-depleted extensions remain small, are mislocalized, and fail to elongate and mature. Total length of the sequence is 195 min. Images were acquired every 3 min. The video plays at 12 frames s^{-1} and is thus accelerated 2,160 times.

Movie 8. DIC time-lapse sequences of HGF-induced extension dynamics and matrix interactions, related to Figure 4.5C. Left panel: Control; right panel: EB1-depleted. The control extension displays persistent outgrowth that correlates with pulling and alignment of collagen fibers. The EB1-depleted cell only weakly engages collagen fibers. Total length of sequence is 97.5 min. Images were acquired every 1.5 min. The video plays at 12 frames s^{-1} and is thus accelerated 1,080 times.

CONCLUSIONS

Epithelial remodeling, the transition from apical-basal cell polarity to migrational polarity, is an important, highly-regulated process that occurs in both normal development and disease. This complex cellular process involves the integration of chemical and mechanical signals from the extracellular environment, changes in intracellular signaling and modulation of gene expression and regulation. Ultimately the cell shape change and migration associated with epithelial remodeling is powered by the dynamic reorganization of the cytoskeleton. Although the field of cytoskeleton and cell migration biology research is large and ever growing, how the cytoskeleton functions and is regulated during the process of epithelial remodeling in a physiological 3D environment is poorly understood. Furthermore the burgeoning field of microtubule +TIPs research over the last decade has rapidly increased our understanding of how the microtubule cytoskeleton is regulated and functions in many different biological processes. I set out on this dissertation research project to investigate how microtubule cytoskeleton dynamics are controlled and contribute to 3D epithelial remodeling. Specifically, do EB1-recruited microtubule +TIP complexes play a role in this process?

In Chapter 1, a chapter we published in Methods In Enzymology, we describe the techniques and methods our lab uses to analyze microtubule dynamics in live cells (Gierke et al., 2010). This includes probes for visualizing dynamic microtubules, microscopy set-up and imaging techniques, and computational methods for analyzing microtubule dynamics. These methods

allow for a comprehensive quantitative analysis of microtubule cytoskeleton dynamics that I used as the underlying basis for the research in this dissertation.

Chapter 2 describes the work that I contributed to a project on the +TIP protein CLASP. The research done in the Wittmann lab on CLASP has strongly contributed to the understanding of how +TIPs interact with microtubules, microtubule plus ends and other intracellular structures. We have also described how CLASP-microtubule binding is regulated by the upstream kinase GSK3β, a finding that may shed light on how other +TIPs are regulated (Kumar et al., 2009; 2012; Kumar and Wittmann, 2012).

In Chapter 3, I describe the use of the MDCK tubulogenesis culture system as a model for epithelial remodeling. We adapted this culture model for high-resolution live-cell imaging of dynamic intracellular proteins. The spherical nature of the apical-basal polarized cysts allows for imaging of all areas of a polarized cell (apical, basal, transverse) in the xy plane, resulting in the best resolution images currently possible on conventional microscope systems. The culture model also allowed for the first time, direct comparison of apical-basal polarized cells and cells in the process of epithelial remodeling in a 3D extracellular matrix environment as described in Chapter 4.

Finally, Chapter 4 is the article published in Current Biology reporting our findings regarding the role of EB1-recruited +TIP complexes in 3D epithelial remodeling (Gierke and Wittmann, 2012). First we quantitatively describe microtubule organization and dynamics in apical-basal polarized cells and during HGF-induced epithelial remodeling. To test a role for +TIPs during epithelial

morphogenesis and remodeling we depleted the central +TIP adapter protein EB1 by lentiviral shRNA. We found that the microtubule cytoskeleton was disorganized and that microtubules underwent extensive retrograde movements, likely resulting from a lack of stabilization toward the leading edge, which was unique to the 3D environment. EB1 depletion did not seem to affect establishment of apical-basal polarity, but profoundly affected HGF-induced extension and migration. We demonstrate that EB1-recruited microtubule +TIP complexes are required to coordinate adhesion and protrusion dynamics, for productive engagement and remodeling of the extracellular matrix, and to form a dominant, productive protrusion. Furthermore, we found that VAMP-3 positive vesicle trafficking, potentially required for delivery of membrane, integrins or matrix metalloprotease transport to the leading edge, was disrupted in EB1-depleted cells likely because they lacked microtubule tracks.

There are still many outstanding questions to be answered. We found that VAMP-3 vesicle trafficking is disrupted EB1-depleted cells. Is this specific to VAMP-3 or is all vesicle trafficking affected? What is the cargo that is being mislocalized? The phenotypes we observed of reduced adhesion maturation and actomyosin contractility could be associated with a defect in integrin activation or recycling. Defective delivery and deposition of fibronectin to the basement membrane could prevent proper integrin activation (Jiang et al., 2000). Localization of the Rho GTPase Cdc42 to the leading edge of a migrating cell has been associated with membrane dynamics and delivery (Osmani et al., 2010), which may be disrupted in EB1 depleted cells. It will also be interesting to

determine what specific +TIPs other than EB1 are important in epithelial remodeling. Is it the ones we would expect to anchor MTs to the cortex, such as APC, ACF7, and CLASP? Or are there other functions of +TIPs besides microtubule stability that are contributing to the EB1-depletion phenotype? Finally, the observation that EB1-depletion did not affect apical-basal polarity but did disrupt remodeling suggests different roles for EB1 depending on cellular context. If EB1 is not required for epithelial maintenance but is required for migration, maybe EB1 could be a potential candidate for metastatic cancer therapy. EB1 overexpression has been associated with breast and colon cancers making it a novel candidate for a tumor biomarker (Sugihara et al., 2012; Dong et al., 2010). It will be interesting in the future to determine if other +TIPs are associated with diseases related to epithelial remodeling and to further understand the role of the diverse microtubule +TIP network.

REFERENCES

Abal, M., M. Piel, V. Bouckson-Castaing, M. Mogensen, J.-B. Sibarita, and M. Bornens. 2002. Microtubule release from the centrosome in migrating cells. *J. Cell Biol.* 159:731–737.

Achler, C., D. Filmer, C. Merte, and D. Drenckhahn. 1989. Role of microtubules in polarized delivery of apical membrane proteins to the brush border of the intestinal epithelium. *J. Cell Biol.* 109:179–189.

Affolter, M., R. Zeller, and E. Caussinus. 2009. Tissue remodelling through branching morphogenesis. *Nat Rev Mol Cell Biol*. 10:831–842.

Akhmanova, A., and M.O. Steinmetz. 2008. Tracking the ends: a dynamic protein network controls the fate of microtubule tips. *Nat Rev Mol Cell Biol*. 9:309–322.

Akhmanova, A., and M.O. Steinmetz. 2010. Microtubule +TIPs at a glance. *Journal of Cell Science*. 123:3415–3419.

Akhmanova, A., S.J. Stehbens, and A.S. Yap. 2009. Touch, grasp, deliver and control: functional cross-talk between microtubules and cell adhesions. *Traffic*. 10:268–274.

Al-Bassam, J., H. Kim, G. Brouhard, A. van Oijen, S.C. Harrison, and F. Chang. 2010. CLASP promotes microtubule rescue by recruiting tubulin dimers to the microtubule. *Developmental Cell*. 19:245–258.

Aldaz, H., L.M. Rice, T. Stearns, and D.A. Agard. 2005. Insights into microtubule nucleation from the crystal structure of human gamma-tubulin. *Nature*. 435:523–527.

Altinok, A., E. Kiris, A.J. Peck, S.C. Feinstein, L. Wilson, B.S. Manjunath, and K. Rose. 2007. Model based dynamics analysis in live cell microtubule images. *BMC Cell Biol.* 8 Suppl 1:S4.

Alves-Silva, J., N. Sánchez-Soriano, R. Beaven, M. Klein, J. Parkin, T.H. Millard, H.J. Bellen, K.J.T. Venken, C. Ballestrem, R.A. Kammerer, and A. Prokop. 2012. Spectraplakins promote microtubule-mediated axonal growth by functioning as structural microtubule-associated proteins and EB1-dependent +TIPs (tip interacting proteins). *J. Neurosci.* 32:9143–9158.

Andrews, P.D., Y. Ovechkina, N. Morrice, M. Wagenbach, K. Duncan, L. Wordeman, and J.R. Swedlow. 2004. Aurora B regulates MCAK at the mitotic centromere. *Developmental Cell*. 6:253–268.

Applegate, K.T., S. Besson, A. Matov, M.H. Bagonis, K. Jaqaman, and G. Danuser. 2011. plusTipTracker: Quantitative image analysis software for the measurement of microtubule dynamics. *J. Struct. Biol.* 176:168–184.

Bacallao, R., C. Antony, C. Dotti, E. Karsenti, E.H. Stelzer, and K. Simons. 1989. The subcellular organization of Madin-Darby canine kidney cells during the formation of a polarized epithelium. *J. Cell Biol.* 109:2817–2832.

Bamburg, J.R., D. Bray, and K. Chapman. 1986. Assembly of microtubules at the tip of growing axons. *Nature*. 321:788–790.

Barth, A.I.M., H.Y. Caro-Gonzalez, and W.J. Nelson. 2008. Role of adenomatous polyposis coli (APC) and microtubules in directional cell migration and neuronal polarization. *Semin. Cell Dev. Biol.* 19:245–251.

Bellett, G., J.M. Carter, J. Keynton, D. Goldspink, C. James, D.K. Moss, and M.M. Mogensen. 2009. Microtubule plus-end and minus-end capture at adherens junctions is involved in the assembly of apico-basal arrays in polarised epithelial cells. *Cell Motil. Cytoskeleton*. 66:893–908.

Bhanot, K., K.G. Young, and R. Kothary. 2011. MAP1B and clathrin are novel interacting partners of the giant cyto-linker dystonin. *J. Proteome Res.* 10:5118–5127.

Bieling, P., L. Laan, H. Schek, E.L. Munteanu, L. Sandblad, M. Dogterom, D. Brunner, and T. Surrey. 2007. Reconstitution of a microtubule plus-end tracking system in vitro. *Nature*. 450:1100–1105.

Bieling, P., S. Kandels-Lewis, I.A. Telley, J. van Dijk, C. Janke, and T. Surrey. 2008. CLIP-170 tracks growing microtubule ends by dynamically recognizing composite EB1/tubulin-binding sites. *J. Cell Biol.* 183:1223–1233.

Birkenfeld, J., P. Nalbant, S.-H. Yoon, and G.M. Bokoch. 2008. Cellular functions of GEF-H1, a microtubule-regulated Rho-GEF: is altered GEF-H1 activity a crucial determinant of disease pathogenesis? *Trends in Cell Biology*. 18:210–219.

Bogdanov, A.M., E.A. Bogdanova, D.M. Chudakov, T.V. Gorodnicheva, S. Lukyanov, and K.A. Lukyanov. 2009. Cell culture medium affects GFP photostability: a solution. *Nat Meth*. 6:859–860.

Bonetta, L. 2005. Microtubules shape the cell. *J. Cell Biol.* 169:553–553.

Bowen, J.R., D. Hwang, X. Bai, D. Roy, and E.T. Spiliotis. 2011. Septin GTPases spatially guide microtubule organization and plus end dynamics in polarizing epithelia. *J. Cell Biol.* 194:187–197.

Brandt, D.T., and R. Grosse. 2007. Get to grips: steering local actin dynamics with IQGAPs. *EMBO Rep.* 8:1019–1023.

Brangwynne, C.P., F.C. MacKintosh, and D.A. Weitz. 2007. Force fluctuations and polymerization dynamics of intracellular microtubules. *Proc. Natl. Acad. Sci. U.S.A.* 104:16128–16133.

Brangwynne, C.P., F.C. MacKintosh, S. Kumar, N.A. Geisse, J. Talbot, L. Mahadevan, K.K. Parker, D.E. Ingber, and D.A. Weitz. 2006. Microtubules can bear enhanced compressive loads in living cells because of lateral reinforcement. *J. Cell Biol.* 173:733–741.

Bré, M.H., R. Pepperkok, A.M. Hill, N. Levilliers, W. Ansorge, E.H. Stelzer, and E. Karsenti. 1990. Regulation of microtubule dynamics and nucleation during polarization in MDCK II cells. *J. Cell Biol.* 111:3013–3021.

Brouhard, G.J., J.H. Stear, T.L. Noetzel, J. Al-Bassam, K. Kinoshita, S.C. Harrison, J. Howard, and A.A. Hyman. 2008. XMAP215 is a processive microtubule polymerase. *Cell*. 132:79–88.

Bryant, D.M., and K.E. Mostov. 2008. From cells to organs: building polarized tissue. *Nat Rev Mol Cell Biol*. 9:887–901.

Bublik, D.R., M. Scolz, G. Triolo, M. Monte, and C. Schneider. 2010. Human GTSE-1 regulates p21(CIP1/WAF1) stability conferring resistance to paclitaxel treatment. *J. Biol. Chem.* 285:5274–5281.

Bulinski, J.C., D.J. Odde, B.J. Howell, T.D. Salmon, and C.M. Waterman-Storer. 2001. Rapid dynamics of the microtubule binding of ensconsin in vivo. *Journal of Cell Science*. 114:3885–3897.

Cai, Y., S. Qiu, X. Gao, S.-Z. Gu, and Z.-J. Liu. 2012. iASPP inhibits p53-independent apoptosis by inhibiting transcriptional activity of p63/p73 on promoters of proapoptotic genes. *Apoptosis*. 17:777–783.

Calderwood, D.A., S.J. Shattil, and M.H. Ginsberg. 2000. Integrins and actin filaments: reciprocal regulation of cell adhesion and signaling. *J. Biol. Chem.* 275:22607–22610.

Cassimeris, L. 2002. The oncoprotein 18/stathmin family of microtubule destabilizers. *Current Opinion in Cell Biology*. 14:18–24.

Caswell, P.T., M. Chan, A.J. Lindsay, M.W. McCaffrey, D. Boettiger, and J.C. Norman. 2008. Rab-coupling protein coordinates recycling of 5 1 integrin and EGFR1 to promote cell migration in 3D microenvironments. *J. Cell Biol.* 183:143–155.

Chang, Y.-C., P. Nalbant, J. Birkenfeld, Z.-F. Chang, and G.M. Bokoch. 2008. GEF-H1 couples nocodazole-induced microtubule disassembly to cell contractility via RhoA. *Mol. Biol. Cell*. 19:2147–2153.

Chiron, S., A. Bobkova, H. Zhou, and M.P. Yaffe. 2008. CLASP regulates mitochondrial distribution in Schizosaccharomyces pombe. *J. Cell Biol.* 182:41–49.

Cohen, D. 2004. Mammalian PAR-1 determines epithelial lumen polarity by organizing the microtubule cytoskeleton. *J. Cell Biol.* 164:717–727.

Conde, C., and A. Cáceres. 2009. Microtubule assembly, organization and dynamics in axons and dendrites. *Nat. Rev. Neurosci.* 10:319–332.

de Forges, H., A. Bouissou, and F. Perez. 2012. Interplay between microtubule dynamics and intracellular organization. *Int. J. Biochem. Cell Biol.* 44:266–274.

De Groot, C.O., I. Jelesarov, F.F. Damberger, S. Bjelic, M.A. Schärer, N.S. Bhavesh, I. Grigoriev, R.M. Buey, K. Wüthrich, G. Capitani, A. Akhmanova, and M.O. Steinmetz. 2010. Molecular insights into mammalian end-binding protein heterodimerization. *J. Biol. Chem.* 285:5802–5814..

Dehmelt, L., and S. Halpain. 2005. The MAP2/Tau family of microtubule-associated proteins. *Genome Biol.* 6:204.

Di Marco, V.B., and G.G. Bombi. 2001. Mathematical functions for the representation of chromatographic peaks. *J Chromatogr A*. 931:1–30.

Dimitrov, A., M. Quesnoit, S. Moutel, I. Cantaloube, C. Poüs, and F. Perez. 2008. Detection of GTP-tubulin conformation in vivo reveals a role for GTP remnants in microtubule rescues. *Science*. 322:1353–1356.

Dixit, R., B. Barnett, J.E. Lazarus, M. Tokito, Y.E. Goldman, and E.L.F. Holzbaur. 2009. Microtubule plus-end tracking by CLIP-170 requires EB1. *Proc. Natl. Acad. Sci. U.S.A.* 106:492–497.

Dogterom, M., J.W.J. Kerssemakers, G. Romet-Lemonne, and M.E. Janson. 2005. Force generation by dynamic microtubules. *Current Opinion in Cell Biology*. 17:67–74.

Dong, X., F. Liu, L. Sun, M. Liu, D. Li, D. Su, Z. Zhu, J.-T. Dong, L. Fu, and J. Zhou. 2010. Oncogenic function of microtubule end-binding protein 1 in breast cancer. *J. Pathol.* 220:361–369.

Doyle, A.D., F.W. Wang, K. Matsumoto, and K.M. Yamada. 2009. One-dimensional topography underlies three-dimensional fibrillar cell migration. *J. Cell Biol.* 184:481–490.

Drabek, K., M. van Ham, T. Stepanova, K. Draegestein, R. van Horssen, C.L. Sayas, A. Akhmanova, T. Ten Hagen, R. Smits, R. Fodde, F. Grosveld, and N. Galjart. 2006. Role of CLASP2 in microtubule stabilization and the regulation of persistent motility. *Current Biology*. 16:2259–2264.

Dragestein, K.A., W.A. van Cappellen, J. van Haren, G.D. Tsibidis, A. Akhmanova, T.A. Knoch, F. Grosveld, and N. Galjart. 2008. Dynamic behavior of GFP-CLIP-170 reveals fast protein turnover on microtubule plus ends. *J. Cell Biol.* 180:729–737.

Drenckhahn, D., and R. Dermietzel. 1988. Organization of the actin filament cytoskeleton in the intestinal brush border: a quantitative and qualitative immunoelectron microscope study. *J. Cell Biol.* 107:1037–1048.

Duband, J.-L. 2010. Diversity in the molecular and cellular strategies of epithelium-to-mesenchyme transitions: Insights from the neural crest. *Cell Adh Migr*. 4:458–482.

Dupin, I., and S. Etienne-Manneville. 2011. Nuclear positioning: mechanisms and functions. *Int. J. Biochem. Cell Biol.* 43:1698–1707.

Efimov, A., A. Kharitonov, N. Efimova, J. Loncarek, P.M. Miller, N. Andreyeva, P. Gleeson, N. Galjart, A.R.R. Maia, and I.X. McLeod. 2007. Asymmetric CLASP-Dependent Nucleation of Noncentrosomal Microtubules at the trans-Golgi Network. *Developmental Cell*. 12:917–930.

Etienne-Manneville, S. 2004. Actin and microtubules in cell motility: which one is in control? *Traffic*. 5:470–477.

Etienne-Manneville, S. 2009. APC in cell migration. *Adv. Exp. Med. Biol.* 656:30–40.

Etienne-Manneville, S. 2012. Adherens junctions during cell migration. *Subcell. Biochem.* 60:225–249.

Etienne-Manneville, S., J.-B. Manneville, S. Nicholls, M.A. Ferenczi, and A. Hall. 2005. Cdc42 and Par6-PKCzeta regulate the spatially localized association of Dlg1 and APC to control cell polarization. *J. Cell Biol.* 170:895–901.

Even-Ram, S., and K.M. Yamada. 2005. Cell migration in 3D matrix. *Current Opinion in Cell Biology*. 17:524–532.

Ferenz, N.P., A. Gable, and P. Wadsworth. 2010. Mitotic functions of kinesin-5. *Semin. Cell Dev. Biol.* 21:255–259.

Feske, S., C. Picard, and A. Fischer. 2010. Immunodeficiency due to mutations in ORAI1 and STIM1. *Clin. Immunol.* 135:169–182.

Fischer, R.S., M. Gardel, X. Ma, R.S. Adelstein, and C.M. Waterman. 2009. Local cortical tension by myosin II guides 3D endothelial cell branching. *Curr. Biol.* 19:260–265.

Folker, E.S., B.M. Baker, and H.V. Goodson. 2005. Interactions between CLIP-170, tubulin, and microtubules: implications for the mechanism of Clip-170 plus-end tracking behavior. *Mol. Biol. Cell*. 16:5373–5384.

Fong, K.-W., S.-Y. Hau, Y.-S. Kho, Y. Jia, L. He, and R.Z. Qi. 2009. Interaction of CDK5RAP2 with EB1 to track growing microtubule tips and to regulate microtubule dynamics. *Mol. Biol. Cell*. 20:3660–3670.

Friedl, P., E. Sahai, S. Weiss, and K.M. Yamada. 2012. New dimensions in cell migration. *Nat Rev Mol Cell Biol*.

Galjart, N. 2010. Plus-end-tracking proteins and their interactions at microtubule ends. *Curr. Biol.* 20:R528–37.

Gardner, M.K., M. Zanic, C. Gell, V. Bormuth, and J. Howard. 2011. Depolymerizing kinesins Kip3 and MCAK shape cellular microtubule architecture by differential control of catastrophe. *Cell*. 147:1092–1103.

Geiger, B., and K.M. Yamada. 2011. Molecular architecture and function of matrix adhesions. *Cold Spring Harb Perspect Biol*. 3.

Geraldo, S., A. Simon, N. Elkhatib, D. Louvard, L. Fetler, and D.M. Vignjevic. 2012. Do cancer cells have distinct adhesions in 3D collagen matrices and in vivo? *Eur J Cell Biol*. 91:930–937.

Gierke, S., and T. Wittmann. 2012. EB1-recruited microtubule +TIP complexes coordinate protrusion dynamics during 3D epithelial remodeling. *Curr. Biol.* 22:753–762.

Gierke, S., P. Kumar, and T. Wittmann. 2010. Analysis of microtubule polymerization dynamics in live cells. *Methods Cell Biol.* 97:15–33.

Goldman, R.D. 1971. The role of three cytoplasmic fibers in BHK-21 cell motility. I. Microtubules and the effects of colchicine. *J. Cell Biol.* 51:752–762.

Goriounov, D., C.L. Leung, and R.K.H. Liem. 2003. Protein products of human Gas2-related genes on chromosomes 17 and 22 (hGAR17 and hGAR22) associate with both microfilaments and microtubules. *Journal of Cell Science*. 116:1045–1058.

Gotlieb, A.I., L. Subrahmanyan, and V.I. Kalnins. 1983. Microtubule-organizing centers and cell migration: effect of inhibition of migration and microtubule disruption in endothelial cells. *J. Cell Biol.* 96:1266–1272.

Grigoriev, I., S.M. Gouveia, B. van der Vaart, J. Demmers, J.T. Smyth, S. Honnappa, D. Splinter, M.O. Steinmetz, J.W. Putney, C.C. Hoogenraad, and A. Akhmanova. 2008. STIM1 is a MT-plus-end-tracking protein involved in remodeling of the ER. *Current Biology*. 18:177–182.

Grohmann, A., K. Tanneberger, A. Alzner, J. Schneikert, and J. Behrens. 2007. AMER1 regulates the distribution of the tumor suppressor APC between microtubules and the plasma membrane. *Journal of Cell Science*. 120:3738–3747.

Gundersen, G.G., E.R. Gomes, and Y. Wen. 2004. Cortical control of microtubule stability and polarization. *Current Opinion in Cell Biology*. 16:106–112.

Hadjidemetriou, S., D. Toomre, and J. Duncan. 2008. Motion tracking of the outer tips of microtubules. *Med Image Anal*. 12:689–702.

Hammond, J.W., D. Cai, and K.J. Verhey. 2008. Tubulin modifications and their cellular functions. *Current Opinion in Cell Biology*. 20:71–76.

Harunaga, J.S., and K.M. Yamada. 2011. Cell-matrix adhesions in 3D. *Matrix Biology*. 30:363–368.

Haynes, J., J. Srivastava, N. Madson, T. Wittmann, and D.L. Barber. 2011. Dynamic actin remodeling during epithelial-mesenchymal transition depends on increased moesin expression. *Mol. Biol. Cell*. 22:4750–4764.

Heck, J.N., S.M. Ponik, M.G. Garcia-Mendoza, C.A. Pehlke, D.R. Inman, K.W. Eliceiri, and P.J. Keely. 2012. Microtubules regulate GEF-H1 in response to extracellular matrix stiffness. *Mol. Biol. Cell*. 23:2583–2592.

Hertzer, K.M., and C.E. Walczak. 2008. The C-termini of tubulin and the specific geometry of tubulin substrates influence the depolymerization activity of MCAK. *Cell Cycle*. 7:2727–2737.

Honnappa, S., C.M. John, D. Kostrewa, F.K. Winkler, and M.O. Steinmetz. 2005. Structural insights into the EB1-APC interaction. *EMBO J.* 24:261–269.

Honnappa, S., S.M. Gouveia, A. Weisbrich, F.F. Damberger, N.S. Bhavesh, H. Jawhari, I. Grigoriev, F.J.A. van Rijssel, R.M. Buey, A. Lawera, I. Jelesarov, F.K. Winkler, K. Wüthrich, A. Akhmanova, and M.O. Steinmetz. 2009. An EB1-binding motif acts as a microtubule tip localization signal. *Cell*. 138:366–376.

Hotta, A., T. Kawakatsu, T. Nakatani, T. Sato, C. Matsui, T. Sukezane, T. Akagi, T. Hamaji, I. Grigoriev, A. Akhmanova, Y. Takai, and Y. Mimori-Kiyosue. 2010. Laminin-based cell adhesion anchors microtubule plus ends to the epithelial cell basal cortex through LL5alpha/beta. *J. Cell Biol.* 189:901–917.

Houlden, H., J. Johnson, C. Gardner-Thorpe, T. Lashley, D. Hernandez, P. Worth, A.B. Singleton, D.A. Hilton, J. Holton, T. Revesz, M.B. Davis, P. Giunti, P. Giunti, and N.W. Wood. 2007. Mutations in TTBK2, encoding a kinase implicated in tau phosphorylation, segregate with spinocerebellar ataxia type 11. *Nat. Genet.* 39:1434–1436.

Howard, J., and A.A. Hyman. 2007. Microtubule polymerases and depolymerases. *Current Opinion in Cell Biology*. 19:31–35.

Hsieh, P.-C., J.-C. Chang, W.-T. Sun, S.-C. Hsieh, M.-C. Wang, and F.-F. Wang. 2007. p53 downstream target DDA3 is a novel microtubule-associated protein that interacts with end-binding protein EB3 and activates beta-catenin pathway. *Oncogene*. 26:4928–4940.

Hyman, A., D. Drechsel, D. Kellogg, S. Salser, K. Sawin, P. Steffen, L. Wordeman, and T. Mitchison. 1991. Preparation of modified tubulins. *Meth. Enzymol.* 196:478–485.

Inoué, S., and E.D. Salmon. 1995. Force generation by microtubule assembly/disassembly in mitosis and related movements. *Mol. Biol. Cell*. 6:1619–1640.

Jang, C.-Y., J. Wong, J.A. Coppinger, A. Seki, J.R. Yates, and G. Fang. 2008. DDA3 recruits microtubule depolymerase Kif2a to spindle poles and controls spindle dynamics and mitotic chromosome movement. *J. Cell Biol.* 181:255–267.

Janke, C., and M. Kneussel. 2010. Tubulin post-translational modifications: encoding functions on the neuronal microtubule cytoskeleton. *Trends Neurosci.* 33:362–372.

Jaqaman, K., D. Loerke, M. Mettlen, H. Kuwata, S. Grinstein, S.L. Schmid, and G. Danuser. 2008. Robust single-particle tracking in live-cell time-lapse sequences. *Nat Meth*. 5:695–702.

Jaulin, F., and G. Kreitzer. 2010. KIF17 stabilizes microtubules and contributes to epithelial morphogenesis by acting at MT plus ends with EB1 and APC. *J. Cell Biol.* 190:443–460.

Jaulin, F., X. Xue, E. Rodriguez-Boulan, and G. Kreitzer. 2007. Polarization-Dependent Selective Transport to the Apical Membrane by KIF5B in MDCK Cells. *Developmental Cell*. 13:511–522.

Jaworski, J., L.C. Kapitein, S.M. Gouveia, B.R. Dortland, P.S. Wulf, I. Grigoriev, P. Camera, S.A. Spangler, P. Di Stefano, J. Demmers, H. Krugers, P. Defilippi, A. Akhmanova, and C.C. Hoogenraad. 2009. Dynamic microtubules regulate dendritic spine morphology and synaptic plasticity. *Neuron*. 61:85–100.

Jiang, K., and A. Akhmanova. 2011. Microtubule tip-interacting proteins: a view from both ends. *Current Opinion in Cell Biology*. 23:94–101.

Jiang, K., G. Toedt, S.M. Gouveia, N.E. Davey, S. Hua, B. van der Vaart, I. Grigoriev, J. Larsen, L.B. Pedersen, K. Bezstarosti, M. Lince-Faria, J. Demmers, M.O. Steinmetz, T.J. Gibson, and A. Akhmanova. 2012. A Proteome-wide Screen for Mammalian SxIP Motif-Containing Microtubule Plus-End Tracking Proteins. *Current Biology*. 22:1800–1807.

Jiang, K., J. Wang, J. Liu, T. Ward, L. Wordeman, A. Davidson, F. Wang, and X. Yao. 2009. TIP150 interacts with and targets MCAK at the microtubule plus ends. *EMBO Rep.* 10:857–865.

Jiang, S.T., W.J. Chuang, and M.J. Tang. 2000. Role of fibronectin deposition in branching morphogenesis of Madin-Darby canine kidney cells. *Kidney Int.* 57:1860–1867.

Kalluri, R., and R.A. Weinberg. 2009. The basics of epithelial-mesenchymal transition. *J. Clin. Invest.* 119:1420–1428.

Kaverina, I., and A. Straube. 2011. Regulation of cell migration by dynamic microtubules. *Semin. Cell Dev. Biol.* 22:968–974.

Kean, M.J., K.C. Williams, M. Skalski, D. Myers, A. Burtnik, D. Foster, and M.G. Coppolino. 2009. VAMP3, syntaxin-13 and SNAP23 are involved in secretion of matrix metalloproteinases, degradation of the extracellular matrix and cell invasion. *Journal of Cell Science*. 122:4089–4098.

Kerssemakers, J.W.J., E.L. Munteanu, L. Laan, T.L. Noetzel, M.E. Janson, and M. Dogterom. 2006. Assembly dynamics of microtubules at molecular resolution. *Nature*. 442:709–712.

Kim, A., and W. Matthew Petroll. 2007. Microtubule regulation of corneal fibroblast morphology and mechanical activity in 3-D culture. *Exp. Eye Res.* 85:546–556.

Kirschner, M.W., and T. Mitchison. 1986. Microtubule dynamics. *Nature*. 324:621.

Kita, K., T. Wittmann, I.S. Näthke, and C.M. Waterman-Storer. 2006. Adenomatous polyposis coli on microtubule plus ends in cell extensions can promote microtubule net growth with or without EB1. *Mol. Biol. Cell*. 17:2331–2345.

Kodama, A., I. Karakesisoglou, E. Wong, A. Vaezi, and E. Fuchs. 2003. ACF7: an essential integrator of microtubule dynamics. *Cell*. 115:343–354.

Kollman, J.M., J.K. Polka, A. Zelter, T.N. Davis, and D.A. Agard. 2010. Microtubule nucleating gamma-TuSC assembles structures with 13-fold microtubule-like symmetry. *Nature*. 466:879–882.

Komarova, Y., C.O. De Groot, I. Grigoriev, S.M. Gouveia, E.L. Munteanu, J.M. Schober, S. Honnappa, R.M. Buey, C.C. Hoogenraad, M. Dogterom, G.G. Borisy, M.O. Steinmetz, and A. Akhmanova. 2009. Mammalian end binding proteins control persistent microtubule growth. *J. Cell Biol.* 184:691–706.

Komarova, Y.A., A.S. Akhmanova, S.-I. Kojima, N. Galjart, and G.G. Borisy. 2002. Cytoplasmic linker proteins promote microtubule rescue in vivo. *J. Cell Biol.* 159:589–599.

Kreitzer, G., J. Schmoranzer, S.H. Low, X. Li, Y. Gan, T. Weimbs, S.M. Simon, and E. Rodriguez-Boulan. 2003. Three-dimensional analysis of post-Golgi carrier exocytosis in epithelial cells. *Nat Cell Biol*. 5:126–136.

Krendel, M., F.T. Zenke, and G.M. Bokoch. 2002. Nucleotide exchange factor GEF-H1 mediates cross-talk between microtubules and the actin cytoskeleton. *Nat Cell Biol*. 4:294–301.

Krylyshkina, O., K.I. Anderson, I. Kaverina, I. Upmann, D.J. Manstein, J.V. Small, and D.K. Toomre. 2003. Nanometer targeting of microtubules to focal adhesions. *J. Cell Biol.* 161:853–859.

Kueh, H.Y., and T.J. Mitchison. 2009. Structural plasticity in actin and tubulin polymer dynamics. *Science*. 325:960–963.

Kuijpers, M., and C.C. Hoogenraad. 2011. Centrosomes, microtubules and neuronal development. *Mol. Cell. Neurosci.* 48:349–358.

Kumar, P., and T. Wittmann. 2012. +TIPs: SxIPping along microtubule ends. *Trends in Cell Biology*. 22:418–428.

Kumar, P., K.S. Lyle, S. Gierke, A. Matov, G. Danuser, and T. Wittmann. 2009. GSK3beta phosphorylation modulates CLASP-microtubule association and lamella microtubule attachment. *J. Cell Biol.* 184:895–908.

Kumar, P., M.S. Chimenti, H. Pemble, A. Schönichen, O. Thompson, M.P. Jacobson, and T. Wittmann. 2012. Multisite phosphorylation disrupts arginine-glutamate salt bridge networks required for binding of cytoplasmic linker-associated protein 2 (CLASP2) to end-binding protein 1 (EB1). *J. Biol. Chem.* 287:17050–17064.

Kwon, S.-H., P.I. Nedvetsky, and K.E. Mostov. 2011. Transcriptional profiling identifies TNS4 function in epithelial tubulogenesis. *Curr. Biol.* 21:161–166.

Laht, P., K. Pill, E. Haller, and A. Veske. 2012. Plexin-B3 interacts with EB-family proteins through a conserved motif. *Biochim. Biophys. Acta*. 1820:888–893.

Lampert, F., P. Hornung, and S. Westermann. 2010. The Dam1 complex confers microtubule plus end-tracking activity to the Ndc80 kinetochore complex. *J. Cell Biol.* 189:641–649.

Lansbergen, G., I. Grigoriev, Y. Mimori-Kiyosue, T. Ohtsuka, S. Higa, I. Kitajima, J. Demmers, N. Galjart, A.B. Houtsmuller, F. Grosveld, and A. Akhmanova. 2006. CLASPs attach microtubule plus ends to the cell cortex through a complex with LL5beta. *Developmental Cell*. 11:21–32.

Lantieri, F., J.T. Glessner, H. Hakonarson, J. Elia, and M. Devoto. 2010. Analysis of GWAS top hits in ADHD suggests association to two polymorphisms located in genes expressed in the cerebellum. *Am. J. Med. Genet. B Neuropsychiatr. Genet.* 153B:1127–1133.

Lechler, T., and E. Fuchs. 2007. Desmoplakin: an unexpected regulator of microtubule organization in the epidermis. *J. Cell Biol.* 176:147–154.

Leroy, P., and K.E. Mostov. 2007. Slug is required for cell survival during partial epithelial-mesenchymal transition of HGF-induced tubulogenesis. *Mol. Biol. Cell*. 18:1943–1952.

Li, W., T. Miki, T. Watanabe, M. Kakeno, I. Sugiyama, K. Kaibuchi, and G. Goshima. 2011. EB1 promotes microtubule dynamics by recruiting Sentin in Drosophila cells. *J. Cell Biol.* 193:973–983.

Li, W., T. Moriwaki, T. Tani, T. Watanabe, K. Kaibuchi, and G. Goshima. 2012. Reconstitution of dynamic microtubules with Drosophila XMAP215, EB1, and Sentin. *J. Cell Biol.* 199:849–862.

Liao, G., T. Nagasaki, and G.G. Gundersen. 1995. Low concentrations of nocodazole interfere with fibroblast locomotion without significantly affecting microtubule level: implications for the role of dynamic microtubules in cell locomotion. *Journal of Cell Science*. 108 (Pt 11):3473–3483.

Liu, X.S., H. Li, B. Song, and X. Liu. 2010. Polo-like kinase 1 phosphorylation of G2 and S-phase-expressed 1 protein is essential for p53 inactivation during G2 checkpoint recovery. *EMBO Rep.* 11:626–632.

Lomakin, A.J., I. Semenova, I. Zaliapin, P. Kraikivski, E. Nadezhdina, B.M. Slepchenko, A. Akhmanova, and V. Rodionov. 2009. CLIP-170-dependent capture of membrane organelles by microtubules initiates minus-end directed transport. *Developmental Cell*. 17:323–333.

Luo, J., Z.-L. Deng, X. Luo, N. Tang, W.-X. Song, J. Chen, K.A. Sharff, H.H. Luu, R.C. Haydon, K.W. Kinzler, B. Vogelstein, and T.-C. He. 2007. A protocol for rapid generation of recombinant adenoviruses using the AdEasy system. *Nat Protoc*. 2:1236–1247.

Ma, H., Q. Cai, W. Lu, Z.-H. Sheng, and S. Mochida. 2009. KIF5B motor adaptor syntabulin maintains synaptic transmission in sympathetic neurons. *J. Neurosci.* 29:13019–13029.

Martins, G.G., and J. Kolega. 2012. A role for microtubules in endothelial cell protrusion in three-dimensional matrices. *Biology of the Cell*. 104:271–286.

Martín-Belmonte, F., A. Gassama, A. Datta, W. Yu, U. Rescher, V. Gerke, and K. Mostov. 2007. PTEN-mediated apical segregation of phosphoinositides controls epithelial morphogenesis through Cdc42. *Cell*. 128:383–397.

Martín-Belmonte, F., and K. Mostov. 2007. Phosphoinositides control epithelial development. *Cell Cycle*. 6:1957–1961.

Martínez-López, M.J., S. Alcántara, C. Mascaró, F. Pérez-Brangulí, P. Ruiz-Lozano, T. Maes, E. Soriano, and C. Buesa. 2005. Mouse neuron navigator 1, a novel microtubule-associated protein involved in neuronal migration. *Mol. Cell. Neurosci.* 28:599–612.

Maruthamuthu, V., B. Sabass, U.S. Schwarz, and M.L. Gardel. 2011. Cell-ECM traction force modulates endogenous tension at cell-cell contacts. *Proc. Natl. Acad. Sci. U.S.A.* 108:4708–4713.

Maruthamuthu, V., Y. Aratyn-Schaus, and M.L. Gardel. 2010. Conserved F-actin dynamics and force transmission at cell adhesions. *Current Opinion in Cell Biology*. 22:583–588.

Matenia, D., and E.-M. Mandelkow. 2009. The tau of MARK: a polarized view of the cytoskeleton. *Trends in Biochemical Sciences*. 34:332–342.

Matov, A., K. Applegate, P. Kumar, C. Thoma, W. Krek, G. Danuser, and T. Wittmann. 2010. Analysis of microtubule dynamic instability using a plus-end growth marker. *Nat Meth*. 7:761–768.

Matsumoto, S., K. Fumoto, T. Okamoto, K. Kaibuchi, and A. Kikuchi. 2010. Binding of APC and dishevelled mediates Wnt5a-regulated focal adhesion dynamics in migrating cells. *EMBO J.* 29:1192–1204.

Maurer, S.P., F.J. Fourniol, G. Bohner, C.A. Moores, and T. Surrey. 2012. EBs Recognize a Nucleotide-Dependent Structural Cap at Growing Microtubule Ends. *Cell*. 149:371–382.

Maurer, S.P., P. Bieling, J. Cope, A. Hoenger, and T. Surrey. 2011. GTPgammaS microtubules mimic the growing microtubule end structure recognized by end-binding proteins (EBs). *Proc. Natl. Acad. Sci. U.S.A.* 108:3988–3993.

Megraw, T.L., J.T. Sharkey, and R.S. Nowakowski. 2011. Cdk5rap2 exposes the centrosomal root of microcephaly syndromes. *Trends in Cell Biology*. 21:470–480.

Meireles, A.M., N.S. Dzhindzhev, and H. Ohkura. 2011. Kebab: kinetochore and EB1 associated basic protein that dynamically changes its localisation during Drosophila mitosis. *PLoS ONE*. 6:e24174.

Mellman, I., and W.J. Nelson. 2008. Coordinated protein sorting, targeting and distribution in polarized cells. *Nat Rev Mol Cell Biol*. 9:833–845.

Meng, W., Y. Mushika, T. Ichii, and M. Takeichi. 2008. Anchorage of Microtubule Minus Ends to Adherens Junctions Regulates Epithelial Cell-Cell Contacts. *Cell*. 135:948–959.

Meyer, A.S., S.K. Hughes-Alford, J.E. Kay, A. Castillo, A. Wells, F.B. Gertler, and D.A. Lauffenburger. 2012. 2D protrusion but not motility predicts growth factor–induced cancer cell migration in 3D collagen. *jcb.rupress.org*.

Mège, R.-M., J. Gavard, and M. Lambert. 2006. Regulation of cell–cell junctions by the cytoskeleton. *Current Opinion in Cell Biology*. 18:541–548.

Miller, P.M., A.W. Folkmann, A.R.R. Maia, N. Efimova, A. Efimov, and I. Kaverina. 2009. Golgi-derived CLASP-dependent microtubules control Golgi organization and polarized trafficking in motile cells. *Nat Cell Biol*. 11:1069–1080.

Mimori-Kiyosue, Y. 2011. Shaping microtubules into diverse patterns: molecular connections for setting up both ends. *Cytoskeleton (Hoboken)*. 68:603–618.

Mimori-Kiyosue, Y., I. Grigoriev, G. Lansbergen, H. Sasaki, C. Matsui, F. Severin, N. Galjart, F. Grosveld, I. Vorobjev, S. Tsukita, and A. Akhmanova. 2005. CLASP1 and CLASP2 bind to EB1 and regulate microtubule plus-end dynamics at the cell cortex. *J. Cell Biol.* 168:141–153.

Mimori-Kiyosue, Y., N. Shiina, and S. Tsukita. 2000. Adenomatous polyposis coli (APC) protein moves along microtubules and concentrates at their growing ends in epithelial cells. *J. Cell Biol.* 148:505–518.

Mitchison, T., and M. Kirschner. 1984. Dynamic instability of microtubule growth. *Nature*. 312:237–242.

Moffat, J., D.A. Grueneberg, X. Yang, S.Y. Kim, A.M. Kloepfer, G. Hinkle, B. Piqani, T.M. Eisenhaure, B. Luo, J.K. Grenier, A.E. Carpenter, S.Y. Foo, S.A. Stewart, B.R. Stockwell, N. Hacohen, W.C. Hahn, E.S. Lander, D.M. Sabatini, and D.E. Root. 2006. A lentiviral RNAi library for human and mouse genes applied to an arrayed viral high-content screen. *Cell*. 124:1283–1298.

Mogensen, M.M., A. Malik, M. Piel, V. Bouckson-Castaing, and M. Bornens. 2000. Microtubule minus-end anchorage at centrosomal and non-centrosomal sites: the role of ninein. *Journal of Cell Science*. 113 (Pt 17):3013–3023.

Montenegro Gouveia, S., K. Leslie, L.C. Kapitein, R.M. Buey, I. Grigoriev, M. Wagenbach, I. Smal, E. Meijering, C.C. Hoogenraad, L. Wordeman, M.O. Steinmetz, and A. Akhmanova. 2010. In vitro reconstitution of the functional interplay between MCAK and EB3 at microtubule plus ends. *Curr. Biol.* 20:1717–1722.

Montenegro-Venegas, C., E. Tortosa, S. Rosso, D. Peretti, F. Bollati, M. Bisbal, I. Jausoro, J. Avila, A. Cáceres, and C. Gonzalez-Billault. 2010. MAP1B regulates axonal development by modulating Rho-GTPase Rac1 activity. *Mol. Biol. Cell*. 21:3518–3528.

Moore, A.T., K.E. Rankin, G. von Dassow, L. Peris, M. Wagenbach, Y. Ovechkina, A. Andrieux, D. Job, and L. Wordeman. 2005. MCAK associates with the tips of polymerizing microtubules. *J. Cell Biol.* 169:391–397.

Moores, C.A., M. Perderiset, C. Kappeler, S. Kain, D. Drummond, S.J. Perkins, J. Chelly, R. Cross, A. Houdusse, and F. Francis. 2006. Distinct roles of doublecortin modulating the microtubule cytoskeleton. *EMBO J.* 25:4448–4457.

Moss, D.K., G. Bellett, J.M. Carter, M. Liovic, J. Keynton, A.R. Prescott, E.B. Lane, and M.M. Mogensen. 2007. Ninein is released from the centrosome and moves bi-directionally along microtubules. *Journal of Cell Science*. 120:3064–3074.

Müsch, A. 2004. Microtubule organization and function in epithelial cells. *Traffic*. 5:1–9.

Myers, K.A., K.T. Applegate, G. Danuser, R.S. Fischer, and C.M. Waterman. 2011. Distinct ECM mechanosensing pathways regulate microtubule dynamics to control endothelial cell branching morphogenesis. *J. Cell Biol.* 192:321–334.

Nagano, T., T. Yoneda, Y. Hatanaka, C. Kubota, F. Murakami, and M. Sato. 2002. Filamin A-interacting protein (FILIP) regulates cortical cell migration out of the ventricular zone. *Nat Cell Biol*. 4:495–501.

Nalbant, P., Y.-C. Chang, J. Birkenfeld, Z.-F. Chang, and G.M. Bokoch. 2009. Guanine nucleotide exchange factor-H1 regulates cell migration via localized activation of RhoA at the leading edge. *Mol. Biol. Cell*. 20:4070–4082.

Näthke, I.S. 2004. THE ADENOMATOUS POLYPOSIS COLI PROTEIN: The Achilles Heel of the Gut Epithelium. *Annu. Rev. Cell Dev. Biol.* 20:337–366.

Nelson, W.J. 1991. Cytoskeleton functions in membrane traffic in polarized epithelial cells. *Semin. Cell Biol.* 2:375–385.

Nelson, W.J. 2009. Remodeling epithelial cell organization: transitions between front-rear and apical-basal polarity. *Cold Spring Harb Perspect Biol*. 1:a000513.

Nogales, E., and H.-W. Wang. 2006. Structural intermediates in microtubule assembly and disassembly: how and why? *Current Opinion in Cell Biology*. 18:179–184.

Notari, M., Y. Hu, S. Koch, M. Lu, I. Ratnayaka, S. Zhong, C. Baer, A. Pagotto, R. Goldin, V. Salter, E. Candi, G. Melino, and X. Lu. 2011. Inhibitor of apoptosis-stimulating protein of p53 (iASPP) prevents senescence and is required for epithelial stratification. *Proc. Natl. Acad. Sci. U.S.A.* 108:16645–16650.

O'Brien, L.E., M.M.P. Zegers, and K.E. Mostov. 2002. Opinion: Building epithelial architecture: insights from three-dimensional culture models. *Nat Rev Mol Cell Biol*. 3:531–537.

O'Brien, L.E., T.S. Jou, A.L. Pollack, Q. Zhang, S.H. Hansen, P. Yurchenco, and K.E. Mostov. 2001. Rac1 orientates epithelial apical polarity through effects on basolateral laminin assembly. *Nat Cell Biol*. 3:831–838.

O'Brien, L.E., W. Yu, K. Tang, T.-S. Jou, M.M.P. Zegers, and K.E. Mostov. 2006. Morphological and biochemical analysis of Rac1 in three-dimensional epithelial cell cultures. *Meth. Enzymol.* 406:676–691.

Ohoka, Y., and Y. Takai. 1998. Isolation and characterization of cortactin isoforms and a novel cortactin-binding protein, CBP90. *Genes Cells*. 3:603–612.

Ojakian, G.K., and R. Schwimmer. 1988. The polarized distribution of an apical cell surface glycoprotein is maintained by interactions with the cytoskeleton of Madin-Darby canine kidney cells. *J. Cell Biol.* 107:2377–2387.

Osmani, N., F. Peglion, P. Chavrier, and S. Etienne-Manneville. 2010. Cdc42 localization and cell polarity depend on membrane traffic. *J. Cell Biol.* 191:1261–1269.

Palazzo, A.F., H.L. Joseph, Y.J. Chen, D.L. Dujardin, A.S. Alberts, K.K. Pfister, R.B. Vallee, and G.G. Gundersen. 2001a. Cdc42, dynein, and dynactin regulate MTOC reorientation independent of Rho-regulated microtubule stabilization. *Current Biology*. 11:1536–1541.

Palazzo, A.F., T.A. Cook, A.S. Alberts, and G.G. Gundersen. 2001b. mDia mediates Rho-regulated formation and orientation of stable microtubules. *Nat Cell Biol*. 3:723–729.

Pankov, R., Y. Endo, S. Even-Ram, M. Araki, K. Clark, E. Cukierman, K. Matsumoto, and K.M. Yamada. 2005. A Rac switch regulates random versus directionally persistent cell migration. *J. Cell Biol.* 170:793–802.

Pegtel, D.M., S.I.J. Ellenbroek, A.E.E. Mertens, R.A. van der Kammen, J. de Rooij, and J.G. Collard. 2007. The Par-Tiam1 complex controls persistent migration by stabilizing microtubule-dependent front-rear polarity. *Current Biology*. 17:1623–1634.

Perez, F., G.S. Diamantopoulos, R. Stalder, and T.E. Kreis. 1999. CLIP-170 highlights growing microtubule ends in vivo. *Cell*. 96:517–527.

Peris, L., M. Thery, J. Fauré, Y. Saoudi, L. Lafanechère, J.K. Chilton, P. Gordon-Weeks, N. Galjart, M. Bornens, L. Wordeman, J. Wehland, A. Andrieux, and D. Job. 2006. Tubulin tyrosination is a major factor affecting the recruitment of CAP-Gly proteins at microtubule plus ends. *J. Cell Biol.* 174:839–849.

Petrie, R.J., A.D. Doyle, and K.M. Yamada. 2009. Random versus directionally persistent cell migration. *Nat Rev Mol Cell Biol*. 10:538–549.

Petrie, R.J., N. Gavara, R.S. Chadwick, and K.M. Yamada. 2012. Nonpolarized signaling reveals two distinct modes of 3D cell migration. *J. Cell Biol.* 197:439–455.

Pézeron, G., G. Lambert, T. Dickmeis, U. Strähle, F.M. Rosa, and P. Mourrain. 2008. Rasl11b knock down in zebrafish suppresses one-eyed-pinhead mutant phenotype. *PLoS ONE*. 3:e1434.

Pfister, A.S., M.V. Hadjihannas, W. Roehrig, A. Schambony, and J. Behrens. 2012. Amer2 interacts with EB1 and APC and controls microtubule stability and cell migration. *J. Biol. Chem.*

Piehl, M., and L. Cassimeris. 2003. Organization and dynamics of growing microtubule plus ends during early mitosis. *Mol. Biol. Cell*. 14:916–925.

Popovici, C., B. Zhang, M.J. Grégoire, P. Jonveaux, M. Lafage-Pochitaloff, D. Birnbaum, and M.J. Pébusque. 1999. The t(6;8)(q27;p11) translocation in a stem cell myeloproliferative disorder fuses a novel gene, FOP, to fibroblast growth factor receptor 1. *Blood*. 93:1381–1389.

Prigozhina, N.L., and C.M. Waterman-Storer. 2006. Decreased polarity and increased random motility in PtK1 epithelial cells correlate with inhibition of endosomal recycling. *Journal of Cell Science*. 119:3571–3582.

Ratheesh, A., and A.S. Yap. 2012. A bigger picture: classical cadherins and the dynamic actin cytoskeleton. *Nat Rev Mol Cell Biol*. 13:673–679.

Reilein, A. 2005. Self-organization of an acentrosomal microtubule network at the basal cortex of polarized epithelial cells. *J. Cell Biol.* 171:845–855.

Reilein, A., and W.J. Nelson. 2005. APC is a component of an organizing template for cortical microtubule networks. *Nat Cell Biol*. 7:463–473.

Ren, Y., R. Li, Y. Zheng, and H. Busch. 1998. Cloning and characterization of GEF-H1, a microtubule-associated guanine nucleotide exchange factor for Rac and Rho GTPases. *J. Biol. Chem.* 273:34954–34960.

Riedl, J., A.H. Crevenna, K. Kessenbrock, J.H. Yu, D. Neukirchen, M. Bista, F. Bradke, D. Jenne, T.A. Holak, Z. Werb, M. Sixt, and R. Wedlich-Soldner. 2008. Lifeact: a versatile marker to visualize F-actin. *Nat Meth*. 5:605–607.

Rogers, S.L., U. Wiedemann, U. Häcker, C. Turck, and R.D. Vale. 2004. Drosophila RhoGEF2 associates with microtubule plus ends in an EB1-dependent manner. *Current Biology*. 14:1827–1833.

Roll-Mecak, A., and F.J. McNally. 2010. Microtubule-severing enzymes. *Current Opinion in Cell Biology*. 22:96–103.

Rooney, C., G. White, A. Nazgiewicz, S.A. Woodcock, K.I. Anderson, C. Ballestrem, and A. Malliri. 2010. The Rac activator STEF (Tiam2) regulates cell migration by microtubule-mediated focal adhesion disassembly. *EMBO Rep.* 11:292–298.

Royal, I., N. Lamarche-Vane, L. Lamorte, K. Kaibuchi, and M. Park. 2000. Activation of cdc42, rac, PAK, and rho-kinase in response to hepatocyte growth factor differentially regulates epithelial cell colony spreading and dissociation. *Mol. Biol. Cell*. 11:1709–1725.

Rusan, N.M., C.J. Fagerstrom, A.M. Yvon, and P. Wadsworth. 2001. Cell cycle-dependent changes in microtubule dynamics in living cells expressing green fluorescent protein-alpha tubulin. *Mol. Biol. Cell*. 12:971–980.

Ryan, S.D., A. Ferrier, and R. Kothary. 2012a. A novel role for the cytoskeletal linker protein dystonin in the maintenance of microtubule stability and the regulation of ER-Golgi transport. *Bioarchitecture*. 2:2–5.

Ryan, S.D., A. Ferrier, T. Sato, R.W. O'Meara, Y. De Repentigny, S.X. Jiang, S.T. Hou, and R. Kothary. 2012b. Neuronal dystonin isoform 2 is a mediator of endoplasmic reticulum structure and function. *Mol. Biol. Cell*. 23:553–566.

Ryan, S.D., K. Bhanot, A. Ferrier, Y. De Repentigny, A. Chu, A. Blais, and R. Kothary. 2012c. Microtubule stability, Golgi organization, and transport flux require dystonin-a2-MAP1B interaction. *J. Cell Biol.* 196:727–742.

Salaycik, K.J., C.J. Fagerstrom, K. Murthy, U.S. Tulu, and P. Wadsworth. 2005. Quantification of microtubule nucleation, growth and dynamics in wound-edge cells. *Journal of Cell Science*. 118:4113–4122.

Sammak, P.J., and G.G. Borisy. 1988. Direct observation of microtubule dynamics in living cells. *Nature*. 332:724–726.

Sandblad, L., K.E. Busch, P. Tittmann, H. Gross, D. Brunner, and A. Hoenger. 2006. The Schizosaccharomyces pombe EB1 homolog Mal3p binds and stabilizes the microtubule lattice seam. *Cell*. 127:1415–1424.

Sato, M., and T. Nagano. 2005. Involvement of filamin A and filamin A-interacting protein (FILIP) in controlling the start and cell shape of radially migrating cortical neurons. *Anat Sci Int*. 80:19–29.

Sato, S., R.L. Cerny, J.L. Buescher, and T. Ikezu. 2006. Tau-tubulin kinase 1 (TTBK1), a neuron-specific tau kinase candidate, is involved in tau phosphorylation and aggregation. *J. Neurochem.* 98:1573–1584.

Schek, H.T., M.K. Gardner, J. Cheng, D.J. Odde, and A.J. Hunt. 2007. Microtubule assembly dynamics at the nanoscale. *Current Biology*. 17:1445–1455.

Schober, J.M., G. Kwon, D. Jayne, and J.M. Cain. 2012. The microtubule-associated protein EB1 maintains cell polarity through activation of protein kinase C. *Biochemical and Biophysical Research Communications*. 417:67–72.

Schober, J.M., J.M. Cain, Y.A. Komarova, and G.G. Borisy. 2009. Migration and actin protrusion in melanoma cells are regulated by EB1 protein. *Cancer Lett.* 284:30–36.

Scolz, M., P.O. Widlund, S. Piazza, D.R. Bublik, S. Reber, L.Y. Peche, Y. Ciani, N. Hubner, M. Isokane, M. Monte, J. Ellenberg, A.A. Hyman, C. Schneider, and A.W. Bird. 2012. GTSE1 Is a Microtubule Plus-End Tracking Protein That Regulates EB1-Dependent Cell Migration. *PLoS ONE*. 7:e51259.

Scrimieri, F., E.S. Calhoun, K. Patel, R. Gupta, D.L. Huso, R.H. Hruban, and S.E. Kern. 2011. FAM190A rearrangements provide a multitude of individualized tumor signatures and neo-antigens in cancer. *Oncotarget*. 2:69–75.

Seetapun, D., B.T. Castle, A.J. McIntyre, P.T. Tran, and D.J. Odde. 2012. Estimating the Microtubule GTP Cap Size In Vivo. *Current Biology*. 22:1681–1687.

Semba, K., K. Araki, Z. Li, K.-I. Matsumoto, M. Suzuki, N. Nakagata, K. Takagi, M. Takeya, K. Yoshinobu, M. Araki, K. Imai, K. Abe, and K.-I. Yamamura. 2006. A novel murine gene, Sickle tail, linked to the Danforth's short tail locus, is required for normal development of the intervertebral disc. *Genetics*.172:445–456.

Shelden, E., and P. Wadsworth. 1993. Observation and quantification of individual microtubule behavior in vivo: microtubule dynamics are cell-type specific. *J. Cell Biol.* 120:935–945.

Siesser, P.F., M. Motolese, M.P. Walker, D. Goldfarb, K. Gewain, F. Yan, R.M. Kulikauskas, A.J. Chien, L. Wordeman, and M.B. Major. 2012. FAM123A Binds to Microtubules and Inhibits the Guanine Nucleotide Exchange Factor ARHGEF2 to Decrease Actomyosin Contractility. *Sci Signal*. 5:ra64.

Skoglund, P., A. Rolo, X. Chen, B.M. Gumbiner, and R. Keller. 2008. Convergence and extension at gastrulation require a myosin IIB-dependent cortical actin network. *Development*. 135:2435–2444.

Skube, S.B., J.M. Chaverri, and H.V. Goodson. 2010. Effect of GFP tags on the localization of EB1 and EB1 fragments in vivo. *Cytoskeleton (Hoboken)*. 67:1–12.

Slep, K.C., S.L. Rogers, S.L. Elliott, H. Ohkura, P.A. Kolodziej, and R.D. Vale. 2005. Structural determinants for EB1-mediated recruitment of APC and spectraplakins to the microtubule plus end. *J. Cell Biol.* 168:587–598.

Smyth, J.T., J.G. Petranka, R.R. Boyles, W.I. DeHaven, M. Fukushima, K.L. Johnson, J.G. Williams, and J.W. Putney. 2009. Phosphorylation of STIM1 underlies suppression of store-operated calcium entry during mitosis. *Nat Cell Biol*. 11:1465–1472.

Stamenović, D., S.M. Mijailovich, I.M. Tolić-Nørrelykke, J. Chen, and N. Wang. 2002. Cell prestress. II. Contribution of microtubules. *Am. J. Physiol., Cell Physiol.* 282:C617–24.

Stehbens, S., and T. Wittmann. 2012. Targeting and transport: How microtubules control focal adhesion dynamics. *J. Cell Biol.* 198:481–489.

Stehbens, S., H. Pemble, L. Murrow, and T. Wittmann. 2012. Imaging intracellular protein dynamics by spinning disk confocal microscopy. *Meth. Enzymol.* 504:293–313.

Stout, J.R., A.L. Yount, J.A. Powers, C. Leblanc, S.C. Ems-McClung, and C.E. Walczak. 2011. Kif18B interacts with EB1 and controls astral microtubule length during mitosis. *Mol. Biol. Cell*. 22:3070–3080.

Sugihara, Y., H. Taniguchi, R. Kushima, H. Tsuda, D. Kubota, H. Ichikawa, K. Sakamoto, Y. Nakamura, T. Tomonaga, S. Fujita, and T. Kondo. 2012. Proteomic-based identification of the APC-binding protein EB1 as a candidate of novel tissue biomarker and therapeutic target for colorectal cancer. *J Proteomics*. 75:5342–5355.

Szymanski, D. 2002. Tubulin folding cofactors: half a dozen for a dimer. *Current Biology*. 12:R767–9.

Tamura, N., and V.M. Draviam. 2012. Microtubule plus-ends within a mitotic cell are “moving platforms” with anchoring, signalling and force-coupling roles. *Open Biology*. 2:120132–120132.

Tanaka, T., F.F. Serneo, C. Higgins, M.J. Gambello, A. Wynshaw-Boris, and J.G. Gleeson. 2004. Lis1 and doublecortin function with dynein to mediate coupling of the nucleus to the centrosome in neuronal migration. *J. Cell Biol.* 165:709–721.

Tanenbaum, M.E., L. Macurek, B. van der Vaart, M. Galli, A. Akhmanova, and R.H. Medema. 2011. A complex of Kif18b and MCAK promotes microtubule depolymerization and is negatively regulated by Aurora kinases. *Curr. Biol.* 21:1356–1365.

Tanos, B., and E. Rodriguez-Boulan. 2008. The epithelial polarity program: machineries involved and their hijacking by cancer. *Oncogene*. 27:6939–6957.

Tran, A.D.-A., T.P. Marmo, A.A. Salam, S. Che, E. Finkelstein, R. Kabarriti, H.S. Xenias, R. Mazitschek, C. Hubbert, Y. Kawaguchi, M.P. Sheetz, T.-P. Yao, and J.C. Bulinski. 2007. HDAC6 deacetylation of tubulin modulates dynamics of cellular adhesions. *Journal of Cell Science*. 120:1469–1479.

van der Vaart, B., A. Akhmanova, and A. Straube. 2009. Regulation of microtubule dynamic instability. *Biochem. Soc. Trans.* 37:1007–1013.

van der Vaart, B., C. Manatschal, I. Grigoriev, V. Olieric, S.M. Gouveia, S. Bjelic, J. Demmers, I. Vorobjev, C.C. Hoogenraad, M.O. Steinmetz, and A. Akhmanova. 2011. SLAIN2 links microtubule plus end-tracking proteins and controls microtubule growth in interphase. *J. Cell Biol.* 193:1083–1099.

Van Gele, M., P. Dynoodt, and J. Lambert. 2009. Griscelli syndrome: a model system to study vesicular trafficking. *Pigment Cell Melanoma Res*. 22:268–282.

van Haren, J., K. Draegestein, N. Keijzer, J.P. Abrahams, F. Grosveld, P.J. Peeters, D. Moechars, and N. Galjart. 2009. Mammalian Navigators are microtubule plus-end tracking proteins that can reorganize the cytoskeleton to induce neurite-like extensions. *Cell Motil. Cytoskeleton*. 66:824–838.

Veale, K.J., C. Offenhäuser, S.P. Whittaker, R.P. Estrella, and R.Z. Murray. 2010. Recycling endosome membrane incorporation into the leading edge regulates lamellipodia formation and macrophage migration. *Traffic*. 11:1370–1379.

Verhey, K.J., and J. Gaertig. 2007. The tubulin code. *Cell Cycle*. 6:2152–2160.

Vicente-Manzanares, M., X. Ma, R.S. Adelstein, and A.R. Horwitz. 2009. Non-muscle myosin II takes centre stage in cell adhesion and migration. *Nat Rev Mol Cell Biol*. 10:778–790.

Walczak, C.E., S. Cai, and A. Khodjakov. 2010. Mechanisms of chromosome behaviour during mitosis. *Nat Rev Mol Cell Biol*.

Walker, R.A., E.T. O'Brien, N.K. Pryer, M.F. Soboeiro, W.A. Voter, H.P. Erickson, and E.D. Salmon. 1988. Dynamic instability of individual microtubules analyzed by video light microscopy: rate constants and transition frequencies. *J. Cell Biol.* 107:1437–1448.

Walpita, D., and E. Hay. 2002. Studying actin-dependent processes in tissue culture. *Nat Rev Mol Cell Biol*. 3:137–141.

Wang, N., K. Naruse, D. Stamenović, J.J. Fredberg, S.M. Mijailovich, I.M. Tolić-Nørrelykke, T. Polte, R. Mannix, and D.E. Ingber. 2001. Mechanical behavior in living cells consistent with the tensegrity model. *Proc. Natl. Acad. Sci. U.S.A.* 98:7765–7770.

Watanabe, T., J. Noritake, M. Kakeno, T. Matsui, T. Harada, S. Wang, N. Itoh, K. Sato, K. Matsuzawa, A. Iwamatsu, N. Galjart, and K. Kaibuchi. 2009. Phosphorylation of CLASP2 by GSK-3 regulates its interaction with IQGAP1, EB1 and microtubules. *Journal of Cell Science*. 122:2969–2979.

Waterman-Storer, C. 2002. Fluorescent speckle microscopy (FSM) of microtubules and actin in living cells. *Curr Protoc Cell Biol*. Chapter 4:Unit 4.10.

Waterman-Storer, C.M., and E.D. Salmon. 1997. Actomyosin-based retrograde flow of microtubules in the lamella of migrating epithelial cells influences microtubule dynamic instability and turnover and is associated with microtubule breakage and treadmilling. *J. Cell Biol.* 139:417–434.

Waterman-Storer, C.M., and E.D. Salmon. 1998. How microtubules get fluorescent speckles. *Biophysj*. 75:2059–2069.

Waterman-Storer, C.M., R.A. Worthylake, B.P. Liu, K. Burridge, and E.D. Salmon. 1999. Microtubule growth activates Rac1 to promote lamellipodial protrusion in fibroblasts. *Nat Cell Biol*. 1:45–50.

Wen, Y., C.H. Eng, J. Schmoranzer, N. Cabrera-Poch, E.J.S. Morris, M. Chen, B.J. Wallar, A.S. Alberts, and G.G. Gundersen. 2004. EB1 and APC bind to mDia to stabilize microtubules downstream of Rho and promote cell migration. *Nat Cell Biol*. 6:820–830.

White, C.D., H.H. Erdemir, and D.B. Sacks. 2012. IQGAP1 and its binding proteins control diverse biological functions. *Cell. Signal.* 24:826–834.

Wiese, C., and Y. Zheng. 2006. Microtubule nucleation: gamma-tubulin and beyond. *Journal of Cell Science*. 119:4143–4153.

Williams, M.J., and P. Clark. 2003. Microscopic analysis of the cellular events during scatter factor/hepatocyte growth factor-induced epithelial tubulogenesis. *J. Anat.* 203:483–503.

Wittmann, T., A. Hyman, and A. Desai. 2001. The spindle: a dynamic assembly of microtubules and motors. *Nat Cell Biol*. 3:E28–34.

Wittmann, T., and C.M. Waterman-Storer. 2001. Cell motility: can Rho GTPases and microtubules point the way? *Journal of Cell Science*. 114:3795–3803.

Wittmann, T., and C.M. Waterman-Storer. 2005. Spatial regulation of CLASP affinity for microtubules by Rac1 and GSK3beta in migrating epithelial cells. *J. Cell Biol.* 169:929–939.

Wittmann, T., G.M. Bokoch, and C.M. Waterman-Storer. 2003. Regulation of leading edge microtubule and actin dynamics downstream of Rac1. *J. Cell Biol.* 161:845–851.

Wittmann, T., G.M. Bokoch, and C.M. Waterman-Storer. 2004a. Regulation of microtubule destabilizing activity of Op18/stathmin downstream of Rac1. *J. Biol. Chem.* 279:6196–6203.

Wittmann, T., R. Littlefield, and C.M. Waterman-Storer. 2004b. Fluorescent Speckle Microscopy of cytoskeletal dynamics in living cells. D.L. Spector and R.D. Goldman, editors. Cold Spring Harbor Press, Woodbury, New York. 18 pp.

Wu, X., A. Kodama, and E. Fuchs. 2008. ACF7 regulates cytoskeletal-focal adhesion dynamics and migration and has ATPase activity. *Cell*. 135:137–148.

Wu, X., Q.-T. Shen, D.S. Oristian, C.P. Lu, Q. Zheng, H.-W. Wang, and E. Fuchs. 2011. Skin stem cells orchestrate directional migration by regulating microtubule-ACF7 connections through GSK3β. *Cell*. 144:341–352.

Xu, J., F. Wang, A. Van Keymeulen, M. Rentel, and H.R. Bourne. 2005. Neutrophil microtubules suppress polarity and enhance directional migration. *Proc. Natl. Acad. Sci. U.S.A.* 102:6884–6889.

Xu, J., S. Lamouille, and R. Derynck. 2009. TGF-beta-induced epithelial to mesenchymal transition. *Cell Res.* 19:156–172.

Yamada, K.M., and E. Cukierman. 2007. Modeling tissue morphogenesis and cancer in 3D. *Cell*. 130:601–610.

Yan, X., R. Habedanck, and E.A. Nigg. 2006. A complex of two centrosomal proteins, CAP350 and FOP, cooperates with EB1 in microtubule anchoring. *Mol. Biol. Cell*. 17:634–644.

Yang, S., X. Liu, Y. Yin, M.N. Fukuda, and J. Zhou. 2008. Tastin is required for bipolar spindle assembly and centrosome integrity during mitosis. *FASEB J.* 22:1960–1972.

Yu, W., L.E. O'Brien, F. Wang, H. Bourne, K.E. Mostov, and M.M.P. Zegers. 2003. Hepatocyte growth factor switches orientation of polarity and mode of movement during morphogenesis of multicellular epithelial structures. *Mol. Biol. Cell*. 14:748–763.

Yvon, A.-M.C., J.W. Walker, B. Danowski, C. Fagerstrom, A. Khodjakov, and P. Wadsworth. 2002. Centrosome reorientation in wound-edge cells is cell type specific. *Mol. Biol. Cell*. 13:1871–1880.

Zanic, M., J.H. Stear, A.A. Hyman, and J. Howard. 2009. EB1 recognizes the nucleotide state of tubulin in the microtubule lattice. *PLoS ONE*. 4:e7585.

Zaoui, K., K. Benseddik, P. Daou, D. Salaün, and A. Badache. 2010. ErbB2 receptor controls microtubule capture by recruiting ACF7 to the plasma membrane of migrating cells. *Proc. Natl. Acad. Sci. U.S.A.* 107:18517–18522.

Zegers, M.M.P., L.E. O'Brien, W. Yu, A. Datta, and K.E. Mostov. 2003. Epithelial polarity and tubulogenesis in vitro. *Trends in Cell Biology*. 13:169–176.

Zimniak, T., V. Fitz, H. Zhou, F. Lampert, S. Opravil, K. Mechtler, P. Stolt-Bergner, and S. Westermann. 2012. Spatiotemporal regulation of Ipl1/Aurora activity by direct Cdk1 phosphorylation. *Curr. Biol.* 22:787–793.

APPENDIX I

Experimental Procedures

DNA Constructs, Adeno- and Lentiviral vectors

To produce the EB1-2xEGFP construct, EGFP was amplified by PCR and inserted into pEGFP-N1-EB1 (Piehl and Cassimeris, 2003) using SmaI and AgeI restriction sites. The QuikChange II Site-Directed Mutagenesis kit (Agilent Technologies) was used to generate the EB1ΔC-2xEGFP construct by deleting the last 20 amino acids of EB1, and to introduce silent point mutations that confer resistance to EB1 shRNA #3 To generate the mCherry-EB1C construct for adenovirus expression, mCherry was amplified by PCR with Vent polymerase (New England Biolabs) and cloned into KpnI and XhoI restriction sites in pShuttle (Agilent Technologies). The C-terminus of EB1 (aa 165-268) was amplified by PCR and subsequently inserted at the 3' end of mCherry using XhoI and EcoRV restriction sites. Replication-deficient mCherry-EB1C adenovirus was produced using the AdEasy system (Agilent Technologies), and concentrated and purified as described (Gierke et al., 2010). For all PCR primers listed in the table below, restriction sites are in italics, homologous sequences are capitalized. For EB1-248 deletion primers, capitalized is homologous to EB1 and lower case is homologous to linker and EGFP to delete last 20 amino acids of EB1. All constructs were verified by sequencing. EGFP-α-tubulin was from Clontech. Non-phosphorylatable EGFP-CLASP2 (340-1084) 9xS/A (Kumar et al., 2009), EGFP-APC C-terminus (Mimori-Kiyosue et al., 2000), EGFP-MCAK (Moore et al., 2005), monomeric mEGFP-N1-Lifeact (Riedl et al., 2008), and EGFP-γ-tubulin

(Yvon et al., 2002) constructs were as described. Paxillin-EGFP and EGFP-VAMP3 expressing cells were gifts from D. Eastburn, D. Bryant and K. Mostov (UCSF).

EB1-2xGFP	
SmaI_EGFP_Forward	ag*cccggg*acATGGTGAGCAAGGGCGAGG
AgeI_EGFP_Reverse	gc*accggt*gtCTTGTACAGCTCGTCCATGC
EB1ΔC-2XGFP	
EB1-248_deletion_Forward	GTAGACATTCTGTATGCCacccgggacatggtgag
EB1-248_deletion_Reverse	ctcaccatgtcccgggtGGCATACAGAATGTCTAC
shRNA#3_rescue_Forward	GGGTGTTGACAAAATAATcCCgGTGGACAAATTAGTAAAAGG
shRNA#3_rescue_Reverse	CCTTTTACTAATTTGTCCACcGGgATTATTTTGTCAACACCC
mCherry-EB1C	
Kpn1_mCherry_Forward	ct*ggtacc*gccaccATGGTGAGCAAGGG
XhoI_mCherry_Reverse	gga*ctcgag*CTTGTACAGCTCGTCCATG
XhoI_EB1C_Forward	gga*ctcgag*TCAACACAGAGAACCGCTGCG
EcoRV_EB1C_Reverse	gga*gatatc*TTAATACTCTTCTTGCTCCTC

3D Epithelial Cyst Cultures

MDCK cells were cultured in minimum essential medium (MEM, Invitrogen), 5% fetal bovine serum (Invitrogen), 100 i.u. ml^{-1} penicillin, 100 µg ml^{-1} streptomycin at 37°C, and 5% CO_2 (O'Brien et al., 2006). Stable MDCK cell lines expressing EGFP-tagged proteins were generated by plasmid DNA transfection with Lipofectamine 2000 (Invitrogen), selected in growth medium supplemented with 1 mg ml^{-1} G418 (Mediatech Inc, Cellgro), and FACS sorted for expression level. Transient transfections were performed using Fugene6 (Roche).

For high-resolution imaging MDCK cysts were prepared essentially as described (Martín-Belmonte et al., 2007) with the following modifications: 35mm, glass-bottom dishes (MatTek) were pre-coated with 4 µl of 100% Matrigel (BD Biosciences, 356234). This resulted in an estimated thickness of the Matrigel

layer between 30-50 μm. #1 coverslip thickness was used to increase the working distance of high N.A. oil objectives. 2 ml of a 9×10^3 cells ml^{-1} single cell suspension in growth medium containing 2% Matrigel were plated on the pre-coated dishes. The growth medium was replaced with fresh medium after 4 days.

For HGF-induced epithelial remodeling assays (O'Brien et al., 2006; Kwon et al., 2011), the Matrigel overlay was removed on day 4 by brief treatment (8-10 minutes or until cysts look bumpy) with 0.25% trypsin containing 0.7 mM EDTA, 0.9 mM Ca^{2+} and 0.5 mM Mg^{2+} at 37°C, quenched with FBS-containing media, washed with PBS containing Ca^{2+} and Mg^{2+}, and overlaid with 2.11 mg ml^{-1} buffered collagen I (Advanced BioMatrix). Collagen was allowed to gel at 37°C without CO_2 before addition of 1 ml growth medium. After ~24 hours, the medium was replaced with 1 ml of growth medium supplemented with 20 ng ml^{-1} HGF (Genentech). Cysts were typically imaged after 16-18 hr of HGF-treatment. For the dominant negative mCherry-EB1C experiment, cysts were trypsinized as usual, then incubated with purified adenovirus for 1 hour before adding collagen and continuing on with the epithelial remodeling assay.

Lentivirus-mediated shRNA

In contrast to the human genome that appears to contain only one EB1 gene, BLAST searches of build 2.1 of the *Canis lupus familiaris* (Boxer) genome revealed surprisingly many well-conserved EB1 homologues on multiple chromosomes. We therefore designed multiple shRNA sequences to homologous areas on several different predicted canine EB1 genes using iRNAi software (www.mekentosj.com):

shRNA	Target Sequence	Target Accession number	Chromosome
Control	CCGCAGGTATGCACGCGT	Non-targeting	n/a
EB1 #1	GTGAAATTCCAGGCTAAAC	XM_846191.1, XM_538061.2 XM_544752.2 XM_533289.2 XM_533170.2 XM_532440.2, XM_534382.2 XM_845932.1	X 30 19 18 14 6 1
EB1 #2	GTGAAATTTCGGGCTAAGC	XM_859882.1, XM_846982.1	17
EB1 #3	ATAATTCCTGTGGACAAAT	XM_846191.1, XM_538061.2 XM_845562.1 XM_544752.2 XM_533170.2 XM_850206.1 XM_534382.2 XM_850108.1 XM_845932.1	X 34 30 18 7 6 4 1
EB1 #4	ATCATTCCTGTGGACAAAT	XM_859882.1, XM_846982.1,	17
EB1 #5	TCATTCCTGTGGACAAATT	XM_859882.1, XM_846982.1,	17
EB1 #6	TTCCTGTGGACAAATTAGT	XM_846191.1, XM_538061.2 XM_845562.1 XM_544752.2 XM_533170.2 XM_859882.1, XM_846982.1 XM_843665.1 XM_850206.1 XM_534382.2 XM_850108.1 XM_845932.1	X 34 30 18 17 13 7 6 4 1
EB1 #7	GTGGCTGTGTTGATTCAGC	XM_859882.1, XM_846982.1	17
EB1 #8	GCAGCTGAATTGATGCAGC	XM_846191.1, XM_538061.2 XM_845562.1 XM_533170.2 XM_532440.2 XM_843665.1 XM_534382.2 XM_850108.1 XM_845932.1	X 34 18 14 13 6 4 1

Sequences indicated in red are targeted by both shRNAs #1 and #3 that yielded the best depletion, and are thus likely to be expressed in MDCK cells. The non-targeting control shRNA has no known target in the canine genome. shRNAs were inserted in the pLKO.1-puro vector (Moffat et al., 2006) following the Addgene pLKO.1 protocol (www.addgene.org, plasmid 8453). For shRNA

lentivirus production, 293-FT cells (Invitrogen) were co-transfected with pLKO.1 plasmid and ViraPower packaging mix (Invitrogen) according to the manufacturer's protocol (Stehbens et al., 2012). Lentivirus-containing supernatants were harvested after 48 hrs, centrifuged, aliquoted, snap frozen in liquid nitrogen, and stored at -80°C. MDCK cells plated in 35 mm dishes were infected with viral supernatant supplemented with 4 μg ml^{-1} Sequabrene (Sigma) 2 hours after plating. After 18 hours, cells were transferred to 10 cm dishes in fresh medium, and 4 μg ml^{-1} puromycin (Invitrogen) was added 24 hrs later. Because puromycin appeared to have some effect on 3D epithelial morphogenesis, cells were selected for at least 7 days before setting up 3D cyst cultures without puromycin. Stable EB1 depletion was verified by immunoblot using a mouse anti-EB1 antibody (Abcam; ab22707) typically 7 days after lentivirus infection, and again after an additional 6-8 days of cell culture in the absence of puromycin (Supplemental Fig. 2). Chemiluminescent immunoblots were quantified using a FluorChem Q gel documentation system (Cell Biosciences).

Immunofluorescence, Live Cell Microscopy and Image Analysis

For F-actin (1:200 Alexa Fluor 488 phalloidin; Invitrogen; A12379), DNA (1 μM Sytox Orange; Invitrogen; S-11368), GP135 (1:1000 mouse anti-GP135 (Ojakian and Schwimmer, 1988)), and phospho-myosin light chain (1:100 pMLC; Rockland Immunochemicals; 600-401-416) staining, 3D MDCK cyst cultures were fixed in paraformaldehyde as described (Martín-Belmonte et al., 2007). To improve penetration of the fixative into epithelial structures, holes were poked

into the collagen matrix prior to fixation. For microtubule staining, 3D cyst cultures were treated with collagenase type VII (Sigma; C-2399) for 10 minutes, fixed in BRB80 (80 mM K-PIPES, pH 6.8, 1 mM $MgCl_2$, 1 mM EGTA) containing 0.25% EM grade glutaraldehyde for 2 minutes, and an additional 20 minutes in the same fixative with 0.1% Triton X-100. Following 3 x 20 minute incubations in PBS with 0.2% $NaBH_4$ to quench glutaraldehyde autofluorescence, cysts were blocked with 7 mg ml^{-1} fish skin gelatin and 0.025% saponin in PBS for 30 minutes. Primary antibodies used for microtubule immunofluorescence were rat-anti-tubulin (1:250, Serotec clone YL1/2) and mouse-anti-acetylated tubulin (1:200, Sigma clone 6-11B-1). Antibody incubations were generally 2 hours at room temperature, except pMLC, which was incubated overnight.

Microtubule fixation in cell extensions in the thick collagen gel was very difficult. An alternative method was used for microtubule array quantification, to better stabilize microtubules during fixation and to increase the number of HGF-induced cell extensions with well-fixed microtubule cytoskeletons. Cultures were pre-treated with 10 μM paclitaxel for 5 minutes before fixation in pre-warmed 0.5% fresh glutaraldehyde, 2% paraformaldehyde in BRB80 for 30 minutes. Cysts were then permeabilized with 0.1% Triton X-100 in TBS for 30 minutes, blocked with 2% BSA, 0.1% Triton X-100 in PBS for 30 min and incubated overnight with rat-anti-tubulin antibody. In this case, $NaBH_4$ quenching was not employed. Although this resulted in increased autofluorescence, hydrogen bubbles forming in the collagen gel often resulted in damage to the embedded epithelial structures.

For live cell microscopy, the growth medium was supplemented with 20 mM HEPES pH 7.5, and the 35 mm glass-bottom dishes were sealed with vacuum grease to prevent medium evaporation. Intracellular EGFP-tagged protein dynamics were imaged at 37°C on an inverted spinning disk confocal microscope system as previously described (Gierke et al., 2010; Kumar et al., 2009; Stehbens et al., 2012). Objectives used were 100x NA 1.49 (CFI APO TIRF; Nikon) for EB1-EGFP and other +TIP constructs, EGFP-α-tubulin, EGFP-VAMP3, high resolution DIC, and fixed cysts stained for microtubules; 60x NA 1.45 (CFI APO TIRF; Nikon) for EGFP-γ-tubulin, GP135/nuclei stained cysts, mEGFP-Lifeact, paxillin-EGFP and fixed cysts stained for pMLC; 60x NA 1.2 (CFI APO VC60WI; Nikon) for F-actin/nuclei stained cysts and fixed cysts stained for microtubule array quantification and 40x (CFI Fluor ELWD DM; Nikon) for phase contrast. Images for figures and videos were processed with a low-pass filter to reduce high-frequency camera noise and an unsharp mask filter to enhance fluorescent features using NIS-Elements software (Nikon). Videos were formatted in Quicktime Pro (Apple).

Cyst morphology was analyzed by inspection of z-stacks through the entire cyst thickness, and any cyst with additional small lumens was considered multi-lumen. Cysts in which the lumen was collapsed or partially filled with cells were considered collapsed. Lengths of HGF-induced extensions, 48-hour HGF-induced tubules, centrosome distances and microtubules to extension end distance were all measured using the Length Measurement tool in NIS-Elements software (Nikon). Fluorescence intensities of +TIP proteins at the microtubule

end were measured using the Intensity Profile Measurement tool in NIS-elements and were normalized to the cytoplasmic intensity. These normalized intensity profiles were least-square fitted with an exponentially-modified Gaussian function (Di Marco and Bombi, 2001) using the Solver tool in Excel (Microsoft):

$$y(x) = \frac{a}{2\tau}\exp\left(\frac{\sigma^2}{2\tau^2} - \frac{x - x_0}{\tau}\right)\left\{1 - erf\left[\frac{1}{\sqrt{2}}\left(\frac{\sigma}{\tau} - \frac{x - x_0}{\sigma}\right)\right]\right\}$$

The focal adhesion axial ratio was measured by dividing the length by the width of the focal adhesion using the Length Measurement tool in NIS elements. The edge/cytoplasm pMLC intensity ratio was measured using the Intensity Profile Measurement tool in NIS-elements. The average intensity of a line drawn along the edge of the cell with a neighborhood width of 2 was divided by the average intensity of a line drawn in the cytoplasm. For VAMP3 analysis, the ratio of mean fluorescence intensity of a region of interest (ROI) around the extension tip to an ROI within the bulk of the extension was measured using the ROI statistics tool in NIS-Elements software. Statistical analysis was performed in Excel (Microsoft) using the Analyze-it add-on (Analyse-it Software Ltd). Significance was determined by 2-tailed t-test. Microtubule growth rates were measured by tracking EB1ΔC-2xEGFP-labeled growing microtubule ends from time-lapse sequences acquired at 2 frames s^{-1} using plusTipTracker software (Danuser Lab, Harvard; http://lccb.hms.harvard.edu/software.html) in MatLab (The MathWorks). The following tracking parameters were used: max gap length = 12, min track length = 6, min search radius = 2, max search radius = 8, max forward angle = 30°, max backward angle = 10°, back velocity multifactor = 1.5,

fluctuation radius = 2. Photobleaching and acquisition speed currently prevent imaging of true 3D volumes, and we therefore only analyzed growth rate differences. We do not report transition frequencies that we expect to be fundamentally affected by tracking errors due to microtubule growth out of the plane of focus.

APPENDIX II

Detailed Protocols

A. Growing MDCK cysts in Matrigel

This is taken from protocol provided by Joan Brugge (Harvard) with some modifications for MDCK by Anirban Datta, David Bryant, and Sarah Gierke (UCSF).

DO EVERYTHING ON ICE!

Day 1

1) Split confluent p10 dish of MDCK 1:10 (to ensure cells are in proliferative mode)

Day 2

2) Pre-cool tips and MatTek coverglass dishes in fridge
3) Thaw some Matrigel (MG; high growth factor) (stored at -80C) on ice for approximately 1 h (DO NOT WARM TO RT)
4) Place coverglass dish on ice in the hood. Quickly remove 3-5 µl 100% MG and spread on coverglass. Spread as thinly as possible, but be sure to cover the whole glass surface.
5) Place in 37 degree TC incubator for ~5 minutes (or less) in a 10 cm dish. It's fine to let this set for longer (i.e. whilst preparing cell dilutions). But don't let it dry out.
6) Trypsinize cells as per usual. If cells are clumpy, pass through cell strainer to get single cell suspension. Count & dilute 20,000 cells/ml in normal MDCK medium
7) Dilute MG in normal MDCK medium (normal media = 5% FBS/MEM) to final concentration of 4%.
8) Mix the cell suspension and 4% MG together (1:1) to give final MG concentration of 2%
9) Add 2ml of this to each well of the coverglass dish.
10) Place in TC incubator.
11) Cysts will be ready in 4 days. Change media (new final concentration 2% Matrigel) every 3-4 days.

B. HGF-induced Tubulogenesis Matrigel Cysts transferred to Collagen

Adapted from Catherine Jacobson's protocol (Mostov Lab) by Sarah Gierke
Refs. Kwon SH et al. Curr Biol. 2011 Jan 25;21(2):161-6
O'Brien et al. Methods Enzymol. 2006;406:676-91.

1. Plate cysts. (see Matrigel cyst protocol for more details)
    a. Layer 4ul 100% MG on coverslip of 35mm coverglass dish.
    b. Dilute cells 1.8 x 10^4 and add 1mL to 1mL of 4% MG.
    c. Plate 2mL in 35mm dish. →37C, 5%CO_2

2. Day 4, Rinse 3x with room temp PBS^+, gently tilting plate back and forth. Aspirate from side of dish, except for last time, aspirate from edge of coverslip to remove all liquid.

3. Place a few drops of room temp 0.25% $Trypsin^+$ (with Ca^{2+} and Mg^{2+}) directly on coverslip (try not to overflow on rest of dish- will need this MG to stick to collagen) and incubate at 37C. (Prepare collagen on ice while cysts are trypsinizing)
    a. Timing is variable. First try a few different times from 6-12 minutes. I usually set up 3 plates and trypsinize different times for each. You want enough digestion to allow for migration, but not so much that the cysts fall apart or the collagen doesn't stick. Cysts should look slightly bumpy.

4. Rinse 3x with PBS^+. Aspirate same as before.
5. Add 1mL ice-cold collagen to side of coverslip on dish bottom, tilt just enough to cover bottom, then avoid any more movement. Place in 37C incubator (without CO_2, within an outer dish) for about 45 minutes or until gelled.
6. Gently add 1mL medium directly on top of collagen (not on edge of dish or it will go underneath collagen and rip it off). Gently place in incubator 37C +5%CO_2.
7. After about 24 hours, tilt plate and gently remove media with P1000 pipet. Add back 1mL 20ng/ml HGF directly on top of collagen. Image between 12-18hrs later.

PBS^+- PBS with 0.9 mM Ca^{2+} and 0.5 mM Mg^{2+}

$Typsin^+$ (0.25% trypsin containing 0.7 mM EDTA, 0.9 mM Ca^{2+} and 0.5 mM Mg^{2+})
10mL fresh 0.25% Trypsin
9uL of 1M $CaCl_2$
5uL of 1M $MgCl_2$
Let come to room temp without heating so that Trypsin activity doesn't decrease. This will make it easier to time the trypsinization step more consistently.

Collagen (2.11 mg ml^{-1} buffered collagen I)

On ice in 15mL conical
5 mL 3mg/mL Collagen (PureCol, Advanced BioMatrix cat # 5005-B)
750 uL 0.2M Glutamine (CCFGB002)
625uL 10xMEM (Gibco cat # 11430)
Gently mix tube by tilting back and forth with lid
625uL $NaHCO_3$ (stock: 5.88g/250mL water, sterile filter, store at 4C)
Mix again
125uL 1M HEPES (CCF)
Mix again.

C. Protocol for staining cyst in Matrigel:

From Dave Bryant, Mostov Lab—Adapted Sarah Gierke

PFA staining. (Non-microtubule staining, i.e. Actin, nuclei)

1) Remove from incubator
2) Wash 2x with warm PBS+, aspirate liquid from coverslip.
3) Immediately treat with fresh 4% PFA in PBS+ for 30 min at RT
4) Wash 2x with PBS+
    a. Can stop here → 4C if needed.
5) Permeabilize with 0.5% Triton-X100 in PBS- 10-15 min RT
6) Block with PFS (PBS+, Fish skin gelatin, saponin), 30min-1hr RT
7) For Actin/Nuclei stain only
    a. 1:50-1:200 phallodin, 0.9uM sytox in PFS, 1 hr.--> skip to step 14.
8) Add primary Ab in PFS for 2hr at RT
9) Wash with PBS- 2x quickly, then 2x 5-10 min each time
10) Add secondary antibody (Alexa conjugates), 1:200 for 2 hrs
    NB: Can also add Alexa-phalloidin or nuclear stain in with 2° Ab.
11) Wash 2x quickly
12) Add Nuclear dye (Hoechst 34580, 200 ng/ml, DAPI 300nM in PBS- (1:50dil) for 30 min at RT (or add nuc dye in with secondary Abs)
13) Wash with PBS- 2x quickly, then 2x 5-10 min each time. MORE IS BETTER.
14) Mount: Can leave cysts in PBS+ azide, parafilim or can use 13mm coverslip and mowiol to mount the dish coverslip.
15) Let dry overnight

PBS- = no $Ca^{2+,}$ Mg^{2+}

PFS = 3.5 g Fish skin gelatin (Sigma G7765- 250mL)

1.25 mLs 10% Saponin (10% in H20, filter, keep at 4C. Calbiochem 558255))

up to 500mLs in PBS+ $Ca^{2+,}$ Mg^{2+}

If using coverglass chamber, put in PBS+ w/ 0.02% NaN3, seal with parafilm, keep at 4C

Publishing Agreement

It is the policy of the University to encourage the distribution of all theses, dissertations, and manuscripts. Copies of all UCSF theses, dissertations, and manuscripts will be routed to the library via the Graduate Division. The library will make all theses, dissertations, and manuscripts accessible to the public and will preserve these to the best of their abilities, in perpetuity.

Please sign the following statement:

I hereby grant permission to the Graduate Division of the University of California, San Francisco to release copies of my thesis, dissertation, or manuscript to the Campus Library to provide access and preservation, in whole or in part, in perpetuity.

Sarah Gaines
Author Signature

1/9/13
Date